PHYSICS 134

ADVANCED PHYSICS LABORATORY

U. C. SANTA CRUZ

Winter Quarter 2022

PHYSICS 134

ADVANCED PHYSICS LABORATORY

U. C. SANTA CRUZ

TABLE OF CONTENTS

CAVENDISH EXPERIMENT

LABORATORY OBJECTIVE

The objective of this experiment is to measure the universal gravitational constant. With this value of the gravitational constant, and the known radius of the earth, calculate the density of planet earth.

INTRODUCTION

G, the gravitational constant, is one of the fundamental constants of our universe. When we measure it, we are measuring the strength of the Newtonian glue that makes apples fall, keeps our solar system in order, and, along with dark energy, determines motions at the greatest visible distances. It is ironic that although this force has been studied longer than any other, *G* is currently known to only four significant figures. Almost every other fundamental constant (the speed of light, Planck's constant, the charge on the electron) is known to six or seven significant figures. We know in detail about photons and how they interact with electrons and other charged particles, but until recently gravitational radiation has eluded direct experimental detection. There is also indirect evidence for gravitational radiation from the orbital decay of binary pulsar systems, for which Hulse and Taylor won the Nobel Prize in 1993.

Recently, interest in measuring *G* has re-emerged. In particular, measurements have been made of the acceleration of the earth and the moon due to the sun's gravity, and it has been found that their accelerations are the same to very high accuracy. The actual measurement is laser ranging between the earth and the moon, accurate on the order of centimeters. Other measurements have tested, at the level of parts per thousand, the equality of inertial mass and gravitational mass for distinct substances. This apparent equality is so striking that Einstein took the equality, which he called the "Principle of Equivalence" to be the foundation of the general theory of relativity.

Some current physical theories, known as string theories, suggest that the law of gravity as we know it may fail at very short distances. Tests are underway to seek deviations from the present law at the scale of millimeters.

The gravitational force, by comparison with the other known forces, is extremely weak. Two bare protons repel each other with an electrostatic force that is many orders stronger than the gravitational force.

Historical note: Cavendish was the richest man in England during his lifetime. He was a recluse, except for his scientific colleagues. He was not interested so much in measuring *G* as he was interested in measuring the density of the earth. He was also considered to be a great chemist; he determined that water was composed of hydrogen and oxygen; he determined that there was an unknown 1% component in air, later identified as argon; and he made important discoveries in thermodynamics.

PHYSICS

The law of gravitation is well known to college freshman. The gravitational force acting between two point masses is given by the formula

$$\mathbf{F}_{12} = \frac{GM_1M_2}{r^2}\hat{\mathbf{e}}_{12} \tag{1}$$

The force is always attractive, and acts along the line joining the two masses. It turns out that this formula is exactly correct for spherical mass distributions, if *r* is the distance between the centers of the distributions. Isaac Newton had to invent integral calculus to prove this theorem.

EXPERIMENTAL METHOD

The experimental method is very straightforward. Two small lead spheres rest on the ends of a boom, which is suspended by a fine tungsten fiber and allowed to rotate freely. Meanwhile, two much larger balls may be brought in close proximity to the two suspended balls, causing the equilibrium angle of the boom to shift. A small mirror is attached to the boom so that a laser beam can be deflected by an angle which is exactly twice the angle of the boom.[1] The position of the reflected beam can be accurately measured with a vertical line on an optical stage, driven by a precision micrometer. The relative angle of the pendulum beam is also sensed by an electronic encoder, which generates a voltage in proportion to the angle.[2]

Assume that the boom has come to rest ($\theta = 0$) with the exterior masses as far from the internal masses as possible, and that we then move the external masses close to the internal masses. The motion of the boom will be simple harmonic, and will be digitally recorded as a time sequence of voltages, which in turn can be related to angles. Simple harmonic oscillators are governed by the differential equation

$$\frac{d^2\theta}{dt^2} + 2b\frac{d\theta}{dt} + \omega_0^2\theta = 0 \tag{2}$$

where *b* is known as the damping constant and ω_0 is the undamped angular frequency. The general solution to equation (2) is given by

$$\theta(t) = \pm\theta_D + A\exp(-bt)\cos(\omega_1 t + \delta) \tag{3}$$

---

[1] The incident beam is focused on to the final slit by two lenses with focal length +1.000 m and −1.000 m, respectively. It turns out that two lenses of equal and opposite focal length separated by a finite distance always result in a net focus.

[2] The electronic encoder is not as accurate nor as repeatable as the laser beam, and so it should only be used to sense the *period* of the oscillations, which it can do very accurately.

where $\omega_1^2 \equiv \omega_0^2 - b^2$; δ is a phase angle that is defined by the origin in time; $\pm\theta_D$ are the equilibrium angles for the two extreme settings of the exterior spheres, and *A* is the initial oscillation amplitude. Our goal is to measure θ_D for two separate extremes of the external lead spheres.

It turns out that the apparatus can be very sensitive to air currents and to various electrostatic forces. To shield against electrostatic forces, the pendulum is enclosed between two grounded aluminum plates, one of which has a window for the laser beam. To shield against air currents, the entire apparatus is surrounded by an aluminum enclosure, also with a port hole for the laser beam. You may notice that if you leave the lid off of the enclosure, there will be annoying parasitic oscillations of the pendulum.

PROCEDURE

The apparatus is fixed in place on the optical table, and it has been carefully aligned. If you bump the apparatus, you risk breaking the tungsten fiber, which will set you back several days! Ask the TA, the instructor, or the lab manager to demonstrate how to move the spheres without breaking the wire.

The capacitive encoder is connected to an oscilloscope, which can be operated at a horizontal sweep speed as slow as 50 seconds per division, or 500 seconds per sweep. This readout is a handy way of observing if the oscillations of the boom have damped, and also where the boom is in its cycle of oscillations. It also offers a handy way of estimating the damping constant, *b*. Finally, it is by far the best way to measure the period of oscillation, which is needed for the determination of *G*. You may set the offset voltage of the encoder to near zero with the potentiometer on the small preamplifier box.

The capacitive encoder is also connected to a Vernier™ data logger, so that you can record and download the time-dependent motion. To use the software, load the application **Logger Lite**. Under **Experiment→Data Collection**, set the dwell time, which should be about 10 seconds per sample. The **Scale** button automatically scales the output graph, and the **Examine** button allows you to interrogate the data set.

Our main experimental objective is to measure the equilibrium angles $\theta_D^{\pm}$ and the period of oscillation of the pendulum. The period of the oscillations can then be determined by measuring the period on the computer. As a bonus, you can check that the equilibrium angles are equal and opposite. Rather than using the complicated forced oscillator method described in the Tel-Atomic manual, use the laser beam make a straightforward measurement of $\theta_D^{\pm}$ with the exterior spheres in the two complementary positions. Finally, don't forget that as the torsion pendulum rotates by δθ, the output beam rotates by 2δθ.

The diode laser beam should be focused by using two lenses, one with $f = 1.00$ m and a second one with $f = -1.00$ m. It can be shown that the effective focal length of a pair of lenses with equal and opposite focal lengths $\pm f$ separated by a distance *d* is always positive, and is given by $f_{eff} = f^2 / d$. Thus, the two lenses in sequence, separated by the correct distance, will give you a sharp focus at the micrometer station. The best way to align

the lenses is to first align the beam without them. Then, as you insert the lenses, one by one, make sure that the spot falls at the same place on the target.

ANALYSIS

The torque arising from the gravitational force of the two large stationary spheres attracting the two pendulum spheres is given by

$$\tau = 2\frac{GmM}{R^2}d \tag{4}$$

The deflection of the pendulum (relative to when the spheres are set midway) is given in terms of the torsion constant *K* by

$$\theta_D = \frac{\tau}{K} = 2\frac{GmM}{R^2}\frac{d}{K} \tag{5}$$

Thus, the gravitational constant is given by

$$G = \frac{KR^2}{2dmM}\theta_D \tag{6}$$

The moment of inertia *I* of the pendulum (needed for evaluating *K*) is given by the moments arising from the lead spheres and from the aluminum support bar:

$$I = 2m(d^2 + (2/5)r^2) + (m_b/12)(l_b^2 + w_b^2) \approx 2md^2 \tag{7}$$

The torsion constant *K* is related to the undamped resonant frequency by $\omega_0^2 = K/I$, and the undamped resonant frequency is related to the observed (damped) frequency by $\omega_0^2 \equiv \omega_1^2 + b^2$. As a consequence, $K/I = \omega_1^2 + b^2$, and so

$$K = (\omega_1^2 + b^2)I = [(2\pi/T)^2 + b^2]I \approx (2\pi/T)^2 I \approx 2md^2(2\pi/T)^2 \tag{8}$$

Using the approximations indicated above, we then get a very simple expression for *G*:

$$\boxed{G \approx \frac{(2\pi/T)^2 R^2 d}{M}\theta_D} \tag{9}$$

Note that *R* is the distance between the *centers* of the large and small spheres. It is given by $R = W/2 + R_L$ (where *W* is the width of the green apparatus enclosure and R_L is the radius of the large sphere) when the large spheres are just touching the glass plates. Also note that as the boom rotates to an angle θ_D, the measured outgoing ray advances an angle equal to $2\theta_D$.

Using the mechanical data tabulated in the Appendix, the measurements of T with the data logger, and the measurements of $\theta_D^{\pm}$ (by rotating the outer lead spheres), determine the gravitational constant G. If your result is within 10% of the latest published value, and if you have time, use the correct expression for the moment of inertia given in equation (7). How big is that effect? Note: In your report, it would be good to make a drawing of the overall light beam path.

ADDITIONAL QUESTIONS

1. Show, by explicit integration, that the gravitational force between a point mass and a uniform spherical shell outside the point mass is the same as the force between the point mass and the shell if all its mass were concentrated at the center.

2. Derive a formula for the ratio of the electrostatic force to the gravitational force for two bare protons. Numerically evaluate this ratio.

3. Derive an expression for the net torque on the two small spheres arising from the two large spheres, as a function of the angle of the exterior boom. Neglect the effect of forces on the aluminum support structure.

4. Why doesn't the small mass m appear in the calculated value of G in equation (9)? After all, the gravitational torque is proportional to m.

REFERENCES

1. H. Cavendish, *Philosophical Transactions of the Royal Society* **88**, 388 (1798).
2. G. G. Luther and W. R. Towler, *Physical Review Letters* **48**, 121 (1982).
3. S. Baessler, B. Heckel, E. Adelberger, J. Gundlach, *Physical Review Letters* **83**, 3585 (1999).

APPENDIX

SYM-BOL	VALUE	UNITS	DEFINITION
θ_D		Radi-ans	Equilibrium angle of the balance
b		s^{-1}	Inverse decay time of the oscillations
ω_0		s^{-1}	Oscillation frequency with no damping
ω_1		s^{-1}	Observed oscillation frequency with damping b
T		s	Observed oscillation period
K			Torsion constant of suspension fiber
I			Moment of inertia of the boom
M	917	g	Mass of each large sphere
R_L	27.4	mm	Radius of the large sphere
m	14.7	g	Mass of each small sphere
r	6.72	mm	Radius of the small sphere
d	66.56	mm	Distance from center of small sphere to rotation axis
D	82.5	mm	Distance from center of large sphere to rotation axis
R	44.9	mm	Dist. betw. the center of the small and the large sphere
l_b	150	mm	Length of the aluminum beam
w_b	12.9	mm	Width of the aluminum beam
h_b	1.73	mm	Thickness of aluminum beam
m_b	8.5	g	Mass of the aluminum beam
m_h	0.34	g	Missing mass of the hole in the beam
W	35.0	mm	Thickness of the apparatus (to exterior glass surfaces)

Table 1. Parameters of the Tel-Atomic apparatus

THE COMPTON EFFECT

LABORATORY OBJECTIVES

The objective of this experiment is to measure the energy of gamma rays scattered by electrons in an aluminum target over a large range in angles, and to compare your results with theory. Along the way you will learn about the interaction of radiation with matter; how a scintillation counter works, how a photomultiplier works, and how a multichannel analyzer can be used.

INTRODUCTION

The scattering of gamma rays by matter provided the first confirmation of the particle-like nature of gamma rays. Although the particle-like nature of visible photons was established in 1906 with Einstein's explanation of the photoelectric effect, the experiments of Compton and Simon in 1925 were the first to definitely establish the quantum nature of gamma rays.[3] Just as importantly, the *intensity* of the scattering of gamma rays by electrons confirmed the relativistic theory of the interaction of electrons and photons proposed by Dirac, and indirectly supported the existence of anti-electrons, now known as positrons.[4]

Today, Compton scattering is an important technique for measuring the momentum distribution of electrons in solids.

PHYSICS

The scattering of electromagnetic radiation by bare electrons was originally known as Thompson scattering. By way of review, for weak scattering,[5] the power of electromagnetic radiation ΔP (in Joules per second) scattered into a solid angle $\Delta\Omega$ is related to the incident power P_0 (also in Joules per second) by the differential cross section $d\sigma / d\Omega$:

$$\Delta P \equiv P_0 \frac{d\sigma}{d\Omega}(nl)\Delta\Omega \qquad (10)$$

where n is the number density of target electrons (in particles/m^3), and l is the thickness of the sample in m.[6] σ *always* has the units of area and $d\Omega$ is dimensionless.

The classical expression for the differential cross section for Thomson scattering of unpolarized (wavelike) radiation is given by

---

[3] A. H. Compton, *Physical Review* **21**, 483 (1923); A. H. Compton and A. W. Simon, *Physical Review* **26**, 889 (1925).

[4] O. Klein and Y. Nishina, *Zeitschr. f. Phys.* **52**, 853 (1929) and Y. Nishina, *Zeitschr. f. Phys.* **52**, 869 (1929).

[5] By "weak" we mean that the total probability of scattering is much less than 1, so that the beam intensity is not diminished as it passes through the sample.

[6] For scattering of particles, P_0 and ΔP are incident and scattered particle rates, respectively, measured in particles/sec.

$$\frac{d\sigma}{d\Omega} = \frac{1}{2} r_0^2 (1 + \cos^2\theta) \quad \text{where } r_0 \equiv \frac{e^2}{4\pi\varepsilon_0 mc^2} = 2.818 \times 10^{-15}\text{m} \tag{11}$$

In this expression, θ is the scattering angle and r_0 is called the *classical radius of the electron*. Notice that the scattering intensity is symmetric with respect to the forward-backward direction.

The Dirac theory of the electron, which ultimately led to the prediction of the positron, required that electromagnetic radiation has particle-like properties satisfying momentum and energy conservation, and be consistent with the special theory of relativity. As a consequence, scattered photons lose energy upon scattering by electrons, according to the following famous formula

$$\frac{1}{E'} = \frac{1}{E} + \frac{(1 - \cos\theta)}{mc^2} \tag{12}$$

where E is the incident photon energy and E' is the scattered photon energy. From this equation, Klein and Nishina calculated the differential cross section, in analogy with the Thompson formula, and showed that

$$\frac{d\sigma}{d\Omega} = \frac{1}{2}\left(\frac{E'(\theta)}{E}\right)^2 r_0^2 \left[\frac{E}{E'(\theta)} + \frac{E'(\theta)}{E} - \sin^2\theta\right] \tag{13}$$

Notice that this cross section does not have forward-backward symmetry, unlike the Thompson cross section, because E' depends upon θ. The verification of this formula was an impressive confirmation of the Dirac theory, and hence served as indirect evidence of the correctness of the idea of the existence of positrons.

EXPERIMENTAL METHOD

The source of gamma rays in this experiment is a sample of ^{137}Cs which undergoes nuclear disintegration, resulting in the emission of gamma rays of energy E = 661.7 keV. The gamma rays emerge from a 3.16 mm diameter source and are collimated by a 4.75 mm diameter by 133 mm long hole in lead. (Refer to Appendix 2 in this section for further details). The gamma-ray beam scatters from an aluminum target which is a 1.00 inch diameter aluminum rod. Scattered gamma rays are absorbed by a 3 inch diameter by 4 inch long NaI crystal, whose scintillation light generates photoelectrons at the cathode of a photomultiplier. Each absorbed gamma ray thus produces an electronic pulse whose amplitude is accurately proportional to the energy of the absorbed quantum. A multichannel analyzer produces and displays a running histogram of the number of pulses with a given energy. A mono-energetic beam of gamma rays would ideally yield a Gaussian histogram with an energy full-width at half maximum of about 7% of the central energy. This width stems from the finite number of scintillation photons emitted by any given photon.

The scattered beam detector is mounted on a rotating carriage, which enables one to accurately measure the scattering rate as a function of angle.

PROCEDURE

With the source shutter closed, mount a ^{137}Cs source about 6 inches from the detector and take calibration spectra with several values of the photomultiplier high voltage. Choose a high voltage that puts the 661.7 keV peak near the upper end of the multichannel analyzer range. You may do a two-point calibration, noting that the low energy peak is the Barium Kα line.

Before proceeding to the main part of the experiment, record the channel number of the ^{137}Cs peak at several lower voltages, and make a log-log plot of the channel number versus the voltage. From this plot estimate the number of dynodes in the photomultiplier. (See Appendix 1 in this section for details).

Now remove the sealed source and collect scattered gamma-ray data at several scattering angles. Since there may be a slight thermal drift of the high voltage and the gain of the amplifier, it would be wise to use the sealed source for intermediate calibrations.

ANALYSIS

Fit each Compton scattering peak with a Gaussian function plus background. From the position of the peaks as a function of angle, verify that gamma rays behave as ballistic, massless particles, satisfying equation (12). In doing so, determine the mass of the electron. From the area of these peaks, plot the relative scattering cross section as a function of angle and compare with the Klein-Nishina formula, equation (13), up to an overall normalization constant.

ADDITIONAL QUESTIONS

1. Verify that equation (10) is dimensionally correct.

2. Show that in the limit $E \ll mc^2$ the Klein-Nishina formula for the cross section approaches the Thompson formula.

3. Explain the presence of the low energy Barium line in the ^{137}Cs spectrum.

4. What is the solid angle of the detector? What is the average thickness of the sample, and what is the number density of electrons in the sample? What other information would you need to know to measure the absolute differential cross section, equation (10) ? Can you suggest how you would go about obtaining this information?

REFERENCES

A. C. Melissinos, *Experiments in Modern Physics*. (New York, Academic Press, 1966).
R. D. Evans**,** *The Atomic Nucleus.* (New York, McGraw Hill, 1955).
X-Ray Data Booklet, http://xrd.lbl.gov
David R. Lide, ed. *Handbook of Chemistry and Physics* **(**CRC Press).

APPENDIX 1: PHOTOMULTIPLIER GAIN

A photomultiplier tube consists of 10-12 electrodes, arranged in a "Venetian blind" configuration, within a vacuum tube. These electrodes are known as "dynodes." By means of a resistive voltage divider, each dynode is about $v = 100$ volts more positive than the preceding dynode. The last dynode is called the anode, and it is where the final charge is collected.

A pulse of n electrons emerging from the photocathode will be attracted to the first dynode. On average, each of these electrons will generate g secondary electrons in colliding with the next dynode. Typically, g~2-4. In other words, the first dynode will receive n electrons and emit ng electrons; the second dynode will receive ng electrons and emit ng^2 electrons, and so forth. Thus, if there are N dynodes, the total number of electrons falling on the final electrode (called the anode) will be ng^N.

The gain per stage, g, depends upon the accelerating voltage per stage, v. To a good approximation, g is proportional to the square root of the accelerating voltage in the operating region; *i.e.* $g(v)=kv^{1/2}$ where k is some constant. Since the accelerating voltage is set by a voltage divider, v is proportional to the overall tube voltage V; say $v = cV$ where c is another proportionality constant. Thus, we may write the final number of electrons as $ng^N = n(kv^{1/2})^N = n(kc^{1/2}V^{1/2})^N$. The final charge Q will be just the number of electrons, multiplied by the charge on the electron: $Q=en(kc^{1/2}V^{1/2})^N$.

With the assumptions given above, we see that $Q \propto V^{N/2}$. That is, the pulse height goes as a high power of the tube voltage. If you were to plot log Q versus log V, you would get roughly a straight line with slope $N/2$. Thus, at a high enough voltage, even a single photoelectron can give rise to an observable pulse at the anode. For example, if $g = 3$ and $N = 10$, the overall multiplication factor will be $3^5 \sim 243$. This is also why it is important to not run the tube at too high a voltage; giant pulses have deleterious effects upon the system. For one thing, residual gas in the tube (mainly helium, which can diffuse through the envelope) can be ionized by the photoelectrons, and give rise to giant, spurious, and intermittent pulses.

APPENDIX 2. THE GAMMA-RAY SOURCE

The gamma-ray source for this experiment is a ~100 mCi (milliCurie) ^{137}Cs sealed source embedded in a thick lead shield, with a locked shutter. ^{137}Cs emits 662 keV gamma rays. It has a half life of about 30 years. There are three important things to know:

1. Only authorized personnel with documented training are permitted to open the locked shutter.
2. There is no need for any one to ever place any part of their body in the direct beam, which is delimited by the cardboard tube.
3. The intensity of the beam scattered from the aluminum post is completely negligible.

Even if you were to put a part of your body, such as a hand, in the direct beam at 1 meter from the source (the closest accessible point), the exposure would be well below the limit for members of the public. here is why:

1. The ^{137}Cs source is effectively pointlike, and situated within the lead shield at a distance of 100 mm from an aperture of 4.8 mm diameter. Thus, the beam is a cone of diameter 47.5 mm (1.87 inches) at the 1 meter point, where the aluminum target is located.
2. The exposure rate from a ^{137}Cs source is 0.32 mR/hour/mCi at 1 meter. For our 100 mCi source this amounts to 32 mR/hour at 1 meter. The exposure limit for members of the public is 100 mR/year.
3. **You would have to expose yourself to the direct beam for three hours to reach the limit for members of the public for one year**. **However, there is no need whatsoever for you to <u>ever</u> place <u>any</u> part of your body in the direct beam.**

ELECTRON SPIN RESONANCE

LABORATORY OBJECTIVES

The objective of this experiment is to learn the fundamentals of microwave theory and instrumentation; to learn the fundamentals of electron spin resonance, and to measure the *g*-factor of an electron in an organic salt known as DPPH.

INTRODUCTION

The fascinating history of the discovery of electron spin has been authoritatively described in the book by Pais.[7] In the mid-1920's, many scientists informally proposed the idea, but the first convincing publication was published by two graduate students, Sam Goudsmidt and George Uhlenbeck.[8] In their seminal article they proposed that the electron had half-integral spin, which qualitatively and quantitatively explained the splitting into doublets of orbital angular momentum states. Today, the electron's spin plays a central role in the magnetism of matter and it is the centerpiece of the modern subject of *spintronics*. At the Stanford Linear Accelerator Center, 50 GeV beams of spin-polarized electrons were once collided with unpolarized positrons at the Z_0 resonance, leading to accurate measurements of an important parameter of the Standard Model.

PHYSICS

Classical treatment: Classical mechanics teaches us that a rigid rotating mass with density function $\rho_m(\mathbf{r})$ may possess a vector spin angular momentum **S**. Likewise, a rotating charge density $\rho_c(\mathbf{r})$ may possess a vector magnetic moment **μ**. These vector quantities are defined by similar expressions:[9]

$$\begin{aligned} \mathbf{S} &\equiv \int (\mathbf{r}\times\mathbf{v})\,\rho_m(\mathbf{r})\,d^3x \\ \boldsymbol{\mu} &\equiv \frac{1}{2}\int (\mathbf{r}\times\mathbf{v})\,\rho_c(\mathbf{r})\,d^3x \end{aligned} \tag{14}$$

In the special case where the charge density is everywhere proportional to the mass density, it is easy to show that

$$\frac{\rho_c(\mathbf{r})}{\rho_m(\mathbf{r})} = \frac{q}{m} \tag{15}$$

and it follows that

$$\boldsymbol{\mu} = (q/2m)\mathbf{S}\,. \tag{16}$$

If, on the other hand, the local ratio of charge density to mass density depends upon position, the magnetic moment will still be proportional to the angular momentum, with the coefficient $q/2m$ scaled by a dimensionless factor known as the *g*-factor:

---

[7] Abraham Pais, *Inward Bound*. Oxford University Press, New York.

[8] G. E. Uhlenbeck and S. Goudsmit, *Naturw*. **13**, 953 (1925).

[9] The curious factor of ½ in the definition of **μ** is chosen so that the energy of a magnetic dipole in an external field **B** is given by $E=-\boldsymbol{\mu}\cdot\mathbf{B}$.

$$\boldsymbol{\mu} = g(q/2m)\mathbf{S} \tag{17}$$

Empirically, for a free electron the *g* factor is measured to be

$$g_e = 2.002\,319\,304\,362 \tag{18}$$

This is one of the most accurately measured quantities in physics. More remarkably, the theory known as *quantum electrodynamics* predicts this number, within the experimental error (±1) in the final digit.

Quantum treatment: When one properly treats an electron quantum mechanically, the fundamental unit of angular momentum is Planck's constant, $\hbar$. In particular, the electron's spin angular momentum along any axis is given by $\pm\hbar/2$. If we arbitrarily take the axis to be the z-axis, then

$$\mu_z = \pm g_e(e/2m_e)(\hbar/2) = \pm(g_e/2)(e\hbar/2m_e) = \pm(g_e/2)\mu_B \tag{19}$$

where we have defined the Bohr magneton, the natural unit of magnetic moment, as $\mu_B \equiv e\hbar/2m_e$.

The *energy* of a spinning charge in a magnetic field is given both classically and quantum-mechanically by the simple formula

$$E = -\boldsymbol{\mu}\bullet\mathbf{B}_{local} \tag{20}$$

where $\mathbf{B}_{local}$ is the local microscopic magnetic field at the site of the electron. Therefore, if $\mathbf{B}_{local}$ is directed along the z-axis, formula (19) tells us that there is an energy difference between the state where an electron is aligned parallel with the field, versus the state when it is aligned anti-parallel. The energy difference will simply be

$$\Delta E = g_e\mu_B B_{local} \tag{21}$$

As a consequence, if we shine photons with energy $\hbar\omega = \Delta E$ on to the sample, we can flip the low-energy spin to a high energy state, or alternatively stimulate a transition from the high energy state to a low energy state. Either way, energy will be absorbed from the photon beam by the electron. Detecting this absorption is the challenge of electron spin resonance.

Now it gets interesting. The magnetic field at the electron's site will be the sum of the externally applied magnetic field and the induced local magnetic field due to neighboring electrons. If the local magnetic field is equal to the externally applied magnetic field, plus an amount proportional to the applied magnetic field, the material is said to be either

paramagnetic or diamagnetic.[10] For this reason, electron spin resonance is sometimes called *electron paramagnetic resonance*, a misnomer since spin resonance occurs perfectly well in nonmagnetic materials. The effective *g*-factor is defined as the coefficient *g* in the formula

$$\Delta E = g\mu_B B_{ext} \tag{22}$$

For most substances, paramagnetism is either weak or absent, and *g* is very close to g_e.[11]

Transitions between the low and high energy states will take place when $\Delta E = \hbar\omega$, where ω is the angular frequency of the incident radiation. Inserting this condition in eq. (22), we get

$$g = \frac{\hbar\omega}{\mu_B B_{ext}} = \frac{2m_e}{e}\frac{\omega}{B_{ext}} = \frac{4\pi m_e}{e}\frac{\nu}{B_{ext}}, \tag{23}$$

where $\nu = \omega/2\pi$ is the frequency of the incident radiation.

EXPERIMENTAL METHOD

The basic method: As previously discussed, microwave energy will be absorbed by a sample when the microwave frequency and the applied magnetic field satisfy the resonance condition. In this experiment we bathe the sample with a known frequency of microwave energy, around 9.7 GHz, and slowly sweep the magnetic field (of order 0.3 T) to observe the absorption profile. Unfortunately, the power absorbed by the sample is only a tiny fraction of the applied power; to achieve high sensitivity, we employ a *bridge* technique where the incident power is effectively subtracted off, so that in the absence of sample absorption, the detector sees little or no microwave power. This method will become clearer in what follows.

Basic Parameters:

1. Nominal microwave frequency: 9.3 GHz
2. Waveguide internal dimensions: 0.400 inches by 0.900 inches
3. Nominal anode voltage: 300 Volts
4. Nominal anode current 30 mA
5. Nominal reflector voltage: 150 Volts
6. Nominal magnet current: 3.4 Amperes
7. Nominal magnetic field 0.33 Tesla

[10] For paramagnets, the local field is increased in magnitude; for diamagnets, the local field is reduced. Paramagnetism in materials is usually far stronger than diamagnetism.
[11] Strictly speaking, *g* is a second-rank tensor, whose principal components can be measured by orienting a single crystal with respect to the external field. We shall neglect this effect.

Magnetic Field: The magnetic field is provided by an electromagnet with water-cooled coils. The power supply is capable of being modulated by an external D.C. coupled input. The approximate calibration of the magnet is 0.1 Tesla/Ampere.

Microwave Source: A klystron *amplifier*, (which we will *not* use) consists of an electron beam that passes through two sequential resonant cavities tuned to the same frequency. Microwave fields introduced into the first cavity modulate the electron speeds, causing the stream of electrons to form bunches. These bunches then induce strong electromagnetic fields in the second cavity, resulting in a large power amplification.

When all that is needed is an oscillator, the two cavities can be cleverly combined into a single cavity; this configuration is known as a *reflex* klystron, as shown in Figure 1, and which we use in this experiment. Such a klystron can oscillate within plus or minus 10% of the central resonant frequency (because the cavity *Q* is about 100). The precise microwave frequency is determined by the so-called reflector voltage, which determines the electron bunch spacing.

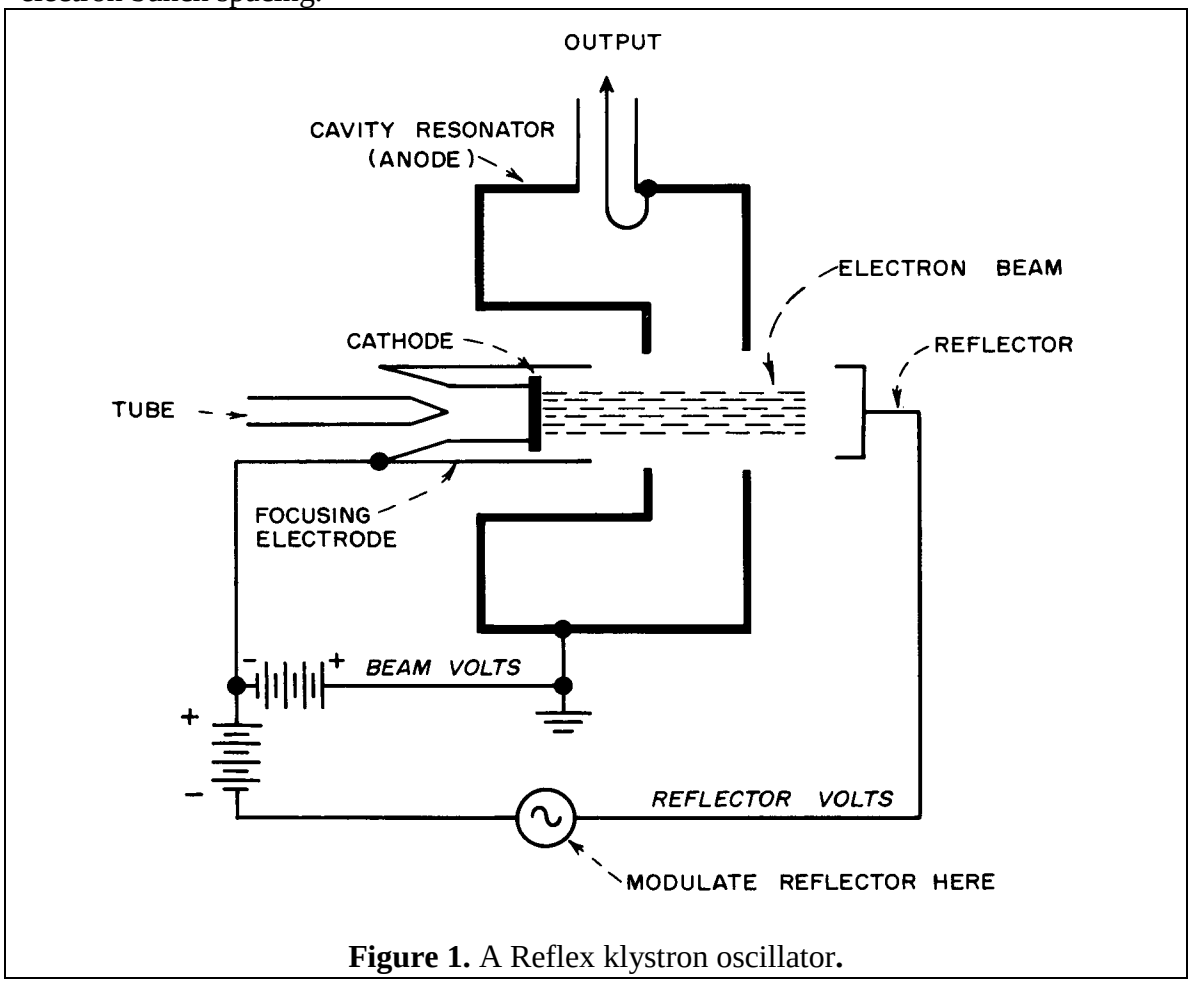

Figure 1. A Reflex klystron oscillator**.**

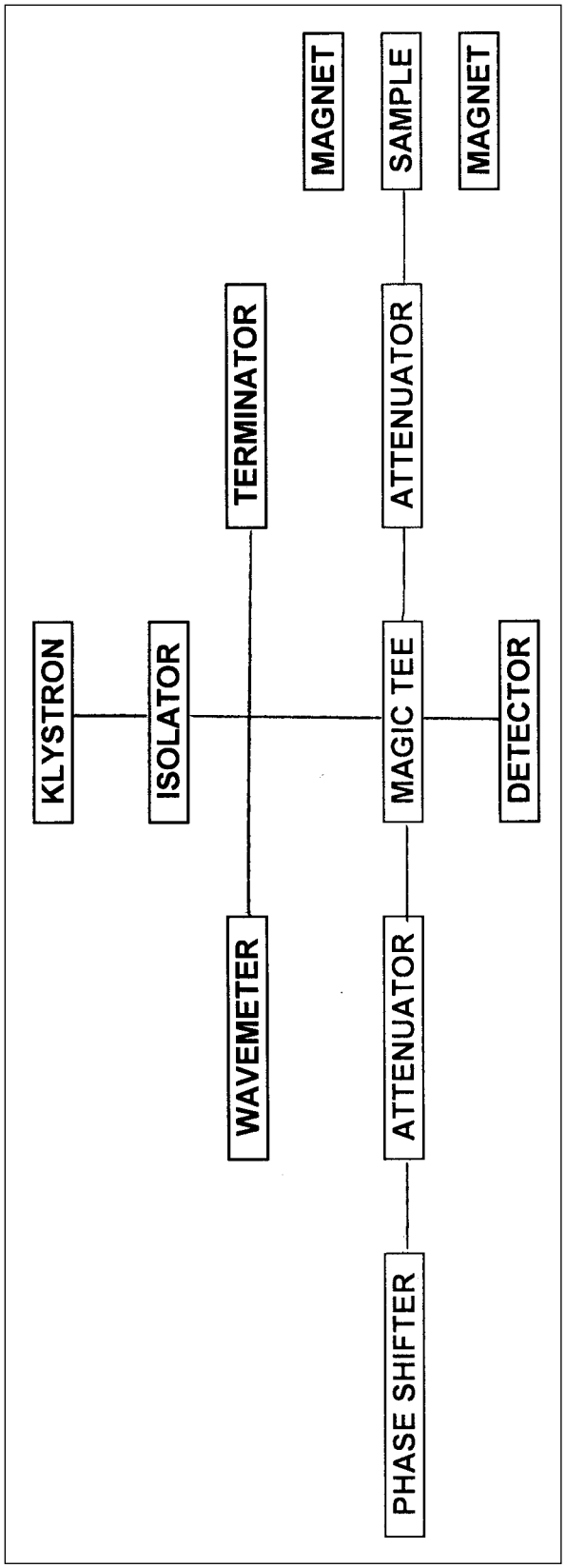

Figure 2. Schematic diagram of the spectrometer circuit.

Microwave oscillator: Following the klystron is an *isolator*, a microwave component that allows power to only flow in one direction, in this case away from the klystron. The isolator protects the klystron from microwave power reflected back from downstream components, power which could damage, or at least disrupt, the action of the klystron.

Microwave Circuit: The full microwave circuit is depicted in Figure 2. The objective of this circuit is to provide a high contrast microwave signal at the detector. By high contrast we mean that variations in the absorption coefficient of the sample with respect to magnetic field (at a constant frequency) appear as a well-defined signal at the detector.

Microwave power is transported to the various components via hollow rectangular waveguides. The power propagating down a waveguide can be resolved into *modes* (*m*,*n*); for any given mode there is a minimum propagation frequency, called the cutoff frequency. Power in this mode can only propagate at frequencies higher than the cutoff frequency. The cutoff frequencies for mode *mn* are given by

$$f_{mn}^{(c)} = \frac{c}{2}\left[\frac{m^2}{a^2} + \frac{n^2}{b^2}\right]^{1/2} \tag{24}$$

If a < b, the mode with the lowest cutoff frequency is the (0, 1) mode, with $f_{(0,1)}^{c} = c/2b = 6.562$ GHz , which is comfortably less than our working frequency, 9.3 GHz. It is easy to show that all other modes have cutoff frequencies greater than 9.3 GHz, so no other mode can propagate in our waveguide.

Wavemeter: Downstream of the isolator, a "tee" diverts[12] a small fraction of the klystron power into a high-*Q* resonant cavity with an adjustable and accurately calibrated piston. A crystal detector downstream of the wavemeter will show a dip in power when the klystron frequency is at resonance. The wavemeter is accordingly used to calibrate the klystron frequency.

Magic Tee: Downstream of the wavemeter circuit, the klystron power encounters a "magic tee." This magic tee is a four-port device with the following remarkable property: all of the power entering the tee from the klystron is evenly split to the two side ports, but none flows to the output port (connected to the final detector). However, power returning from the two side ports *coherently* combines at the tee but only flows to the output port.

Sample Chamber: One of the two symmetric ports of the magic tee, the *sample arm*, provides power to the sample chamber; the other port provides power to a variable reactance. (See below).

[12] Half the diverted power goes to the wavemeter and half to a dummy matched load. An equivalent approach would have been to use a *directional coupler* connected only to the wavemeter, instead of a tee to two arms.

The sample chamber is a short piece of waveguide (a = 0.400 inches, b= 0.900 inches) of internal length d = 1.543 inches, soldered to the sample arm. Signal enters the sample cavity via a small hole drilled in the upper face of the sample arm waveguide. The sample is contained in a miniature test tube which slips into a hole in the upper part of the sample chamber. By suspending the sample in a resonant cavity, one substantially increases the electromagnetic fields at the sample over the fields in the waveguide proper.[13] Since the sample is close to the conducting boundary of the cavity, the oscillating electric field **E** is small, but the oscillating magnetic field **B** is large.

A perfectly conducting rectangular cavity with no apertures has an infinite Q and an infinite spectrum of resonances, given by the formula

$$f_{lmn} = \frac{c}{2}\left[\left(\frac{l}{a}\right)^2 + \left(\frac{m}{b}\right)^2 + \left(\frac{n}{d}\right)^2\right]^{1/2}. \qquad (25)$$

Because our chamber has finite conductivity and a large hole to admit the sample, the resonant frequency is significantly shifted downward, and the Q is substantially reduced.[14]

The ideal configuration of the sample arm occurs when most of the power traveling down the sample arm is absorbed by the resonant cavity walls, and by the sample itself. This is called a "matched" configuration. It occurs when the aperture admitting the power to the chamber is exactly the right size, and when the fields are at a maximum at the aperture. Maximizing the fields at the aperture is accomplished by terminating the sample arm in an adjustable short, which sets up standing waves in the sample arm, with maxima separated by λ_g. When the aperture is adjusted to be a distance $(p+½)\lambda_g$ from the short (where p is any integer), the coupling will be optimal. In practice, this adjustment is made empirically. (See below).

Variable reactance: The other symmetric port of the magic tee is connected to a calibrated variable attenuator, followed by a variable reactance. The variable attenuator is a masterpiece in engineering: It reduces the power transmitted to the downstream components, yet it always presents a matched impedance to the waveguide, so no power is reflected back by the attenuator. It is also symmetric in this regard.

The purpose of this circuit is to reflect power back to the magic tee with a phase and amplitude that nearly cancels the power reflected from the sample chamber when the spin resonance condition (B, ω) is *not* met. Then, when the spin resonance condition is met (in

[13] The spectrometer described in Mellisinos has the sample suspended in the standing wave field of the waveguide, rather than in a high-Q resonator. The signal in such a spectrometer is much smaller.

[14] A closed copper cavity at these frequencies typically has a Q of about 10,000. The apertures in our sample chamber reduce the Q to of order 100, which is still a huge improvement over the Mellisinos method.

our case by varying B at fixed ω) the bridge will be unbalanced and a net signal will flow to the output detector.

Detector: The microwave detector is a simple semiconductor diode placed in the wave-guide at the point of maximum electric field. The diode rectifies the applied electric field, producing a D.C. signal whose amplitude increases with the applied electric field. The current versus voltage is shown in Figure 3:

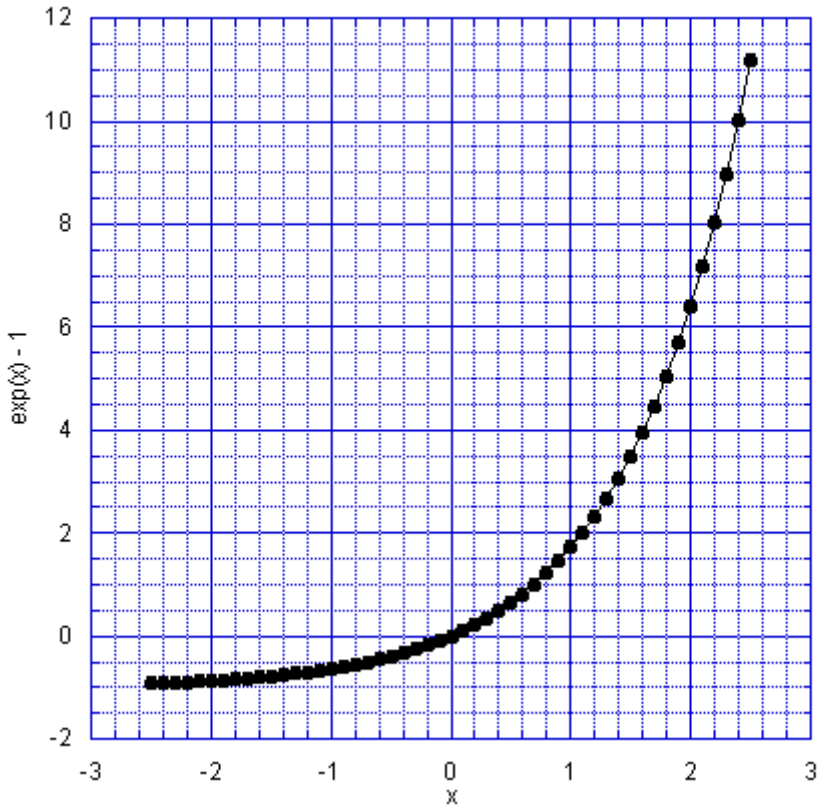

Figure 3. Current versus voltage in a p-n diode (Ebers-Moll formula).

As we shall show below, the DC signal output is proportional to the square of the electric field at the diode, by the following argument. A well-made *pn* junction diode has a current-voltage relationship given by the Ebers-Moll formula:

$$i(t) = i_0[\exp(ev(t)/kT) - 1] \tag{26}$$

where k is the Boltzmann constant,[15] i_0 is the asymptotic reverse current in the diode, and $v(t) = v_0 \cos(\omega t)$ is the voltage across the diode, which is oscillating at the microwave frequency. Ordinarily the argument of the exponential is small compared to 1, so we may expand this expression in a power series:

[15] At room temperature, kT/e = 0.025 volts.

$$i(t) = i_0[(ev(t)/kT) + (1/2)(ev(t)/kT)^2 + \cdots] \quad (27)$$

Recalling that $v(t)$ is oscillating at roughly 10 GHz, and that our detector is measuring the DC, or average value of i, the first term vanishes, and, using $<\cos^2 \omega t>=1/2$,

$$<i(t)> \approx (i_0/2)<(ev(t)/kT)^2> = (i_0/4)(ev_0/kT)^2 . \quad (28)$$

Thus the diode current is proportional to the average of the square of the incident microwave voltage, hence proportional to the incident power.

PROCEDURE

Preliminaries: The first step is to turn on the power strip on the desktop. This supplies power to a cooling fan for the klystron.

CAUTION: THE HIGH VOLTAGE LEADS OF THE KLYSTRON ARE PARTIALLY EXPOSED AT THE KLYSTRON. BE CAREFUL TO NOT TOUCH THE EXPOSED LEADS WITH YOUR HAND OR WITH A CONDUCTING TOOL.

Klystron tuning: The goal of this section is to tune the klystron oscillator so that it oscillates at the resonant frequency of the sample chamber. First, the klystron *cavity* must be mechanically tuned so that its resonant frequency is centered at the frequency of the sample chamber. Then, the precise klystron frequency is set by the *reflector voltage*, which should be in the neighborhood of 200 volts.

1. Connect channel 1 of the oscilloscope to the output of the crystal detector. The sensitivity should be about 200 mV/cm.
2. Connect the BK signal generator to channel 2 of the oscilloscope and set the signal generator to triangle wave at about 1 kHz. The scope sensitivity should be 5 V/cm.
3. Also connect the BK signal generator to EXT. MOD. on the klystron power supply. Be mindful of the *ground* tab on the banana connector.
4. Set the BEAM VOLTS dial to 300.
5. Set the REFL. VOLTS dial to 150.
6. Turn on the klystron cooling fan.
7. Switch the klystron power supply ON. This activates the klystron filament.
8. Wait 2 minutes for the klystron filament to warm up.
9. Turn REFL. RANGE dial to 0-300 setting. This applies a voltage to the klystron reflector.
10. Set the MODULATION dial to CW. This will apply an anode voltage to the klystron, resulting in microwave emission.
11. Set the calibrated microwave attenuator in the variable reactance arm to maximum attenuation; *i.e.* 50 dB. The attenuator will then absorb virtually all of the incident power in that arm.

12. Vary the reflector voltage (REFL. VOLTS) between 0 and 300 volts by hand and observe the klystron modes as a function of reflector voltage. Then set the reflector voltage near the peak of one of the modes.
13. Turn the MODULATION dial to EXT. This allows the externally applied signal from the BK signal generator to modulate the reflector voltage. With the BK signal generator at maximum voltage, the crystal output should look like Figure 4, when the klystron cavity, the reflector voltage, the modulation amplitude, and the sample tuning short are properly set. This will be accomplished by the procedure given below.

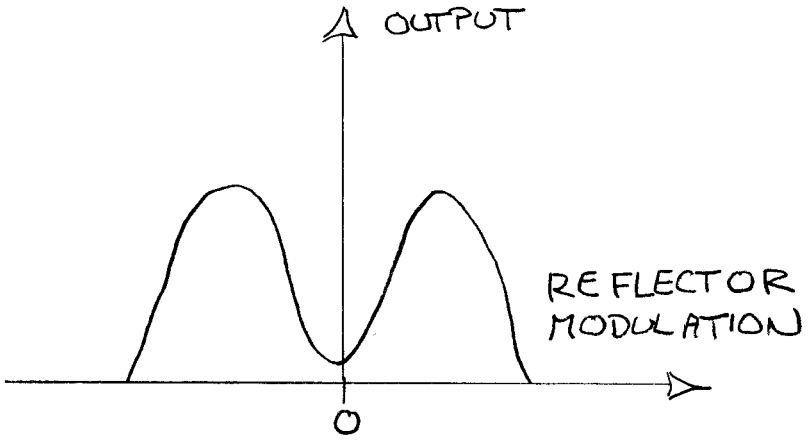

Figure 4. Crystal output as a function of reflector modulation when the klystron cavity and the reflector voltage are set properly. The klystron cavity is first tuned to put the sample dip into the center of the output peak; and the klystron voltage is then set so that the dip occurs at 0 reflector modulation.

Here is what is happening: As the reflector voltage sweeps over its full range, the klystron oscillator comes to life and oscillates with a frequency that increases as the magnitude of the reflector voltage increases. This is because the bunch spacing in the klystron beam becomes progressively shorter as the reflector voltage is increased. However, the klystron will only oscillate when the electron bunch frequency is near the resonant frequency of the klystron cavity, which in turn is determined by the internal dimensions of the cavity, tunable with the tuning screw on the klystron.

The dip in the klystron peak is the resonant absorption of the sample cavity. Since the *Q* of the sample cavity is somewhat higher than the *Q* of the klystron, the dip is fairly well resolved within the positive peak.

To achieve the proper tuning, perform the following steps:

1. Mechanically match the klystron cavity resonant frequency to the center of the fixed sample chamber resonant frequency. This is accomplished by adjusting the tuning screw on the klystron until the sample chamber “dip” is centered on the klystron peak.

2. Now adjust the reflector voltage until the center of the preceding "dipped peak" falls at 0 reflector modulation voltage (as observed on channel 2, which is the output of the BK signal generator). You are now very close to the final tuning.
3. Now reduce the modulation voltage at the BK signal generator by about a factor of two, and repeat step 2.
4. Keep repeating steps 1-3 until the sweep amplitude is zero. The reflector voltage, the klystron cavity, and the sample cavity are now tuned to the same frequency. Note that you will eventually need to pull out the BK signal generator knob to put it in low amplitude mode.
5. Now switch the MODULATION knob to CW. This will ensure that the reflector is no longer modulating the signal.

To measure the resonant frequency of the sample cavity, repeat steps 1 and 2 above. Then connect channel 2 of the oscilloscope to the wavemeter crystal. (The wavemeter is an accurately calibrated, adjustable resonant cavity). Adjust the knob of the wavemeter until a sharp dip appears at the center of the "dipped peak." You may now read out the resonant frequency to high precision.

Now adjust the phase and the amplitude of the signal reflected from the bridge circuit (the attenuator and the phase shifter) so that the reflected signal exactly cancels the residual signal from the sample chamber. Once you have tuned the bridge to exactly null the sample signal you need to "spoil" the tune by detuning the attenuator by about 3 dB away from its null setting. This is because the detector is sensitive to the *curvature* of the diode response curve at the operating point.

You are now ready to turn on the magnet. To do this, turn on the magnet power supply, and simultaneously adjust the coarse and fine current control knobs to a current of about 3.4 Amperes.

Meanwhile, you may turn on the Hall probe power supply, and measure the magnetic field. Be sure that the Hall sensor plane is perpendicular to the magnetic field.

If you slowly by hand adjust the current in the magnet, you will see the resonance! By carefully sweeping the current by hand, you may set the field to maximum absorption, and thus calculate g using equation (23).

Magnetic Sweep: The final step is to sweep the magnet current with a slow triangular waveform. This is accomplished by connecting the BK sweep generator to the magnet power supply and to channel 2 of the oscilloscope. (A good choice of frequency would be about 2 Hz.) You should be able to observe the resonance waveform. To improve the signal and suppress the noise, you might try the signal averaging capability of the oscilloscope, by setting Average in the Acquire menu. Why does the resonance appear at a different current going up, as compared to going down? Once you have a nice waveform you should download it to a flash drive for further analysis.

Phase-sensitive detection: You will notice that the signal appears on top of a background. There is a very clever and well-established method for dramatically reducing the background noise, known variously as *phase-sensitive* detection, *synchronous* detection, and *lock-in* detection. With this technique, one superimposes a tiny sinusoidal current at, say, 1,000 Hz, on top of the normal sweep current.[16] One then observes the variation of the output signal at the same frequency (*e.g.* 1 kHz) within a narrow bandwidth, determined by the averaging time. (When you do the complete analysis, you discover that the output signal is proportional to the derivative, with respect to the magnet current, of the original signal). This method rejects all noise not falling within this narrow bandwidth.

The setup is relatively straightforward.

1. Connect the 1 kHz sinusoidal output of the lock-in amplifier to the Radio Shack audio amplifier, and connect the output of the audio amplifier to the sweep coils of the magnet.
2. Connect the crystal detector to the input of the lock-in amplifier.
3. Connect the output of the lock-in amplifier to channel 1 of the oscilloscope.
4. The settings of the lock-in amplifier should be: Time constant, 30 ms.; sensitivity, 10 mV.

Presto! You will see a dramatic improvement in the signal-to-noise ratio, at the expense of outputting the derivative of the signal.

ANALYSIS

From your measurements of the resonant frequency and of the magnetic field, determine the *g*-factor of the electron for the DPPH signal. Compare to the established value, $g = 2.0036$. You should include in your report the plots of signal versus magnet current, with an estimate of the hysteresis effects in the magnet.

FURTHER QUESTIONS AND MEASUREMENTS

1. In your own words, briefly describe how the following microwave components work, and their properties: a) reflex klystron, b) isolator, c) wavemeter, d) magic tee, e) attenuator, f) diode detector.

2. With the wavemeter, measure the range of frequencies over which the klystron oscillates. Similarly, estimate the *Q* of the wavemeter and of the sample cavity.

3. The waveguide internal dimensions are 0.400″ x 0.900″. Calculate the five lowest cutoff frequencies.

4. The internal dimensions of the sample resonant cavity are 0.400″ x 0.900″ x 1.543″. What are the six lowest resonant frequencies of the cavity, assuming one can neglect the sample opening?

[16] By "tiny," we mean small enough so that the resulting sinusoidal magnetic field variation is small in comparison to the "width" of the signal.

APPENDIX

At first glance, one might expect that the instrument would be most sensitive when, off resonance, the microwave bridge is perfectly balanced. This way, one can amplify the signal as much as one pleases, since the "background" signal has been eliminated. This is almost, but not quite, correct. Recall from equation (28) that the D.C. signal that one measures, for an incident microwave voltage across the detector diode, is

$$< i(t) > \approx (i_0 / 2) < (ev(t) / kT)^2 > = (i_0 / 4)(ev_0 / kT)^2 \tag{29}$$

If we take Δv to be the change in voltage amplitude at the detector caused by absorption, and Δi to be the corresponding change in detector current, it follows that

$$\begin{aligned} &< i + \Delta i > \approx (i_0 / 4)(e(v_0 + \Delta v) / kT)^2 \\ &< i + \Delta i > - < i > \approx (i_0 / 4)(e^2(2v_0 \Delta v + (\Delta v)^2) / k^2 T^2) \end{aligned} \tag{30}$$

To first order, the change in current is proportional to v_0, the "unbalanced" voltage! Thus, to the extent that we can electronically subtract the baseline average current, we gain in signal by deliberately unbalancing the bridge.

REFERENCES

General references:

A. C. Melissinos, *Experiments in Modern Physics*. New York, Academic Press, 1966). Note that Melissinos has the sample situated in the waveguide but not in a resonant cavity.

Microwave Instrumentation:

T. H. Wilmshurst, *Electron Spin Resonance Spectrometers*. Plenum Press, 1968.

Edward L. Ginzton, *Microwave Measurements*. McGraw-Hill Book Company (1957).

Carol G. Montgomery, *Techniques of Microwave Measurements*. McGraw-Hill, 1947.

Simon Ramo, John Whinnery, Theodore van Duzer, *Fields and Waves in Modern Communications.* John Wiley and Sons, 1984.

Electron Spin Resonance; Paramagnetism:

Richard P. Feynman, Robert B. Leighton, and Matthew Sands, *The Feynman Lectures on Physics, vol. II.* Addison-Wesley, 1964.

G. E. Pake, *Paramagnetic Resonance*. W. A. Benjamin, 1962.

Charles P. Poole, *Electron Spin Resonance*. John Wiley, 1967 and 1983.

GAMMA RAY SPECTROSCOPY

LABORATORY OBJECTIVES

The objective of this experiment is 1) to measure the gamma-ray emission lines from four radioactive nuclei, and 2) to measure the absorption coefficient of gamma rays from various absorbers. You will learn the fundamentals of the interaction of radiation with matter; how a scintillator and photomultiplier work; and how a multichannel analyzer works.

INTRODUCTION

As described in the Appendix at the end of this manual, gamma rays and x-rays are synonymous. X-rays were discovered by Roentgen in 1895 as resulting from the collisions of energetic electrons with matter. Gamma rays were discovered by Villard[17] in 1900 as 'emanations' emitted by some unstable nuclei. Their equivalence was settled by Andrade and Rutherford[18] in 1914 when they successfully diffracted gamma rays, of nuclear origin, from crystals.

PHYSICS

Nuclear decay can happen through many channels, too numerous to describe in this manual. For details, consult any textbook on modern physics or on nuclear physics; the classic is the book by Evans.[19] We are interested in decay processes that result in the emission of mono-energetic gamma rays, either directly by the nucleus, or by secondary processes resulting from the nuclear decay, involving atomic electrons. The following section discusses the four isotopes that we will be using in this lab.

Cesium-137: ^{137}Cs has a half life of 30.17 years. It decays into the metastable state of ^{137m}Ba by *beta decay* (electron and antineutrino emission). ^{137m}Ba then decays with a half life of 133 seconds via the electric dipole transition, resulting in the stable isotope ^{137}Ba. This latter transition is accompanied by the emission of a 662 keV gamma ray. The decay chain is summarized below:

$$^{137}\mathrm{Cs} \rightarrow {}^{137m}\mathrm{Ba} + e^- + \bar{\nu}_e$$

$$^{137m}\mathrm{Ba} \rightarrow {}^{137}\mathrm{Ba} + \gamma\ (662\ \mathrm{keV})$$

Thus a ^{137}Cs sample is characterized by the emission of an electron (beta-ray), an antineutrino, and a gamma ray. For our sealed sources, the window is thin enough on the top (label) side that one can observe the broad spectrum electrons. The underside of the sealed source is thick enough to absorb the electrons, but thin enough to allow the passage of the gamma rays.

For the subsequent reaction, the emerging gamma ray can be photoelectrically absorbed by a barium K-shell electron, resulting in a fast photoelectron and a barium K-shell fluorescence x-ray of energy 32 keV. This latter photon will show up as a low-energy peak in your spectrum, and will be useful for calibration.

---

[17] P. Villard, *Comptes Rendus* **130**, 1010, 1178 (1900).
[18] E. Rutherford and E. N. C. Andrade, *Phil. Mag*. **27**, 854 (1914).
[19] R. D. Evans, *The Atomic Nucleus*, McGraw-Hill Book Company, 1955.

Owing to the short half life of ^{137}Cs, it does not occur naturally, but is a by-product of nuclear reactions in nuclear reactors and nuclear weapons. Unsealed sources of Cesium-137 are unhealthy because organisms mistake it for sodium, and readily take it up via ingestion.

Barium-133: ^{133}Ba decays by *electron capture*. That is, the nucleus absorbs a nearby K-shell electron, resulting in an excited ^{133}Cs' nucleus and an electron neutrino. The excited ^{133}Cs' then decays to the stable ^{133}Cs via the emission of two successive gamma rays. The reactions are as follows:

$$^{133}\text{Ba} + e^- \rightarrow {}^{133}\text{Cs}' + \nu_e$$
$$^{133}\text{Cs}' \rightarrow {}^{133}\text{Cs}'' + \gamma\ (81\ \text{keV})$$
$$^{133}\text{Cs}'' \rightarrow {}^{133}\text{Cs} + \gamma\ (356\ \text{keV})$$

For the first reaction, the capture of a K-shell electron results in a ^{133}Cs' with a missing K-shell electron. This electron shell is usually filled with an L-shell electron, resulting mostly in the emission of Cs K_α radiation (31 keV).

Notice the odd fact that ^{137}Cs → ^{137}Ba (electron emission) but ^{133}Ba → ^{133}Cs (electron capture). This follows the general pattern of neutron-rich nuclei tending to decay by beta decay (electron *emission*), and electron-poor nuclei tending to decay by electron *capture*. These two reactions can be symbolically represented by the "inverse" reactions

$$n \rightarrow p + e\text{-} + \bar{\nu}_e$$
$$p + e^- \rightarrow n + \nu_e$$

Sodium-22: ^{22}Na decays via two possible chains: *positron emission*, and by *electron capture* (as with ^{133}Ba). The positron emission reaction is

$$^{22}\text{Na} \rightarrow {}^{22}\text{Ne} + e^+ + \nu_e$$

This reaction is very interesting because the positron ultimately comes to rest and meets an electron, and both are annihilated into two back-to-back gamma rays, each with 511 keV energy:

$$e^+ + e^- \rightarrow \gamma + \gamma$$

The second possibility is *electron capture*, followed by two successive gamma decays:

$$^{22}\text{Na} + e^- \rightarrow {}^{22}\text{Ne}' + \nu_e$$
$$^{22}\text{Ne}' \rightarrow {}^{22}\text{Ne}'' + \gamma\ (1274.5\ \text{keV})$$
$$^{22}\text{Ne}'' \rightarrow {}^{22}\text{Ne} + \gamma\ (99.9\ \text{keV})$$

As with ^{133}Ba, the ^{22}Ne atom is left with a K-shell vacancy. When this vacancy is filled, a 0.9 keV K_α x-ray is emitted. the x-ray energy, however, is way too low to be observed with our detector.

Cobalt-60: ^{60}Co decays eventually to ^{60}Ni through a chain of three reactions, beginning with beta-decay:

$$^{60}\text{Co} \rightarrow {}^{60}\text{Ni}' + e^- + \bar{\nu}_e$$
$$^{60}\text{Ni}' \rightarrow {}^{60}\text{Ni}'' + \gamma\ (1173.2\ \text{keV})$$
$$^{60}\text{Ni}'' \rightarrow {}^{60}\text{Ni} + \gamma\ (1332.5\ \text{keV})$$

As with ^{137}Cs, the ^{60}Ni may be photoionized by one of the outgoing γ-rays, leading to a ^{60}Ni K-shell vacancy. When this vacancy is filled, usually by an L-shell electron, a 7.5 keV x-ray is emitted. As before, this x-ray energy is way too low to be observed by our detector.

ABSORPTION AND SCATTERING

There are three important physical processes that remove photons from an incident beam: elastic scattering by the atoms or by the lattice; Compton scattering by atomic electrons; and photoelectric absorption. These processes are discussed in detail in the Appendix at the end of this manual.

EXPERIMENTAL METHOD

Gamma rays originate with the disintegration of some radioactive nuclei. These gamma rays are highly monochromatic. As a consequence their presence is exhibited as peaks in the energy absorbed by detectors sensitive to individual quanta.

The detector is a sodium iodide crystal coupled to a photomultiplier, it is described in greater detail in the appendix to this manual. The amplitude of the output pulses of the photomultiplier are accurately given by a linear function of the gamma-ray energy. The high voltage on the photomultiplier tube can be monitored by the test point on the tube base via a 1000:1 voltage divider, and the voltage can be adjusted by turning the potentiometer, also on the tube base.

The distribution of pulse amplitudes is displayed on the computer screen as a histogram. Each pulse is assigned a channel number, which is a linear function of the pulse amplitude. The horizontal axis of the display is the channel number, and the vertical axis is the number of events in each channel.

PROCEDURE

Spectroscopy. Before taking spectra you will need to know how to calibrate the multichannel analyzer. Since the pulse amplitude is a linear function of the gamma-ray energy, there will be a one-to-one correspondence between channel number and gamma-ray energy. If you only have one feature in the spectrum that you can identify, you may do a one-point calibration, which implicitly assumes that channel 0 corresponds to 0 energy. (The assumption of zero offset). If you have two identified features separated by a large energy difference, as in the case of ^{137}Cs, you may do a 2-point calibration.

Collect gamma-ray spectra with the ^{137}Cs source, and do a 2-point calibration. Then collect gamma-ray spectra from the ^{60}Co source, the ^{133}Ba source, and from the ^{22}Na source.

In all cases, adjust the detector height above the sample to keep the dead time below 10%. Identify peak positions and compare them with the published results.

Photomultiplier response. Using a single gamma-ray line, measure the pulse height spectrum for a wide range of photomultiplier voltages, and plot the peak position versus voltage on a log-log plot. From this plot determine the approximate number of dynodes in the photomultiplier (See Appendix 2 for details).

Absorption. Measure the total cross-section in cm^2 of graphite, aluminum, and lead over a wide range of gamma-ray energies, using the isotopes provided. The best measure of the density of the material is made by weighing the sample and by measuring the two large dimensions.

ANALYSIS

Spectroscopy. Identify all of the spectral features that you observe with each element.

Dead Time. For a sample that has a high count rate, measure a line energy as a function of dead time by adjusting the detector height. Interpret your result.

Absorption. From the appropriate plots, determine the mass absorption coefficient for gamma rays in lead, graphite, and aluminum. Compare your results with the tabulated values.

ADDITIONAL QUESTIONS

1. Using the CRC Handbook or other sources, tabulate the expected gamma-ray energies from the four isotopes used in this experiment.
2. Why might you expect the gain of a photomultiplier to follow a power law expression?
3. If you were to improve the geometry of this experiment, how would you minimize the effect of Compton scattering?

REFERENCES

R. D. Evans, *The Atomic Nucleus.* (New York, McGraw Hill, 1955).
David R. Lide, ed. *Handbook of Chemistry and Physics*. (CRC Press).
X-Ray Data booklet, http://xdb.lbl.gov.

APPENDIX 1: PHOTOMULTIPLIER GAIN

A photomultiplier tube consists of 10-12 electrodes, arranged in a "Venetian blind" configuration, within a vacuum tube. These electrodes are known as "dynodes." By means of a resistive voltage divider, each dynode is about $v = 100$ volts more positive than the preceding dynode. The last dynode is called the anode, and it is where the final charge is collected.

A pulse of n electrons emerging from the photocathode will be attracted to the first dynode. On average, each of these electrons will generate g secondary electrons in colliding with the next dynode. Typically, g~2-4. In other words, the first dynode will receive n electrons and emit ng electrons; the second dynode will receive ng electrons and emit ng^2

electrons, and so forth. Thus, if there are N dynodes, the total number of electrons falling on the final electrode (called the anode) will be ng^N.

The gain per stage, g, depends upon the accelerating voltage per stage, v. To a good approximation, g is proportional to the square root of the accelerating voltage in the operating region; *i.e.* $g(v)=kv^{1/2}$ where k is some constant. Since the accelerating voltage is set by a voltage divider, v is proportional to the overall tube voltage V; say $v = cV$ where c is another proportionality constant. Thus, we may write the final number of electrons as $ng^N = n(kv^{1/2})^N = n(kc^{1/2}V^{1/2})^N$. The final charge Q will be just the number of electrons, multiplied by the charge on the electron: $Q=en(kc^{1/2}V^{1/2})^N$.

With the assumptions given above, we see that $Q \propto V^{N/2}$. That is, the pulse height goes as a high power of the tube voltage. If you were to plot log Q versus log V, you would get roughly a straight line with slope $N/2$. Thus, at a high enough voltage, even a single photoelectron can give rise to an observable pulse at the anode. For example, if $g = 3$ and $N = 10$, the overall multiplication factor will be $3^5 \sim 243$. This is also why it is important to not run the tube at too high a voltage; giant pulses have deleterious effects upon the system. For one thing, residual gas in the tube (mainly helium, which can diffuse through the envelope) can be ionized by the photoelectrons, and give rise to giant, spurious, and intermittent pulses.

APPENDIX 2: ABSORPTION AND SCATTERING COEFFICIENTS

If a beam of gamma rays is incident upon an absorber, some of the gamma rays may be photoelectrically absorbed, Compton scattered, or elastically scattered. The intensity of the emerging beam is related to the intensity of the incident beam by the familiar Beer's law:

$$I = I_0 \exp(-nL\sigma_{tot}) \tag{31}$$

where n is the number of atoms per cm^3, L is the thickness of the absorber in cm, and σ_{tot} is the total cross section in cm^2. Note that some care needs to be taken with the geometry so that one minimizes detection of the scattered radiation. The product nL is given by

$$nL = \frac{N_{av}\rho}{A_{wt}} L = \frac{N_{av}}{A_{wt}} \rho L = \frac{N_{av}}{A_{wt}} \frac{M}{A} \tag{32}$$

Where $N_{av} = 6.023\text{x}10^{23}$ atoms/mole is Avogadro's number; A_{wt} is the atomic weight in grams per mole, ρ is the density in grams per cm^3, M is the mass of the sample, and A is the area of the sample in cm^2.

The total cross section is just the sum of the cross-sections for the three processes.

$$\sigma_{tot} = \sigma_{photo} + \sigma_{elastic} + \sigma_{compton} \tag{33}$$

The three separate cross-sections are each functions of energy. It turns out that the energy dependence of each cross section can be fit reasonably well by a ln-ln plot. For example,

$$\ln(\sigma_{photo}) = A_0^{photo} + A_1^{photo}(\ln E) + A_2^{photo}(\ln E)^2 + A_3^{photo}(\ln E)^3 \qquad (34)$$

In the following tables, we tabulate the coefficients for carbon, aluminum, and lead. Please note that the units of E are keV and the cross sections are in units of 10^{-24} cm. per atom.

COEFFICIENT	PHOTOELECTRIC	ELASTIC	COMPTON
A0	10.68790	3.108610	−0.982878
A1	−2.71400	−0.260580	1.466930
A2	−0.20053	−0.271974	−0.293743
A3	0.02072	0.013518	0.015600

Table 2. Absorption and scattering coefficients for Carbon.

COEFFICIENT	PHOTOELECTRIC	ELASTIC	COMPTON
A0	13.17380	4.519950	−0.439322
A1	−2.18203	0.140549	1.30867
A2	−0.25896	−0.352441	−0.211648
A3	0.022284	0.019369	0.00754

Table 3. Absorption and scattering coefficients for Aluminum

COEFFICIENT	PHOTOELECTRIC	ELASTIC	COMPTON
A0	8.63374	8.15996	0.182167
A1	3.69400	0.418031	1.54661
A2	−1.21312	−0.35233	−0.195793
A3	0.07746	0.01647	0.003907

Table 4. Absorption and scattering coefficients for Lead.

To make life a bit simpler, we have calculated the cross-sections for these three materials at an energy of 1000 keV (1 MeV) so that you can check your calculations. The units of cross section are 10^{-24} cm^2 per atom.

	PHOTOELECTRIC	ELASTIC	COMPTON
CARBON	2.042E−5	7.37E−4	1.318E+0
ALUMINUM	9.970E−4	7.14E−3	2.682E+0
LEAD	6.030E+0	7.15E−1	1.663E+1

Table 5. Cross-sections for carbon, aluminum, and lead at 1000 keV.

MILLIKAN OIL DROP EXPERIMENT

LABORATORY OBJECTIVES

The objective of this experiment is to measure the charge on the electron, using an apparatus similar to that used by Robert Millikan. Along the way, you will learn about Stokes' law, which yields the terminal velocity of a sphere in a viscous fluid.

INTRODUCTION

In the early twentieth century, estimates of the absolute charge of the electron were established, but Robert Millikan was the first to precisely measure the charge, by studying the rate of fall of charged oil drops in air.[20] For this work he won the Nobel Prize in 1923.

PHYSICS

Tiny oil drops emitted by an atomizer may be neutral, but often may contain one or more electrons. Thus, if an oil drop is sprayed into a volume with a uniform electric field, the droplet's fall may be increased, decreased, or even reversed by the electric field, depending upon the sign and the magnitude of the electric field. The droplet will ultimately move at a constant equilibrium speed, the *terminal velocity*, as a consequence of the three forces acting on it: the gravitational force $m\mathbf{g}$, the electric force $q\mathbf{E}$, and the viscous force $\mathbf{F} = -k\mathbf{v}$, where, for a sphere, $k = 6\pi a\eta_{eff}(a)$, $\eta_{eff}(a)$ is the effective viscosity of air, and a is the radius of the droplet.[21] The minus sign tells us that the force is always directed in opposition to the velocity. The effective viscosity departs from the macroscopic viscosity for values of the droplet radius approaching the mean free path of the air molecules. A first order expression for the effective viscosity, in terms of the tabulated viscosity η_0, is given by

$$\eta_{eff}(a) = \frac{\eta_0}{1 + b/\,pa} \tag{35}$$

Where b is the viscosity correction factor in N/m and p is the atmospheric pressure in N/m^2. Once the droplet reaches its terminal velocity,[22] the acceleration vanishes, so by Newton's second law the total force on the droplet is zero:

$$\boxed{m\mathbf{g} + q\mathbf{E} - k\mathbf{v} = 0 \text{ where } k = 6\pi a\eta_{eff}(a)} \tag{36}$$

We will use equation (36) both with and without an applied electric field to determine the charge on the electron.

For definiteness, let us define a coordinate system with the vertical axis as the y-axis and that the unit vector $\mathbf{e}_y$ is pointing *downward*; that m, g, η, and a are all positive constants; and that $E_y = +V/d$ where V is the voltage across the plates (positive if the upper plate is

[20] Robert A. Millikan, *Philosophical Magazine*, February, 1910.
[21] At the level of accuracy of this experiment, we may neglect the buoyant force of the air on the droplet.
[22] In this experiment, terminal velocity is reached in a few milliseconds.

positive with respect to the lower plate) and d is the (positive) distance between the plates. With this convention, $g_y = g = 9.80\ \text{ms}^{-2}$. We will make no a priori assumption about the sign of the charge of droplet, q, although in hindsight we know that for an excess of electrons on the droplet, $q < 0$.

Determination of the radius *a*: Using Stokes' law in the absence of an electric field, *i.e.* free fall, we can determine the radius of the droplet, by taking the y-component of equation (36) with no field applied:

$$\begin{aligned} & mg - 6\pi a\eta_{eff}(a)v_{y0} = 0 \\ \Rightarrow\ & \frac{4}{3}\pi a^3\rho g - 6\pi a\eta_{eff}(a)v_{y0} = 0 \\ \Rightarrow\ & a = \left(\frac{9\eta_{eff}(a)v_{y0}}{2g\rho}\right)^{1/2} \end{aligned} \tag{37}$$

We need now to insert equation (35), the expression for $\eta_{eff}(a)$:

$$a = \left(\frac{9\eta_0 v_{y0}}{2g\rho(1+b/\,pa)}\right)^{1/2} \tag{38}$$

If we square both sides of (38), we get a quadratic equation for a, whose solution is

$$a = \left[\frac{9\eta_0 v_{y0}}{2g\rho} + \left(\frac{b}{2p}\right)^2\right]^{1/2} - \left(\frac{b}{2p}\right) \tag{39}$$

We conclude that by measuring the speed of a falling droplet in the absence of an electric field, we can determine the radius a of the droplet.

Determination of *q*: By taking the y-component of equation (36) alternately in the absence, and then in the presence of an electric field, we get

$$\begin{aligned} & mg - kv_{y0} = 0 \qquad (V = 0) \\ & mg + q\frac{V}{d} - kv_{yE} = 0 \quad (V \neq 0) \end{aligned} \tag{40}$$

We can eliminate k, the viscosity coefficient, from these two equations, yielding

$$q = mg\frac{d}{V}\frac{v_{yE} - v_{y0}}{v_{y0}}, \text{ or}$$
$$q = \frac{4}{3}\pi a^3 \rho g \frac{d}{V}\frac{v_{yE} - v_{y0}}{v_{y0}} \tag{41}$$

Let's check the signs. For a very large and positive applied field and voltage (upper plate positive), we have $q \approx (mgd/V)(v_{yE}/v_{y0})$. We know that v_{y0} is greater than zero (the droplet falls in the absence of a field). So if q is negative, v_{yE} must also be negative (rising droplet). This squares with our understanding that in this circumstance a negatively charged droplet will be attracted to the positively charged upper plate.

For completeness, we incorporate into (41) the explicit expression for a:[23]

$$q = \frac{4}{3}\pi\rho g \frac{d}{V}\left\{\left[\frac{9\eta_0 v_{y0}}{2g\rho} + \left(\frac{b}{2p}\right)^2\right]^{1/2} - \left(\frac{b}{2p}\right)\right\}^3 \frac{v_{yE} - v_{y0}}{v_{y0}} \tag{42}$$

Thus, by measuring a by means of the free-fall velocity v_{y0}, we can then compute q from the velocity under the action of the electric field. Incidentally, to compare with the formulas in the PASCO manual, $v_f = v_{y0}$ because v_f is the field-free "falling velocity," and $v_r = -v_{yE}$ because v_r is the "rising velocity."

As an alternative to (42), we can derive an alternative expression for q that is sometimes more convenient. This is done by incorporating the original expression for a, equation (38) into (41):[24]

$$q = \frac{4}{3}\pi\rho g\left(\frac{9\eta_0 v_{y0}}{2g\rho(1 + b/pa)}\right)^{3/2}\frac{d}{V}\frac{v_{yE} - v_{y0}}{v_{y0}}$$
$$q = 18\pi d\left(\frac{\eta_0^3}{2g\rho}\right)^{1/2} \times \left(\frac{1}{(1 + b/pa)}\right)^{3/2} (v_{y0})^{1/2} \times \frac{1}{V}(v_{yE} - v_{y0}) \tag{43}$$

This expression is the product of three terms: the first term comprises instrument parameters and physical constants; the middle term is specific to a particular drop radius (determined from equation (39), which requires the field-free velocity v_{y0}), and the third term comprises measured velocities and the plate voltage. For this reason this expression is sometimes computationally useful if exhaustive studies are performed on a single drop with the variable charge.

[23] This is the same as the result presented on page 12 of the PASCO manual.
[24] Beware! The formula on the top of page 3 (equation 10) of the PASCO manual is expressed in esu units, and has some errors.

EXPERIMENTAL METHOD

Please refer to the PASCO manual for a description of the experimental method. Please note that we have installed a recording video camera, to enable one to record the motion of droplets and to analyze them off-line.

PROCEDURE

Please refer to the PASCO manual for a description of the experimental procedure.

ANALYSIS

For a given droplet, use equation (39) to determine the droplet radius a. Then use equation (41) to calculate the total charge on the droplet. Measure several different droplets, and, for a single droplet, several charges.

ADDITIONAL QUESTIONS

1. Calculate the ratio of the buoyant force to the gravitational force for an oil droplet.
2. Derive equation (39) from equation (38).

REFERENCES

A. C. Melissinos, **Experiments in Modern Physics.** (New York, Academic Press, 1966).
R. A. Millikan, **The Electron**. University of Chicago Press.

APPENDIX: GLOSSARY OF TERMS

Note: all quantities should be expressed in SI units

SYMBOL	VALUE	UNITS	DESCRIPTION
a		m	Droplet radius
b	8.20×10^{-3}	N/m	Viscosity correction factor
d		m	Separation of plates
g	9.80	m/s^2	Acceleration of gravity
p	1.013×10^5	N/m^2	Atmospheric pressure
q		C	Droplet charge
v_{y0}		m/s	Droplet downward velocity with no field
v_{yE}		m/s	Droplet downward velocity with field E
V		V	Voltage across the plates
η_0	1.824×10^{-5}	$N\text{-}s/m^2$	Viscosity of air, uncorrected for radius
$\eta_{eff}(a)$		$N\text{-}s/m^2$	Viscosity of air, corrected for radius
ρ	8.86×10^2	kg/m^3	Density of oil droplet

MUON PHYSICS

INTRODUCTION

This experiment is based upon an instrument designed by Thomas Coan and Jingbo Ye at Southern Methodist University in Dallas, Texas. The experiment will enable you to learn many of the basic techniques of experimental particle physics. This is possible because we have a free high energy physics lab: At sea level, we are bombarded by energetic (on average, 4 GeV) $\mu^{\pm}$ particles at a rate of about 170 particles per second per square meter. These particles have a mean lifetime in free space of about 2 μs, which we will determine to high accuracy.

Please carefully read the manual *Muon Physics* by Coan and Ye. (The manual can be found online at http://www.matphys.com/muon_manual.pdf) Then perform experiments 1-10 outlined on pages 31 and 32 of the manual. Afterwards, analyze your data according to the procedure below.

All of the programs that you will need are located in the folder muon lifetime. The data collection program is called muon, with self explanatory buttons. If you wish to pause to analyze the data using the built-in programs, you will need to enter the password muon. After you have finished taking data, press quit.

DATA ANALYSIS

Data retrieval: After you have collected a few days worth of data, and have quit the program, the data will be stored in a file named muon.data. This will be a huge file, because it will contain many events where a muon (or other charged particle) entered but then left the detector without decaying. So the first thing that you need to do is filter the data using the program sift. This program will output a new file (which you are free to name) which will only contain muon-like events; *i.e.* double pulses separated by 20 μsec or less. You may inspect the contents of this file using the utility program called notepad, which will be invoked if you double-click on the data file.

Data format: Each line of the sifted data will consist of two numbers: the pulse separation time in nanoseconds, and a date and time stamp. For our purposes, only the first number is relevant. You should read these numbers into whatever file you find appropriate; Excel is certainly a convenient and easy choice.

Data Binning: You should now bin the data in bins of width 0.1 - 1.0 μsec, for events with pulse separations between 0 and, say, 10 μsec. This will result in 10-100 bins of data.

Analysis: Let us suppose that the number of events in bin j will be d_j, with statistical variance $(d_j)^{1/2}$. Our goal is to find a function that best fits the number of events in each bin. For particle decay, the function would be

$$y(t_j) = A\exp(-t_j / \tau) + B \qquad (44)$$

Where t_j ($j = 1 \ldots N$) is the pulse separation associated with the center of bin j, τ is the muon lifetime, and B is a constant background arising from accidental double pulses.

For sound statistical reasons, we define our 'best' fit to be the values of A, B, and τ that minimize the sums of the squares of the discrepancies between our data and our fit, where the discrepancy is normalized for each bin to its statistical variance. The sum of the squares of the normalized discrepancies is called χ^2 (chi-squared) and is a key measure of the quality of the fit. The mathematical definition is as follows, where j is the bin index:

$$\chi^2 \equiv \sum_{j=1}^{N} \frac{(y_j - d_j)^2}{\sigma_j^2} = \sum_{j=1}^{N} \frac{(y_j - d_j)^2}{d_j} = \sum_{j=1}^{N} \left(\frac{y_j^2}{d_j} - 2y_j + d_j\right) \tag{45}$$

Nowadays it is straightforward to do a numerical minimization of this function over all three parameters A, B, and τ on a computer. (This is what we suggest you do). It is interesting to note that if you did not have access to this capability, it is possible to analytically solve for the best fit values of two of the parameters in terms of the third, reducing it to a one-dimensional problem that can more readily be solved by trial and error. The procedure is as follows. Inserting our trial function given in equation (44), we get

$$\chi^2 = \sum_{j=1}^{N} \left\{ \frac{(A\exp(-t_j/\tau) + B)^2}{d_j} - 2(A\exp(-t_j/\tau) + B) + d_j \right\} \tag{46}$$

Our job is now to minimize this sum by varying the values of A, B, and τ. That is, we wish to set

$$\frac{\partial \chi^2}{\partial A} = 0, \quad \frac{\partial \chi^2}{\partial B} = 0, \quad \frac{\partial \chi^2}{\partial \tau} = 0 \tag{47}$$

Since we have three equations in three unknowns, in principle the solution is unique. Unfortunately, because of the exponential, the equations are nonlinear in the parameters! However, it turns out that because our trial function is linear in A and in B, we can explicitly solve equations (47) for a given trial value of τ, and thus minimize χ^2. We can then manually adjust τ until χ^2 is further reduced. The math is as follows, where the sums are over the N bins:

$$\begin{aligned} \frac{\partial \chi^2}{\partial A} = 0 &\Rightarrow \sum \left[\frac{2}{d_j} [(A\exp(-t_j/\tau) + B)\exp(-t_j/\tau)] - 2\exp(-t_j/\tau) \right] = 0 \\ \frac{\partial \chi^2}{\partial B} = 0 &\Rightarrow \sum \left[\frac{2}{d_j} [A\exp(-t_j/\tau) + B] - 2 \right] = 0 \end{aligned} \tag{48}$$

A close inspection of these two equations tells us that they are two linear equations in two unknowns. Let us define the following six sums (recall τ is a trial number that we put in by hand):

$$N \equiv \sum 1 \quad \alpha \equiv \sum d_j \quad \beta \equiv \sum \exp(-t_j / \tau)$$
$$\gamma \equiv \sum \frac{1}{d_j} \quad \delta \equiv \sum \frac{\exp(-t_j / \tau)}{d_j} \quad \lambda \equiv \frac{\exp(-2t_j / \tau)}{d_j} \tag{49}$$

Then our two equations read

$$\frac{\partial \chi^2}{\partial A} = 0 \Rightarrow \lambda A + \delta B = \beta$$
$$\frac{\partial \chi^2}{\partial B} = 0 \Rightarrow \delta A + \gamma B = N \tag{50}$$

Presto! We can solve immediately for *A* and *B*:

$$A = \frac{\beta\gamma - N\delta}{\lambda\gamma - \delta^2} \quad B = \frac{N\lambda - \beta\delta}{\lambda\gamma - \delta^2} \tag{51}$$

Finally, we can calculate χ^2 by rewriting our expression (46):

$$\chi^2 = \lambda A^2 + 2\delta AB + \gamma B^2 - 2\beta A - 2NB + \alpha \tag{52}$$

In summary:

1. Pick a trial value of τ, say 2 μs.
2. Evaluate the sums in equation (49).
3. Evaluate the coefficients *A* and *B* in equation (51).
4. Evaluate χ^2 from equation (52).
5. Vary τ by hand until χ^2 is minimized.

Experimental errors: The value of χ^2 resulting from the optimization of the three parameters carries valuable information about the quality of the data and the appropriateness of the fitting function, sometimes called the *goodness of fit*. χ^2 should be roughly equal to *v*, the number of *degrees of freedom* in the experiment. For our experiment, *v* is equal to the number of bins, *N*, minus the number of free parameters (3). For an experiment with measurements characterized by accurate statistical uncertainties, and for which the fitting function is appropriate, χ^2 should fall roughly in the range

$$\nu - \sqrt{2\nu} \le \chi^2 \le \nu + \sqrt{2\nu} \quad \text{for} \quad \nu \ge 30 \tag{53}$$

That is, if we were to repeat the entire experiment a large number of times, χ^2 should roughly obey a normal distribution and fall within the range given above.[25] If χ^2 falls well on the low side of this range, it means that we have overestimated the individual

[25] This statement should only be used as a rough guide, and fails for low values of *v*. More precise formulations of the "chisquared function for *v* degrees of freedom" that are correct for all values of *v* can be found in textbooks on statistics.

data variances, so the fit looks artificially good. On the other hand, if χ^2 falls well beyond the high side of this range, it means that we have either underestimated the individual data variances, or that we have systematic errors that are not accounted for, or that the fitting function was not appropriate for the experiment.

The χ^2 minimization program that you use to obtain the fit parameters should also return errors on the parameters (perhaps in the form of an error matrix). Use these errors and the χ^2 value discussed in the introductory lectures to evaluate the goodness of fit and the uncertainty in the muon lifetime.

Final Observation: Using the methods of Baysean statistics, one can calculate the most probable value of τ by the very simple formula:

$$\tau = < t_i > \tag{54}$$

That is, the "most probable value" of the physical lifetime is just the average of all of the individual lifetimes. This is why τ is sometimes called the "mean lifetime." If you have time, try calculating τ this way. Unfortunately, since there is a significant background to our data, arising from "accidental" double pulses, the value will not correspond exactly to the better value that you calculated above. However, for very small data sets, for which binning the data is meaningless, this method gives surprisingly accurate values. So if you have time, try calculating the mean lifetime this way.

NONLINEAR DYNAMICS AND CHAOS

LABORATORY OBJECTIVES

In this experiment you will observe the transition from deterministic response to chaotic response in a simple 3-component nonlinear circuit driven by a sinusoidal oscillator. You will write the differential equations governing the response of the circuit, and you will observe period doubling and tripling, and eventually the chaotic behavior.

INTRODUCTION

Much of the history of physics before the 1960's was reductive in nature; that is, physicists sought ever more fundamental and deeper principles governing the physical universe. Moreover, prior to the advent of quantum mechanics, it was hoped that the physical world could be reduced to "clockwork." It was hoped that the knowledge of physical laws, and the precise knowledge of the initial conditions of particles in the universe would be enough to predict, in principle, the evolution of the universe.

We have known since the 1920's that quantum mechanics completely rules out this possibility, because of the uncertainty principle. However, we now know that even if the world were governed by classical principles, our ability to predict the future for even very simple real systems is severely limited. Most real systems are governed by nonlinear differential equations, and it happens that the solutions to these equations are invariably extremely sensitive to initial conditions. Roughly speaking, the time horizon over which we can predict the evolution of a system is proportional to the logarithm of the certainty with which we can establish the initial conditions. The most familiar everyday example is the weather: We have vastly more detailed information today about the temperature, humidity, wind velocity, and so forth, around the globe, but our ability to predict the weather even a day in advance is scarcely better than it was five decades ago. This sensitivity to initial conditions is the hallmark of what is now known as *chaos*.

PHYSICS

By now you should be familiar with the fact that the laws of physics are frequently cast as relations among rates of change (temporal and spatial) of various physical quantities. Here are some important examples:

$$\begin{aligned} \mathbf{F} &= m\frac{d\mathbf{v}}{dt} \text{ (Newton's second law)} \\ v(t) &= L\frac{di(t)}{dt} \text{ (Voltage across an inductor)} \\ v(t) &= \frac{1}{C}\int i(t)dt \text{ (Voltage across a capacitor)} \end{aligned} \tag{55}$$

These are but a few of the many, many examples of differential relations in physics. Other prominent examples include Maxwell's equations; the Navier-Stokes equations of fluid flow; the Schrödinger equation (and its relativistic generalization, the Dirac equation); the Einstein field equations of the general theory of relativity; and so forth.

In formulating a physical phenomenon, one often assembles a set of differential equations. These equations are said to be *linear* if linear combinations of solutions to the equations are also solutions. That is, if $y_1(t)$ and $y_2(t)$ are solutions to a time-dependent differential equation, then $Ay_1(t)+By_2(t)$ is also a solution, for arbitrary constants A and B. In other words, the solutions obey the *principle of superposition*.

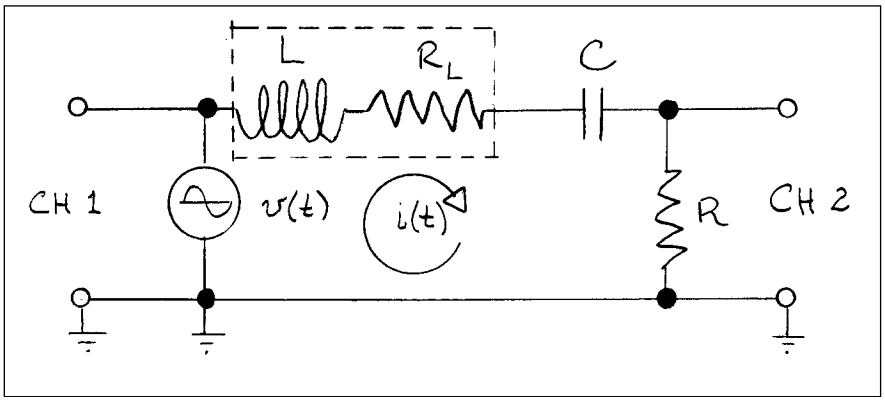

Figure 5. The LRC series circuit.

As an example of a linear set of equations, consider an L-C-R circuit driven by a sinusoidal voltage source, as shown in Figure 5. For this example, assume that $R_T = R+R_L$ is the total series resistance, consisting of R, the sensing resistor, and R_L, the series resistance of the inductor.

$$L\frac{di}{dt}+\frac{1}{C}\int i dt + R_T i = V_0 \sin \omega t \tag{56}$$

By differentiating once in time, and dividing by L, one obtains

$$\frac{d^2 i}{dt^2}+\frac{R_T}{L}\frac{di}{dt}+\frac{1}{LC}i = \omega \frac{V_0}{L}\cos \omega t \tag{57}$$

Equation (57), which is linear, has well-known solutions which can be divided into the transient response due to the turning on of the driving signal at $t = 0$, and the long-term response, insensitive to the initial conditions and valid after the transients have died down. A similar equation describes the motion of a forced pendulum, oscillating through angles small compared to one radian.

It is convenient to write equation (57) with the symbols consolidated, by defining $\Gamma \equiv R_T / L$ and $\omega_0^2 \equiv 1/LC$:

$$\frac{d^2 i}{dt^2}+\Gamma\frac{di}{dt}+\omega_0^2 i = V_0 \frac{\omega}{L}\cos \omega t \tag{58}$$

After the transients have died down, the solution to equation (58), written in terms of the voltage across the sensing resistor *R*, is the following:[26]

$$i(t) = \frac{V_0 \omega / L}{\sqrt{(\omega_0^2 - \omega^2)^2 + \omega^2 \Gamma^2}} \sin(\omega t - \phi)$$

$$v_R(t) = Ri(t) = V_0 \frac{\omega R / L}{\sqrt{(\omega_0^2 - \omega^2)^2 + \omega^2 \Gamma^2}} \sin(\omega t - \phi) \qquad (59)$$

$$\text{where } \tan\phi = \frac{\omega^2 - \omega_0^2}{\omega \Gamma}$$

We thus see that the current in the circuit, and thus the voltage across the sensing resistor, oscillates at the same frequency as the driving voltage, but with an amplitude and phase dependence. At peak response (resonance), $\omega^2 = \omega_0^2$ and $\phi = 0$, and the voltage across the resistor is given by

$$v_R(t) = Ri(t) = V_0 (R / R_T) \sin(\omega t) \qquad (60)$$

In other words, at resonance the impressed voltage appears entirely across the sensing resistor (reduced by the factor R/R_T), with the voltages across the inductor and capacitor exactly canceling.

It is possible to show that the periodic long-term solutions of forced linear equations can only have frequencies that are equal to the driving frequency. Other frequencies, including harmonics and sub-harmonics, are disallowed. And, of course, the principle of superposition is strictly obeyed, by definition.

Equations not obeying the principle of superposition are said to be *nonlinear*. Solutions to such equations can be bizarre, exhibiting harmonics (integer multiples of the driving frequency), sub-harmonics (period doubling, tripling, etc.), chaos, and so forth. We will be studying a physical example of such a system, shown in Figure 6. This system closely resembles the LCR circuit described above, with a diode replacing the capacitor.

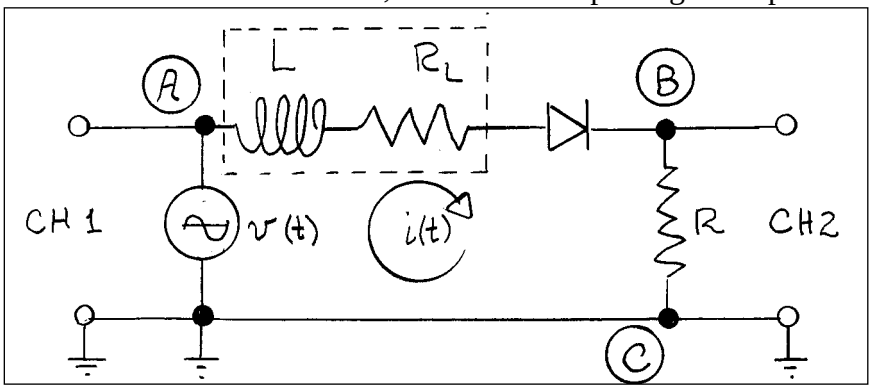

Figure 6. A diode in series with an inductor and resistor.

[26] *E.g.* Marion and Thorton, *Classical Dynamics of Particles and Fields.* Brooks Cole.

A diode, formed as a junction between p-type silicon and n-type silicon, is one of the most ubiquitous circuit elements in modern electronics. It is safe to say that there are of order 10^6 p-n junctions in a typical laptop computer! The static behavior of a p-n junction is extremely nonlinear: the current through the junction is related to the voltage by the following expression (the Ebers-Moll formula):

$$i = i_R[\exp(ev/kT) - 1] \tag{61}$$

In this expression, i_R is the reverse current (which depends upon the parameters of the specific device), e is the charge on the electron, k is Boltzmann's constant, and T is the temperature. At room temperature (294 K), kT/e = 0.025 volts. Notice that at small voltages,

$$v = \frac{i}{i_R}\frac{kT}{e} = 0.025\frac{i}{i_R} \tag{62}$$

Thus the p-n junction behaves, at low voltages, like a linear resistor of resistance R_d = .025/i_R.

The p-n junction also acts as a capacitor, with a capacitance that is a complicated function of the impressed voltage.[27] Most importantly, the capacitance is always present, whether the junction is reverse or forward biased. At very small bias voltages, there is a relatively constant capacitance arising from the width of the diode depletion layer. From this we conclude that the above circuit, at small excitation voltages, should exhibit identical behavior to the LCR circuit described above, provided that we can neglect the effect of the large parallel resistance R_d. At larger impressed voltages, the best model is that of an ideal diode (following the Ebers-Moll formula) in parallel with a voltage-dependent capacitance. This circuit is illustrated below, in Figure 7.

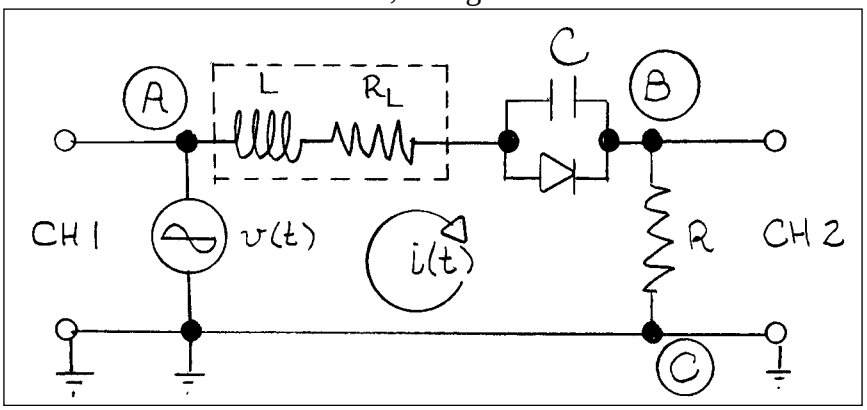

Figure 7. An inductor in series with a model of a real diode, replaced by an ideal (Ebers-Moll) diode in parallel with a voltage-dependent capacitance $C(v)$. A, B, and C indicate the test points on the box.

[27] S. M. Sze, *Semiconductor Devices: Physics and Technology*. John Wiley and Sons, 1985.

Now the fun begins. One can show that a system described by a second order (or higher) nonlinear differential equation that is forced by a periodic function can exhibit a wealth of phenomena that are absent in comparable linear equations. These phenomena include period doubling, bifurcation, and chaos. By chaos we mean that the time evolution of the system is exquisitely sensitive to the initial conditions, so that the exact long-term behavior of the system is unpredictable (like the weather, which has very similar properties, being governed by highly nonlinear equations).

EXPERIMENTAL METHOD

The first part of the experiment will be to explore the behavior of a linear series resonant circuit. You will excite the circuit with a sinusoidal voltage source, and observe the voltage across a resistor with an oscilloscope. The voltage across the resistor will be proportional to the current in the loop. Using the oscilloscope, you may also observe the Fourier transform of the output voltage, to determine the frequency spectrum.

In the second part of the experiment, you will drive the nonlinear circuit with a sinusoidal voltage of adjustable frequency and amplitude. In this circuit the inductance is 25 mH, the resistance is 3,300 Ohms, and the diode is 1N4004. The response of the circuit will be taken to be the voltage across the resistor; this voltage will serve as a proxy for the loop current, by Ohm's law.

PROCEDURE

For part 1 of the experiment, connect an 15 mH inductor, a 10 nF capacitor, and a 100 ohm resistor in series. Connect a signal generator to this loop, and monitor the output of the signal generator with channel 1 of the oscilloscope. Connect channel 2 of the oscilloscope to the resistor, bearing in mind that the oscilloscope inputs and the signal generator all have a common ground. Perform the following experiments:

1. Predict the resonant frequency of the circuit.
2. Adjust the signal generator to the actual resonant frequency of the circuit. What is the resonant frequency?
3. Make a series of about 10 measurements of the phase and amplitude voltage response of the circuit in the vicinity of the resonance, covering it fully. (Be sure to record the input voltage at each point. You should not assume that the signal generator puts out a load-independent voltage). Find values of ω_0 and Γ that best fit the data. From these data determine the intrinsic resistance of the inductor.

The second experiment is to study the *linear* behavior of the *nonlinear* circuit at low amplitudes. To do this, measure the amplitude and the phase of the loop current as a function of frequency at a driving voltage near the lowest setting of the signal generator, using the attenuated output (by pulling the amplitude knob out). (If you need further attenuation you may use the attenuator provided). You should observe a distinct resonance. From the resonant frequency and the known value of L, calculate the low-amplitude capacitance of the diode junction. Using the FFT (Fast Fourier Transform) function on the oscilloscope, verify that the response frequency is equal to the driving frequency.

Now raise the driving amplitude to a level where you observe other frequencies besides the fundamental frequency. In all, you should see four regions:

1. The linear region, where the output frequency is always equal to the input frequency,
2. The distortion region, where the output is a mildly distorted sine wave, with frequency components that are integer multiples of the fundamental;
3. The highly nonlinear region, where the output shows, in addition to the higher harmonics, sub harmonics of the fundamental. The signal is still steady.
4. The chaotic region, where higher harmonics and sub harmonics both occur, but the signal is unsteady.

ANALYSIS

With this oscilloscope you can capture both a waveform and its Fourier Transform. Capture a series of waves demonstrating regions 1-4. In particular, show a series of waveforms in region (4) that demonstrate that the response is not deterministic.

FURTHER QUESTIONS

Write down the system of differential equations that characterizes the circuit in Figure 7. What order is the equation?

CHUA CIRCUIT

You will find on an electronic breadboard the so-called Chua circuit.[28] This circuit consists of three energy storage devices; two capacitors and one inductor. These are connected to two operational amplifiers in a positive-feedback configuration. The two operational amplifiers simulate a negative resistance $N_R < 0$, such that $V = -I\left|N_R\right|$. Because there are three energy storage devices, the circuit has the ability to oscillate without any external driver, unlike the previous circuit. Not only does it oscillate, but for certain values of the feedback resistance *R*, the circuit can oscillate chaotically. This chaotic oscillation is best observed with an analog oscilloscope in x-y format.

You should observe the behavior of the circuit as you vary the feedback resistance *R*. You may gain a better understanding of what's going on by connecting the two signals to the two channels of the digital oscilloscope, and observing the two signals simultaneously.

REFERENCES

Steven H. Strogatz, *Nonlinear Dynamics and Chaos.* Perseus Book Publishing, 1994.
S. M. Sze, *Semiconductor Devices: Physics and Technology*. John Wiley & Sons, 1985.
Michael P. Kennedy, *IEEE Transactions on Circuits and Systems* **40**, 657 (1993).

[28] Michael P. Kennedy, IEEE Transactions on Circuits and Systems **40**, 657 (1993).

NUCLEAR MAGNETIC RESONANCE

In classical terms, the nucleus of an atom may be thought of as a spinning dipole magnet. As such, it possesses both angular momentum and a magnetic moment. Such a magnet will precess in an external magnetic field with a well-defined precession frequency. Fortunately, this classical precession phenomenon carries over mostly intact in a correct quantum mechanical treatment. The main difference is that the energy of a spinning magnet is quantized, so that a spin ½ particle, such as the proton, has only two distinct energy states, with spin pointed either parallel or anti-parallel to the magnetic field, and separated by an energy ΔE . The precession frequency ν is then given by $h\nu = \Delta E$.

In a macroscopic sample immersed in a static magnetic field, the nuclei will normally be in thermal equilibrium with the atoms in the sample. Since at room temperature the two energy states of a proton are much closer together than kT, in thermal equilibrium there will be only a slight excess of protons in the lower energy state, resulting in a slight overall magnetization of the sample. However, by applying a radio-frequency magnetic field at the precession frequency, higher energy states may be stimulated downward, resulting in equalizing the two populations, resulting in a non-equilibrium population distribution. Upon removal of the RF, this non-equilibrium state will decay back to equilibrium with a time constant called the *spin-lattice* relaxation time, or *longitudinal* relaxation time, T_1. (This terminology is used even in a liquid or gas, where there is no "lattice.") It is called the spin-lattice relaxation time, because it quantifies the irreversible thermal relaxation of the spins. It is called the longitudinal relaxation time because it quantifies the relaxation of the total spin in the direction of the external field (the longitudinal direction).

Using methods described below, it is possible, with the application of a radio frequency pulse, to rotate the net magnetization vector from the longitudinal direction (z-axis) to the plane perpendicular to the z-axis (x-y plane). The net magnetization vector will then rotate in the x-y plane at the Larmor frequency, given above. However, because there may be local magnetic fields within the molecular system, there may be dephasing of the net magnetization vector, resulting in an exponential decrease in the net transverse magnetization, with time constant defined as T_2. Thus, T_2 is called the *spin-spin* relaxation time, as well as called the *transverse* relaxation time. *T_2 is the time of most interest in molecular physics research, as it contains information about the electronic and molecular structure of the material T_1. The spin-lattice time constant, is of far less interest.*

Although T_2 is the time constant of most interest, it was hard to measure in the early days of NMR, because unavoidable tiny inhomogeneities in the externally applied magnetic field contributed to the dephasing. The main advantage of pulsed NMR is that the method cleverly cancels out the dephasing arising from the imperfect externally applied magnetic field, allowing one to make clean measurements of T_2.

EXPERIMENTS

Read carefully the sections from Feynman and from Melissinos. Also read *A Conceptual Tour of Teach-Spin's Pulsed NMR*, and pages 1-35 of *Pulsed Nuclear Magnetic Resonance Spectrometer*.

General Hints. The leftmost module in the instrument bay is the 15 MHz receiver. It is basically a tuned amplifier with an adjustable central frequency and gain. Ordinarily the gain should be adjusted to about 20% of the maximum value, to prevent overload distortion. The tuning frequency should be adjusted for maximum signal. The RF OUT connector gives you the amplified output of the amplifier; it should ordinarily be connected to the MIXER IN connector of the third module from the right. The DETECTOR OUT is basically the RF OUT, but with the 15 MHz signal averaged out. Thus, if $\text{RF OUT} = A\exp(-t/\tau)\cos(\omega t)$, then $\text{DETECTOR OUT} = A\exp(-t/\tau)$. It is customary to monitor DETECTOR OUT with channel 1 on the oscilloscope.

The MIXER OUT is the other important signal to monitor with the oscilloscope. Note that CW-RF OUT is the constant amplitude output of the 15 MHz oscillator.[29] The mixer multiplies CW-RF OUT by the detector RF OUT, and then averages out the 15 MHz oscillations. Symbolically,

$$\text{MIXER OUT} = <(\text{CW-RF OUT})(\text{RF OUT})> \tag{63}$$

Thus, if the oscillator output is $R\cos(\omega_1 t)$ and the RF OUT is $A\cos(\omega_2 t)\exp(-t/\tau)$, the time-filtered mixer output will be $(1/2)RA\exp(-t/\tau)\cos(\omega_1 - \omega_2)t$. The mixer output signal will exhibit beats if the oscillator ω_1 is not tuned precisely to the nuclear precession frequency ω_2.

Free Induction Decay (pp 29-31). In this experiment you will apply a single 90° pulse to the sample, which will rotate the magnetization into the x-y plane. To prepare a 90° pulse, observe the strength of the signal as the A-width is varied from 0 to 100%. The first maximum, around 20%, signifies a 90° pulse; and the subsequent minimum signifies a 180° pulse. You should be able to adjust the width all the way just past 450°.

The rotating magnetization will induce an oscillating signal in the detector at the precession frequency. The signal will diminish quickly with time, owing to the dephasing arising from the magnetic field inhomogeneities. From the time constant of the signal, and of the characteristic size of the sample, estimate the relative magnetic field gradient $(1/B)(dB/dx)$.

Spin-Lattice Relaxation Time T_1 (p. 32). As discussed earlier, T_1 is the irreversible thermal relaxation time between the spins and the lattice in which the spins are embedded. That is, if the main magnetic field could be turned on (or off) instantaneously, T_1 represents the time that it takes for the spins to adjust to their new magnetic environment.

---

[29] The abbreviation CW is an ancient radio shorthand for *Continuous Wave*.

The first, crude way to estimate T_1 is to repeat the free induction decay experiment above, but with a repetition frequency that prevents the spins from reaching equilibrium. This will give you a direct "feel" for the relaxation time.

The second, much more accurate way to measure T_1 is as follows:

1. Apply a 180° pulse to the sample (resulting in 0 signal, of course).
2. Wait a delay time *t*, using the DELAY TIME switches.
3. Apply a 90° pulse ("B") and measure the amplitude $A(t)$.
4. Repeat this experiment with different delay times *t*.

SETUP: Use the Free Induction Decay setup, but enable the second pulse by switching B on with 1 B pulse. To achieve a 90° B pulse, use the same method as with the 90° A pulse. Note that you can trigger the scope on the B pulse with the SYNCH switch, so that you always see the B pulse. Show that, for an exponential relaxation time T_1, the result should be

$$A(t) = A_0 \left| 2\exp(-t/T_1) - 1 \right| \tag{64}$$

Fitting this function will give you an accurate value for T_1.

Spin-Spin Relaxation Time T_2 (p. 34). Recall that with the free-induction decay experiment, we rotated the magnetization from the z-axis to the x-y plane by applying a 90° pulse. Owing to magnetic field inhomogeneities, the magnetization vector quickly dispersed and the signal dissipated far faster than T_2, the time that it would have dissipated in a perfectly homogeneous field. Fortunately, with clever pulsing techniques, we can "reverse" the dispersion arising from the inhomogeneities, so that they no longer spoil the signal. The three methods, in order of sophistication, are the Hahn two-pulse spin-echo method, the Carr-Purcell multiple pulse method, and the Meiboom-Gill multiple pulse method. These methods are closely related, and are discussed in the Appendix to this chapter.

Please measure T_2 for mineral oil with each of these methods.

REFERENCES

Feynman, Leighton, and Sands, *The Feynman Lectures on Physics*, Volume 1, pp 35-10 to 35-12. Addison Wesley, 1963.

Melissinos and Napolitano, *Experiments in Modern Physics*, 2nd Edition, pp 252-273. Academic Press, 2003.

Eric D. Black, *Nuclear Magnetic Resonance(NMR)*. California Institute of Technology.

Wolff-Reichert, *A Conceptual Tour of Teach-Spin's Pulsed NMR*. Teach-Spin, Inc.

Wolff-Reichert, *Pulsed Nuclear Magnetic Resonance Spectrometer*, Teach-Spin, Inc., 1997.

Thomas C Farrar and Edwin D. Becker, *Pulse and Fourier Transform NMR*, Academic Press, 1971.

APPENDIX

Hahn *vs.* Carr-Purcell *vs.* Meiboom-Gill

In this appendix we describe the pulse timing sequences associated with the Hahn method (two pulse spin echo), Carr-Purcell method (multiple pulse spin echo) and the Meiboom-Gill method (multiple pulse spin echo, with a twist).

Hahn. Erwin Hahn invented the two-pulse spin echo method.[30] The sequence is as follows:

1. Rotate spins 90 degrees about *y*-axis, going from *z*-axis to *x*-axis.
2. Coast for a time $\tau/2$.
3. Rotate spins 180 degrees about *y*-axis.
4. Coast for a time $\tau/2$. Echo appears at $t = \tau$; spins coincide on $-x$ axis.
5. Manually repeat steps 1-4 with various values of τ and record the echo amplitude as a function of τ.

In a series of experiments with increasing total delay time τ, the amplitude of the echo will decrease exponentially. This exponential time constant will be T_2, the spin-spin (or transverse) relaxation time. The method inherently cancels out effects due to inhomogeneities in the applied magnetic field, at least for motionless molecules (solids).

The drawback of this method is that molecules may not be stationary. Rather, their motions may cause them to diffuse sufficiently rapidly that the magnetic field homogeneities result in a shorter dephasing time than T_2. In order to correct for this diffusion, Carr and Purcell invented the multiple pulse spin echo.

Carr-Purcell. Carr-Purcell uses a multiple pulse sequence, starting out with the Hahn sequence.[31] The method is illustrated in Figure 8:

1. Rotate spins 90 degrees about *y*-axis, going from *z*-axis to $+x$-axis.
2. Coast for a time $\tau/2$.
3. Rotate spins 180 degrees about y-axis.
4. Coast for a time $\tau/2$. Echo then appears at $t = \tau$; spins coincide on $-x$ axis.
5. Coast for a time $\tau/2$.
6. Rotate spins 180 degrees about *y*-axis again.
7. Coast for a time $\tau/2$. Echo then appears at $t = 2\tau$; spins coincide on $+x$ axis.
8. Automatically continue with steps 2-7, indefinitely.

At times τ, 2τ, 3τ, 4τ,..., spin echoes appear, diminishing in amplitude exponentially with time constant T_2.[32] Thus, rather than having to conduct a sequence of measurements per Hahn, one sweep reveals the exponential attenuation of the amplitude. Moreover, For reasons beyond the scope of this manual, this method cancels, to first order, the effect of diffusion of the molecules in the inhomogeneous magnetic field.

---

[30] E. L. Hahn, *Phys. Rev*. **80**, 580 (1950)

[31] H. Y. Carr and E. M. Purcell, *Phys. Rev*. **94**, 630 (1954).

[32] Note that the first four steps of the Carr-Purcell sequence are identical to the first four steps of the original Hahn sequence.

The problem with this method is that can be very difficult to form an exact 180 degree pulse, so that the spins may wind up with a small z-component. The resulting error is cumulative, giving a value of T_2 that is shorter than the actual value. To circumvent this problem, Meiboom and Gill invented a slight variation on Carr-Purcell, avoiding this problem.

Meiboom-Gill. The M-G sequence is as follows,[33] and is depicted in Figure 8 (below).

1. Rotate spins 90 degrees about *y*-axis, going from *z*-axis to +*x*-axis.
2. Coast for a time $\tau/2$.
3. Rotate spins 180 degrees about *x*-axis (not the *y*-axis as in C-P).
4. Coast for a time $\tau/2$. Echo then appears at $t = \tau$; spins coincide on +*x* axis.
5. Coast for a time $\tau/2$.
6. Rotate spins 180 degrees about *x*-axis again.
7. Coast for a time $\tau/2$. Echo then appears at $t = 2\tau$; spins coincide on +*x* axis.
8. Automatically continue with steps 2-7, indefinitely.

As with Carr-Purcell, at times τ, 2τ, 3τ, 4τ,..., spin echoes appear, diminishing in amplitude exponentially with time constant T_2. As can be seen by comparing C-P with M-G, C-P always rotates spins about the *y*-axis; while, for M-G, once the spins are initially in the *x*-*y* plane, the rotations are performed about the *x*-axis. This method causes errors in the 180 degree pulse to cancel rather than accumulate.

Figure 8 (Below). A comparison of the Carr-Purcell sequence with the Meiboom-Gill sequence, shown in the rotating frame. The vector **A** represents spins slowly drifting counter clockwise, and the vector **B** represents spins drifting slowly clockwise.

[33] S. Meiboom and D. Gill, *Rev. Sci. Inst.* **29**, 688 (1958).

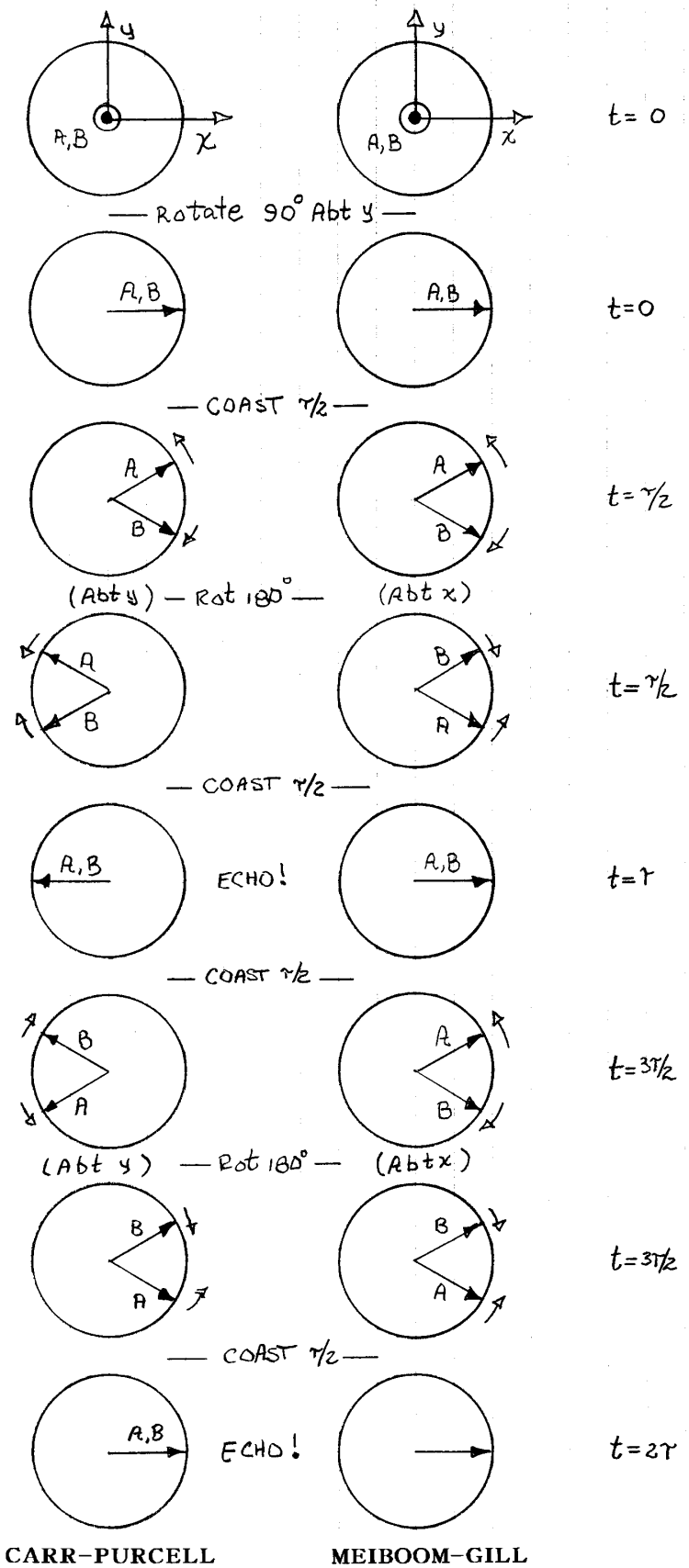
y
A,B
x
t= 0
— Rotate 90° Abt y —
t=0
— COAST τ/2 —
A
B
t= τ/2
(Abt y) — Rot 180° — (Abt x)
t= τ/2
— COAST τ/2 —
ECHO!
t=τ
— COAST τ/2 —
t=3τ/2
(Abt y) — Rot 180° — (Abtx)
t=3τ/2
— COAST τ/2 —
ECHO!
t=2τ
CARR–PURCELL
MEIBOOM–GILL

OPTICAL PUMPING

INTRODUCTION

The hydrogen atom, the simplest atom in the periodic table, exhibits an extremely rich optical spectrum when subjected to an external magnetic field. The ground electronic state ($n = 1$), as well as the excited electronic states, are split into sublevels by the magnetic field. These energy level splittings make themselves evident in the complex optical absorption and emission spectra of the atoms, known as the *Zeeman effect*. The energy level splittings also manifest themselves in the radio frequency absorption and emission spectra, involving transitions among sublevels that would be degenerate in the absence of a magnetic field. Finally, under certain circumstances, non-equilibrium populations can be established, which is the subject of this experiment, *i.e. optical pumping*.

Rubidium, along with the other alkali metals (lithium, sodium, potassium, cesium and francium) has an atomic spectrum very similar to atomic hydrogen. This is because each alkali atom consists of a rare-gas, inert, closed shell electron configuration, plus a single valence electron. Rubidium is convenient because it has a significant vapor pressure at modest temperatures, although similar studies have been performed on the other alkali metals, as well as on atomic hydrogen.

ENERGY LEVELS IN HYDROGEN-LIKE ATOMS

Figure 10 depicts the four categories of energy levels of a hydrogen-like atom (in this case rubidium) when it is immersed in a magnetic field. The respective energy levels are

1. Electronic structure (Coulomb force).
2. Electron spin-orbit fine structure (L-S coupling)
3. Nuclear spin interaction with electron's angular momentum (hyperfine structure).
4. Magnetic interaction with atom's total angular momentum (Zeeman effect).

Electronic Structure and spin-orbit structure. The three lowest *electronic* states ($n = 5$) of atomic rubidium are the $5S_{1/2}$, $5P_{1/2}$ and $5P_{3/2}$ states. The $5P_{1/2}$ and $5P_{3/2}$ states have transition wavelengths to the ground state $5S_{1/2}$ at 795 nm and 780 nm, respectively. Both of these orbital states (P) have orbital quantum number $l = 1$. The $P_{3/2}$ state has $j = 3/2$, and the $P_{1/2}$ state has $j = 1/2$, where j is the sum of the electron spin angular momentum and the electron orbital angular momentum.[34] Since the final electronic state in each case is $S_{1/2}$, we are only considering $j = 1/2$ to $j = 1/2$ transitions.[35]

---

[34] To simplify the observations, the $P_{3/2}$ transition will be blocked by the interference filter.

[35] From the text one can see that there are significant differences between the spectrum of the alkali metals and atomic hydrogen. Hydrogen's electron sees a precise $1/r$ Coulomb potential, while the alkali valence electron sees a quite different, albeit spherically symmetric potential. There are several consequences: 1) the ground state of hydrogen has only one electronic state, the $1S_{1/2}$ state, and no states with $l > 0$. By contrast, the n = 5 lowest energy states of rubidium are $5S_{1/2}$, $5P_{1/2}$, and $5P_{3/2}$ states, all with distinct energies. 2) the hydrogen $2S_{1/2}$, $2P_{1/2}$, and $2P_{3/2}$ states are degenerate (modulo a tiny QED

Hyperfine Structure. Hyperfine structure results from the interaction of the nuclear spin **I** with the total electronic angular momentum **J**. We will be dealing with two separate nuclei, ^{85}Rb (nuclear spin 5/2) and ^{87}Rb (nuclear spin 3/2). The hyperfine transition frequency for the ^{87}Rb $5S_{1/2}$ state is $\nu = \Delta W / h =$ 6,834,682,610.904 Hz. It is the basis for rubidium atomic clocks. The hyperfine transition for the ^{87}Rb $5P_{1/2}$ state is 818 MHz.[36]

The hyperfine interaction Hamiltonian is $\mathbf{H} = A_{nlj}\mathbf{I}\bullet\mathbf{J}$ where **I** is the nuclear spin operator, $\mathbf{J} = \mathbf{S}+\mathbf{L}$ is the total angular momentum operator for the valence electron, A_{nlj} is a constant depending upon the nucleus, and the *n*, *l*, and *j* quantum numbers. From experiments, $A_{5,0,1/2}$ = 3417.3 MHz, and $A_{5,1,1/2}$ = 409 MHz. The hyperfine energy shifts are given as follows:

$$E_{nljf} = E_{nlj} + \frac{1}{2}[f(f+1) - i(i+1) - j(j+1)]A_{nlj} \tag{65}$$

The energy splitting between the state *f* and the state *f*−1 will then be

$$\Delta E = A_{nlj} f \tag{66}$$

Magnetic interaction (Zeeman effect). The interaction of an external magnetic field with an atom is a complex subject, the full treatment of which is beyond the scope of this manual. The reader is encouraged to consult any introductory book on quantum mechanics for the details; we will mainly concentrate on the results.

Recall that the total angular momentum operator for a complex system is the sum of the operators associated with the individual constituents:

1. **S** is the operator associated with the electron spin.
2. **L** is the operator associated with the electron's orbital angular momentum.
3. **J = S + L** is the operator associated with the sum of the spin an orbital angular momentum.
4. **I** is the operator associated with the nuclear spin.
5. **F** = **S** + **L** + **I** = **J** + **I** is the total angular momentum operator.

Each of these operators has two quantum numbers associated with them: the *z*-component of angular momentum, and the total angular momentum quantum number. For example, for a single electron spin, the *z*-component of angular momentum is $\hbar m_s = \pm\hbar/2$, and the square of the total spin angular momentum is $\hbar^2 s^2 (s+1)^2 = \hbar^2 (1/2)^2 (1/2+1)^2 = (3\hbar/4)^2$. For a single electron characterized by orbital angular momentum quantum number *l*, the z-component of orbital angular momentum can take on the values $\hbar m_l = \hbar l, \hbar(l-1), \ldots, -\hbar l$, and the square of the total orbital angular momentum is $\hbar^2 l^2 (l+1)^2$. For a nucleus characterized by spin angular momentum quantum number *i*, the z-component of orbital angular momentum can take on the values

---

shift called the Lamb shift), while the levels are quite separate in the alkalis, owing to the non-Coulomb like potential.

[36] Alan Corney, *Atomic and Laser Spectroscopy*. Oxford University Press (1977).

$\hbar m_i = \hbar i, \hbar(i-1), \ldots, -\hbar i$, and the square of the total nuclear spin angular momentum is $\hbar^2 i^2 (i+1)^2$.

To combine angular momenta, we need to define the so-called *g*-factors for the electron spin, electron orbital angular momentum, electron total angular momentum, and nuclear spin angular momentum. They are, respectively,

Electron spin:

$$g_s = 2(1+\alpha/2\pi + O(\alpha^2)) \cong 2.002319304362 \cong 2 \tag{67}$$

Electron orbital angular momentum:

$$g_l = 1 \tag{68}$$

Electron spin plus orbital angular momentum:

$$g_j = g_s \frac{j(j+1)+s(s+1)-l(l+1)}{2j(j+1)} + g_l \frac{j(j+1)-s(s+1)+l(l+1)}{2j(j+1)} \tag{69}$$

Since $g_l = 1$ and $g_s \approx 2$, to a very good approximation:

$$g_j \cong 1 + \frac{j(j+1)+s(s+1)-l(l+1)}{2j(j+1)} \tag{70}$$

This is known as the *Lande g-factor*.

Nuclear spin alone: g_i. Since the interaction of a particle with an external magnetic field is always given by the Hamiltonian $\mathbf{H} = -\boldsymbol{\mu}\bullet\mathbf{B}$, for the nucleus it will be $\mathbf{H} = -\boldsymbol{\mu}_i\bullet\mathbf{B}$. The magnetic moment operator $\boldsymbol{\mu}$ is always proportional to the spin angular momentum operator. We will adopt the convention used in the Reichart manual, that $\boldsymbol{\mu}_i \equiv g_i \mu_B \mathbf{I}$, where μ_B is the Bohr magneton $\mu_B \equiv e\hbar/2m_e$. The magnitude of the magnetic moment is related to g_i by $\mu_i = g_i \mu_B i$. (Please refer to the appendix for an alternative definition of g_i.)

From the tables by Stone,[37] $\mu_i = 2.7515\mu_N$, where $\mu_N \equiv e\hbar/2m_p$ is the so-called *nuclear magneton*. Since $i = 3/2$ for ^{87}Rb, This gives $g_i \mu_B i = 2.7515\mu_N$, or $g_i = 2.7515\mu_N / \mu_B i = 1.8343(m_e/m_p)$ = 1.00x10^{-3}. From this we draw the important conclusion that $g_i \ll g_j$.

Electron spin plus electron orbital angular momentum plus nuclear spin angular momentum:

$$g_f = g_j \frac{f(f+1)-i(i+1)+j(j+1)}{2f(f+1)} - g_i \frac{f(f+1)+i(i+1)-j(j+1)}{2f(f+1)} \tag{71}$$

[37] N. J. Stone, *Atomic and Nuclear Data Tables* **90**, 96 (2005)

Since g_j is of order 1 and and g_i is of order 10^{-3},

$$g_f \cong g_j \frac{f(f+1)-i(i+1)+j(j+1)}{2f(f+1)} \tag{72}$$

We now have the vocabulary necessary to compute the energy shifts of the electronic levels, arising from the nuclear spin and from the applied magnetic field. The standard approach is to write down the Hamiltonian, including the hyperfine and magnetic interactions:

$$\mathbf{H} = A\mathbf{I}\bullet\mathbf{J} - \vec{\mu}\bullet\mathbf{B} = A\mathbf{I}\bullet\mathbf{J} + \mu_B(g_j\mathbf{J} + g_i\mathbf{I})\bullet\mathbf{B} \tag{73}$$

where the first term represents the interaction of the nuclear spin with the electron's total angular momentum, and the second term represents the interaction of the total magnetic moment of the atom with the magnetic field.

It turns out that for $j = 1/2$, we can calculate the energy shifts analytically, resulting in the famous Breit-Rabi formula:[38]

$$\Delta E_{f=i\pm1/2} = -\frac{\Delta W_{hf}}{2(2i+1)} - \frac{\mu_i}{i} mB_z \pm \frac{\Delta W_{hf}}{2}\left(1+\frac{4mx}{2i+1}+x^2\right)^{1/2} \tag{74}$$

where $\Delta W_{hf} \equiv (A/2)(2i+1)$ is the zero-field hyperfine splitting, x is defined by $x \equiv \mu_B(g_j - g_i)B_z / \Delta W_{hf}$, and $m\hbar$ is the z-component of total angular momentum. For ^{87}Rb, the nuclear spin quantum number is $i = 3/2$, so f can take on the values $3/2 \pm 1/2 = 2,1$ (because we are restricting our discussion to $j = 1/2$). This function is plotted in Figure 9.

[38] For j not equal to 1/2, the formula is much more complicated, involving roots of cubic and higher equations.

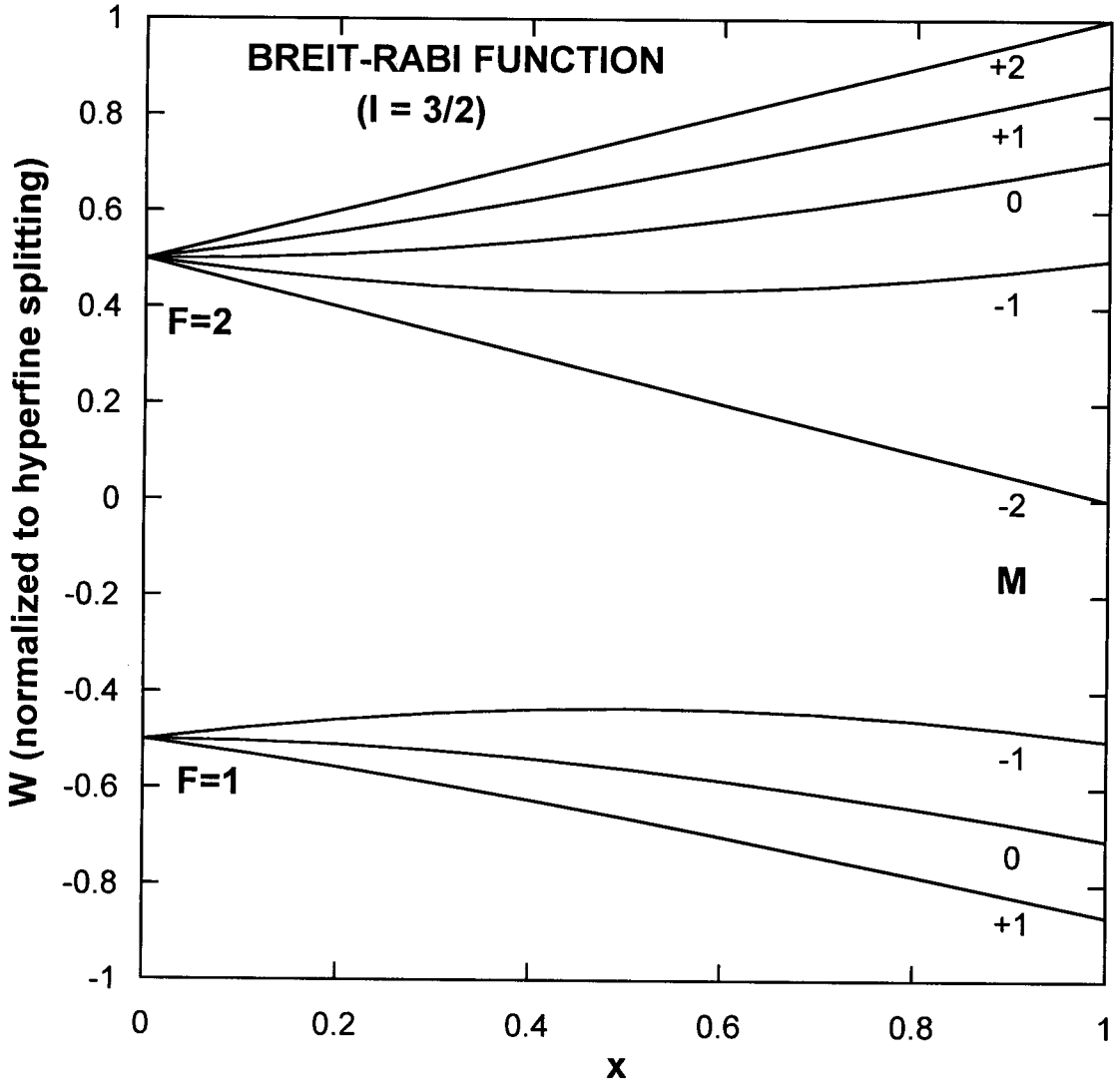

Figure 9. The normalized Breit-Rabi energy shifts of the valence electron of an atom with the following quantum numbers: s = 1/2, l = 0 or 1, j = 1/2, i = 3/2, f = 1 or 2. This diagram would apply to ^{87}Rb, and where the j = 3/2 level is disregarded because an optical filter is used. M is the z-component of the total angular momentum. The parameter x is given by $x \equiv (g_j - g_i)\mu_B B_z / \Delta W_{hf} \cong g_j \mu_B B_z / \Delta W_{hf}$.

For $x \ll 1$ and for $x \gg 1$the energy shifts of the levels are linear in B_z. However, for $x \ll 1$we can further expand equation (74) in powers of x, retaining the quadratic terms:

$$\begin{aligned}(1+\frac{4mx}{2i+1}+x^2)^{1/2} &\cong 1+\frac{1}{2}(\frac{4mx}{2i+1}+x^2)-\frac{1}{4}(\frac{4mx}{2i+1}+x^2)^2 \\ &\simeq 1+\frac{2m}{2i+1}x+\left[\frac{1}{2}-\frac{4m^2}{(2i+1)^2}\right]x^2\end{aligned} \tag{75}$$

Using equation (75), we can calculate the frequencies of RF transitions between sub-levels m_a and m_b, denoting the average $\bar{m} \equiv (m_A + m_B)/2$.

$$f = 2: h\nu_{\bar{m}} = \left(\frac{g_j \mu_B B}{2i+1}\right) - \frac{2\bar{m}}{\Delta W_{hf}}\left(\frac{g_j \mu_B B}{2i+1}\right)^2$$
$$f = 1: h\nu_{\bar{m}} = \left(\frac{g_j \mu_B B}{2i+1}\right) + \frac{2\bar{m}}{\Delta W_{hf}}\left(\frac{g_j \mu_B B}{2i+1}\right)^2 \qquad (76)$$

The transitions are summarized pictorially in Figure 10.

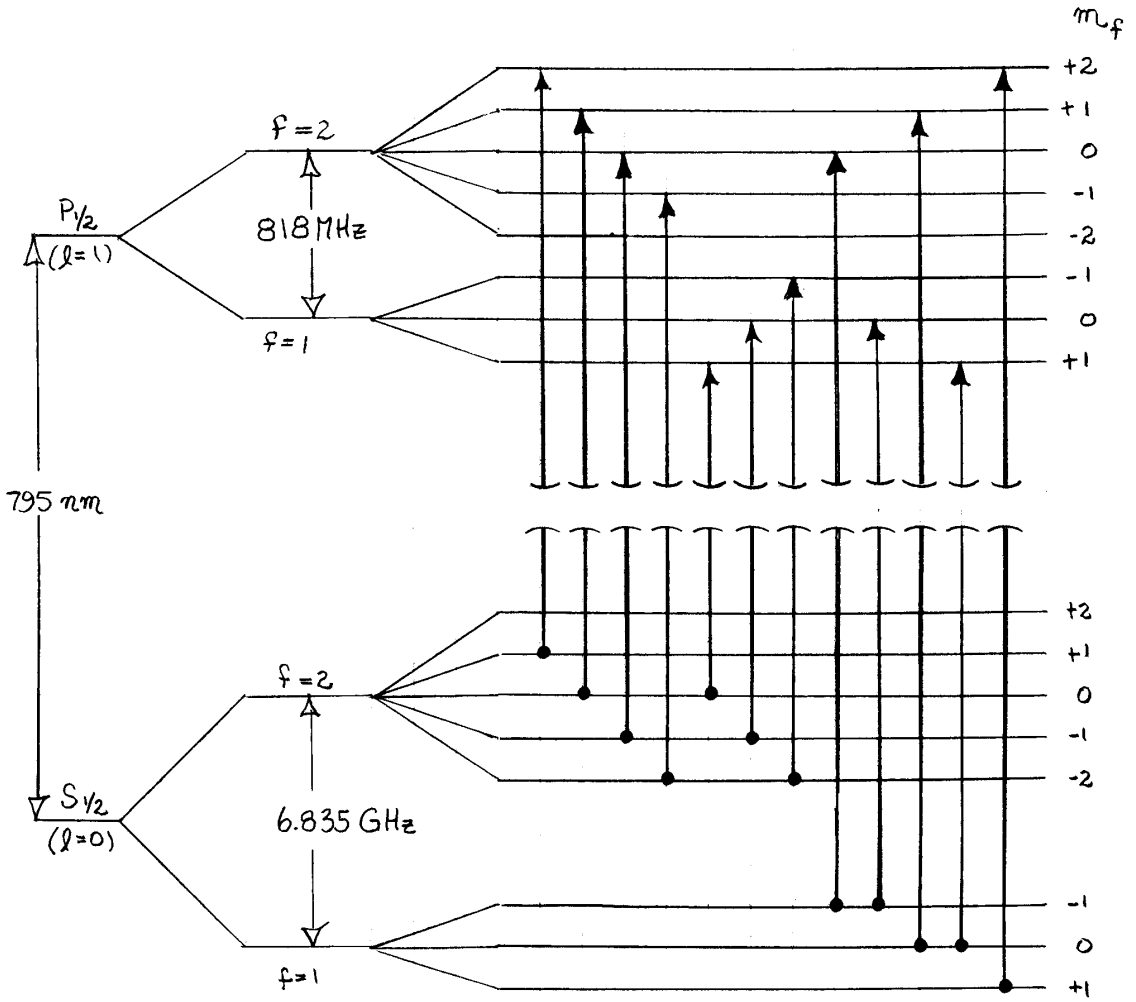

Figure 10. The schematic (not to scale) energy levels and dipole-allowed optical excitations from the $S_{1/2}$ levels to the $P_{1/2}$ levels in ^{87}Rb. (Recall that we have filtered out transitions involving the $P_{3/2}$, and we are using circularly polarized light, so $\Delta m = +1$ only).

Optical Pumping. "Optical pumping" refers to the production of a non-equilibrium population of atomic states, obtained by cleverly shining light of a particular wavelength on to a sample. The sample is said to experience a "population inversion."

Figure 10 (above) depicts the energy levels of the rubidium valence electron when subjected to a static magnetic field along the z-axis. It also depicts the allowed optical absorption transitions from the ground state to the first excited state, when the incident light is circularly polarized. The selection rule is $\Delta m = +1$.

Once an upward transition to a $P_{1/2}$ state has occurred, the atom may soon relax back to the original $S_{1/2}$ state. However, the various *f, m* levels of the ground electronic state ($S_{1/2}$) are now unequally populated, because of the unequal depletion caused by the optical absorption. For example, with circularly polarized incident light, there is no allowed upward transition from the $S_{1/2}$ $f = 2$ $m = 2$ state, so this state will have an excess population relative to the other $S_{1/2}$ states, which do have allowed upward transitions. (This is the essence of optical pumping). One can calculate the relative absorption probabilities for the various $S_{1/2}$ states:[39]

F	1	1	1	2	2	2	2	2
M	+1	0	−1	2	1	0	−1	−2
P	1	2	3	0	1	2	3	4

If we now subject the rubidium sample to a radio frequency signal that is tuned to a pair of adjacent $S_{1/2}$ magnetic states, the populations will be re-equalized.[40] The population inversion will have been undone, and the sample will be slightly more absorptive.

EXPERIMENT

Low-field resonances (4B)

(Please note that it is best to keep the instrument covered with the black cloth provided. This will reduce stray light and will help stabilize the oven temperature).

1. An absorption dip will occur as the magnetic field is swept through zero magnetic field, even with no RF field applied. Please observe this dip.

2. At relatively low but nonzero applied magnetic fields, the Zeeman splitting will be linear in the magnetic field, and one only needs to be concerned with the first term in Equation (76). If the sample is subjected to a constant RF frequency (134 kHz in this case), when the B-field is swept, a resonance will appear at the field satisfying this equation. Please observe the absorption dip for the ^{87}Rb and ^{85}Rb isotopes. Details are given in the TeachSpin manual.

---

[39] W. Franzen and A.G. Emslie, *Physical Review* **108**, 1453 (1957). Note that the TeachSpin manual is vague on this point, suggesting that the only levels with an anomalous populations are the levels for which downward transitions are completely forbidden.
[40] This can be accomplished by having a fixed RF frequency and a variable magnetic field, or a variable (swept) RF frequency and a fixed magnetic field.

Intermediate field Resonances (4C)

At intermediate magnetic fields, the splitting in the magnetic sublevels will start to exhibit the quadratic dependence shown in Equation (76). Please observe and explain these resonances as described in the manual.

Transient Effects (4D)

The preceding experiments were steady state; that is, the sample was subjected to a constant incident light beam, a constant or slowly varying magnetic field, and a constant radio frequency field. It is also possible to observe the response of the system in the time domain, by pulsing the radio frequency field.

Please perform the suite of experiments in this section.

APPENDIX I

Alternate Definition of g_i

We have used a definition of g_i, the nuclear g-factor, that is consistent with the TeachSpin manual, and also consistent with the current Wikipedia articles on the Zeeman effect and on the hyperfine structure. This convention references the nuclear magnetic moment to the Bohr magneton, $\mu_B \equiv e\hbar / 2m_e$.

There is an alternative definition of g_i, which references g_i to the *nuclear* magneton, $\mu_N \equiv e\hbar / 2m_p$. This convention results in a nuclear *g*-factor of order unity rather than of order 10^{-3}. This convention is consistent with the monographs by Corney[41] and by Bernheim,[42] and perhaps others. We shall refer to this convention as $g_i^{(alt)}$. Here are the key formulas, translated to this convention:

$$\boldsymbol{\mu}_i \equiv g_i^{(alt)} \mu_N \mathbf{I} \tag{77}$$

$$g_i^{(alt)} \equiv \mu_i / (\mu_N i) \tag{78}$$

$$g_f = g_j \frac{f(f+1) - i(i+1) + j(j+1)}{2f(f+1)} - g_i^{(alt)} \frac{m_e}{m_p} \frac{f(f+1) + i(i+1) - j(j+1)}{2f(f+1)} \tag{79}$$

$$x \equiv (g_j \mu_B - g_i^{(alt)} \mu_N) B_z / \Delta W_{hf} \cong g_j \mu_B B_z / \Delta W_{hf} \tag{80}$$

From the tables by Stone,[43] $\mu_i = 2.7515 \mu_N$. Since i = 3/2 for ^{87}Rb, This gives $g_i^{(alt)} = 2.7515 / i = 1.8343$. The basic conclusion remains; *i.e.* that we can neglect the second term in equation (79).

---

[41] Alan Corney, *Atomic and Laser Spectroscopy*. Oxford University Press (1977).
[42] Robert Bernheim, *Optical Pumping*. W. A. Benjamin (1965).
[43] N. J. Stone, *Atomic and Nuclear Data Tables* **90**, 96 (2005)

SECOND SOUND

(Not presently offered)

INTRODUCTION

At pressures below 25 atmospheres, and at temperatures between 0.00 and 4.21 Kelvin, helium (^{4}He) vapor coexists with the liquid phase. Below temperatures of 2.172 Kelvin (the lambda point) the liquid behaves as if it were composed of a mixture of two interpenetrating fluids, one with normal liquid properties (non-vanishing viscosity), and one with superfluid properties (zero viscosity, zero entropy, infinite thermal conductivity). Since the partial densities of the respective fluids depends only upon the temperature, a temperature variation within the fluid implies a corresponding density variation of the separate components. This is the fundamental origin of second sound.

The two fluids taken together support the propagation of ordinary sound waves, which are density waves associated with the compressibility of the total fluid. Thus, *ordinary* sound propagates with a speed c_1 given by

$$c_1^2 = \left(\frac{\partial P}{\partial \rho}\right)_S \tag{81}$$

Because temperature variations imply density variations as discussed above, there must be temperature (or equivalently entropy) waves.[44] [45] [46] Below the lambda point, temperature fluctuations satisfy a second order wave equation,

$$\nabla^2 T = \frac{1}{c_2^2}\frac{\partial^2 T}{\partial t^2} \tag{82}$$

Where c_2 is given by

$$c_2^2 = S^2\left(\frac{\partial T}{\partial S}\right)_S\left(\frac{\rho_s}{\rho_n}\right) = \frac{S^2 T}{C_P}\left(\frac{\rho_s}{\rho_n}\right) \tag{83}$$

By contrast, the temperature distribution in ordinary matter satisfies the diffusion equation (84):

$$\nabla^2 T = \kappa\frac{\partial T}{\partial t} \tag{84}$$

The time dependence of this equation is typically a damped exponential, rather than an oscillatory function.

---

[44] J. Wilks, *The Properties of Liquid and Solid Helium***.** Clarendon Press, Oxford (1967).
[45] K. R. Atkins, *Liquid Helium*. Cambridge University Press (1959).
[46] R. J. Donnelly, *Experimental Superfluidity*. The University of Chicago Press (1967).

Some insight into this phenomenon may be gained by considering temperatures below about 1 Kelvin. In this temperature range, the thermal agitation of the atoms may be though of as an ideal gas of phonons propagating at the speed c_1. The density of phonons is a direct measure of the temperature of the fluid; and fluctuations in the density of phonons are a corresponding measure of fluctuations in temperature. Now it is well known that the speed of sound in an ordinary ideal gas is $1/\sqrt{3}$ times the r.m.s. speed of the physical particles. By the same token, in this temperature range the speed of second sound is just $1/\sqrt{3}$ times the r.m.s. speed of the phonons.

APPARATUS

The apparatus has a heat source (transmitter) and a heat detector (receiver, a.k.a. *bolometer*) at two ends of a closed cylindrical cavity of length L = 10.05 cm that is immersed in, and filled with, liquid helium. Both the transmitter and the bolometer are carbon film resistors, which have an electrical resistance that varies with the temperature, according to the approximate three-parameter formula

$$R_B = R_0 (1 + a \exp(T_0 / T)) \tag{85}$$

where $R_0(1+a)$ is the room temperature resistance and T_0<<300 K is a characteristic temperature of the resistor. Thus, the temperature fluctuations at the bolometer are manifested as resistance fluctuations. If one biases the receiver with a current source, resistance fluctuations will be manifested as voltage fluctuations.

In essence, the experiment is to apply a known voltage waveform (sinusoidal wave or pulses) to the transmitter, resulting in the propagation of second sound waves. These waves will be picked up as a voltage waveform across the current-biased bolometer.

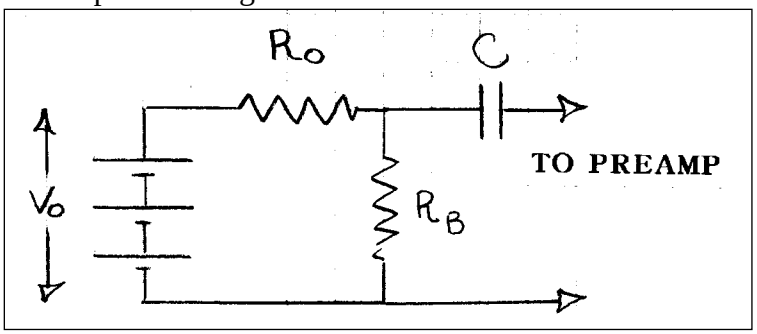

Figure 11. Bolometer bias circuit.

The bolometer current bias comes from the simple circuit shown in Figure 11. A battery pack of total voltage V_0 is wired in series with a bias resistor R_0, which is in turn is wired in series with the bolometer R_B. The voltage across the bolometer resistance is given by

$$V_B = V_0 \frac{R_B}{R_B + R_0} \tag{86}$$

If the bolometer resistance changes by an amount ΔR_B, the bolometer voltage will change by

$$\Delta V_B = \Delta R_B \frac{\partial V_B}{\partial R_B} = V_0 \frac{R_0 \Delta R_B}{\left(R_B + R_0\right)^2} \tag{87}$$

If we are given a bolometer resistance R_B, we can determine the optimum series resistance R_0 by differentiating this expression with respect to R_0 and setting it to zero. (we leave it as an exercise for the reader). The result is that the optimum R_0 is given by R_B. In our circuit, we choose R_0 = 51 kΩ and V_0 = 36 volts (three 9 Volt batteries in series). This gives an average power dissipation in the bolometer of about $18^2/51000 \sim 6$ mW.

A final note about the biasing circuit: The capacitor C in Figure 11 blocks the DC voltage across R_B, so that only the AC voltage appears at the input of the preamplifier.

The output of the biasing circuit is connected to a high quality low-noise preamplifier, whose output is in turn connected to a digital oscilloscope. To minimize low frequency noise, set the high pass filter to 10 Hz; and to minimize the high frequency noise, set the low-pass filter to 10 kHz. Signals in the range $10 < f < 10^4$ Hz will be passed faithfully on to the oscilloscope and all other frequencies will be suppressed.

EXPERIMENT

Pulse method: By pulsing the transmitter with a single short pulse, one can observe the receipt of the pulse at the Bolometer a time $T = L/c_2$ seconds later. This will be followed by echoes at multiples of $2L/c_2$ seconds, each echo being damped and somewhat broadened with respect to the earlier echo. Knowing L, one can straightforwardly determine c_2. The challenge of this method is that, near the lambda point, the echoes become fainter than the background noise. This challenge can be overcome by the *coherent pulse* method.

Coherent Pulse Method: As with the pulse method, one pulses the transmitter with a short pulse, but this time as part of a *continuous* pulse train, with pulses separated by a time $2L/c_2$; i.e. a pulse train of *frequency* $c_2/2L$. Now, the amplitude of each echo is continuously reinforced, so its amplitude now rises above the noise.

Resonance method: The wavelength and frequency of a sine (or cosine) wave propagating with speed c_2 are related by the elementary formula $\lambda f = c_2$. If the wave is confined to a one-dimensional cavity of length L with identical boundaries, the wavelengths can only take on discrete values given by $\lambda_n = 2L/n$, where $n = 1, 2, 3, \ldots$ As a consequence, the frequencies take on only the discrete values $f_n = c_2/\lambda_n = n(c_2/2L)$. Thus if we excite the transmitter *power* at or very close to a frequency f_n, we will observe a large signal at the bolometer.

With the resonance method, it is important to keep in mind the fact that a *voltage* waveform of frequency f results in a *power* waveform which is a constant plus a cosine wave at $2f$. This follows from the fact that $P(t) = V^2(t)/R_0$, and the identities

$$\sin^2 \omega t = \frac{1-\cos 2\omega t}{2}$$
$$\cos^2 \omega t = \frac{1+\cos 2\omega t}{2} \tag{88}$$

In other words, exciting the transmitter with a sine (or cosine) *voltage V* results in an average power dissipation $V^2/2R$, plus a cosine *power* at *twice* the frequency.

APPENDIX 1. INITIAL SETUP

OVERVIEW

The vacuum system consists of three independent vacuum volumes:

1. The outer (tertiary) volume jacket is permanently evacuated and sealed. It is effectively a thermos bottle, ultimately holding liquid nitrogen and the inner Dewars.
2. The secondary volume can be evacuated with a small mechanical pump. It needs to be evacuated and slightly backfilled before each run to remove any residual helium, which would conduct heat from the liquid helium to the outside world. The slight backfill of air provides a conductive heat path from the innermost volume to the liquid nitrogen during the initial cool-down. The air will then freeze when liquid helium is introduced into the innermost volume.
3. The tertiary (innermost) volume, after flushing with helium gas, is kept just above atmospheric pressure while it is cooled with liquid nitrogen. The large mechanical pump[47] is first used as part of the flushing process, and then used to reduce the vapor pressure when liquid helium is introduced, thereby cooling the liquid helium. The mechanical gauges measure the pressure within the chamber. At thermal equilibrium, the pressure is uniquely related to the temperature of the liquid helium.

Bottom line: Ultimately, there should be no air nor water in the innermost volume; and ultimately, there should be no helium in the secondary volume.

PRELIMINARY CHECKS

1. Check oil level of large pump (with pump running).
2. Pump out inner (primary) dewar. Pressure should go to zero on the gauge.
3. Check oil level of small pump (with pump running).
4. Pump out secondary dewar. Pressure should fall below 10 mTorr.
5. Check transmitter resistance. Should be about 300 Ω.
6. Check bolometer resistance. Should be about 11 kΩ.
7. Check output of bias box. Should be about 36-40 volts.
8. Evacuate the vacuum jacket of the helium transfer line using the high vacuum pump. (This should be done once per quarter).

[47] The power switch does not work on the main pump. You need to power up by plugging in.

PROCEDURE[48]

1. **Prepare the secondary (jacket) volume**. Be sure that the liquid helium storage Dewar is outside the room, so that no helium gas will contaminate the jacket volume.
   1.1. Open the two jacket valves and close the small pump vent valve. Evacuate the volume to about 10 mTorr or better, using the small mechanical pump.
   1.2. Admit a small amount of air into the jacket using the following procedure:
      1.2.1. Close the valve nearest the vacuum jacket.
      1.2.2. Turn off the pump and open the vent valve to air.
      1.2.3. Close the *next* nearest valve to the vacuum chamber.
      1.2.4. Open the nearest valve to the vacuum chamber. This will admit a small, well-defined amount of air into the vacuum jacket.
2. **Prepare the primary (inner) volume (starting at atmospheric pressure)**.
   2.1. Connect the helium gas cylinder to the primary volume venting valve with a rubber hose.
   2.2. Open the primary volume venting valve.
   2.3. With the giant pump, evacuate the primary chamber and rubber tubing leading to the gas cylinder. When you reach 1 mm Hg (1 Torr) or less, valve off the giant pump at the gate valve but leave the pump running.
   2.4. With the cylinder pressure set at about 2 psig, while monitoring the chamber pressure, slowly open the needle valve at the gas cylinder to bring the chamber up to just above atmospheric pressure. (The three plugs on top of the brass flange will prevent over-pressurization of the the chamber).
3. **Cool system with liquid nitrogen**.
   3.1. Transfer liquid nitrogen to the appropriate volume using the plastic funnel at the top of the platform.
   3.2. Top up the liquid every 15 minutes, for a period of about two hours. This procedure will eventually bring all inner systems to about 77 K.
4. **Introduce liquid helium into the primary volume**.
   4.1. Roll the liquid helium storage Dewar into the room.
   4.2. Remove the cap at the top of the storage Dewar.
   4.3. Open the valve at the top of the storage Dewar. A puff of helium gas will emerge as the liquid comes to equilibrium with the atmosphere.
   4.4. Having purged the rubber tubing from the gas cylinder at about 2 psig, connect the rubber tubing to the storage Dewar.
   4.5. Remove the three plugs on the top flange of the vacuum system.
   4.6. Simultaneously insert the transfer tube into the tank and into the primary chamber. Be sure to use gloves and a face mask.
   4.7. Open the gas valve at the storage Dewar to pressurize the Dewar.
   4.8. When the liquid helium reaches about ¾ full, close the gas cylinder valve, retract the transfer tube, and replace the three plugs.
   4.9. Begin pumping on the liquid helium by opening the isolation valves. You will notice that the helium ceases to boil at the lambda point, 37.9 mm Hg = 37.9

[48] 1 Torr = 1 mm Hg; 1 mTorr = 10^{-3} mm Hg = 1 μm Hg.

Torr. The pressure (and hence the temperature) may be tuned with the valves.

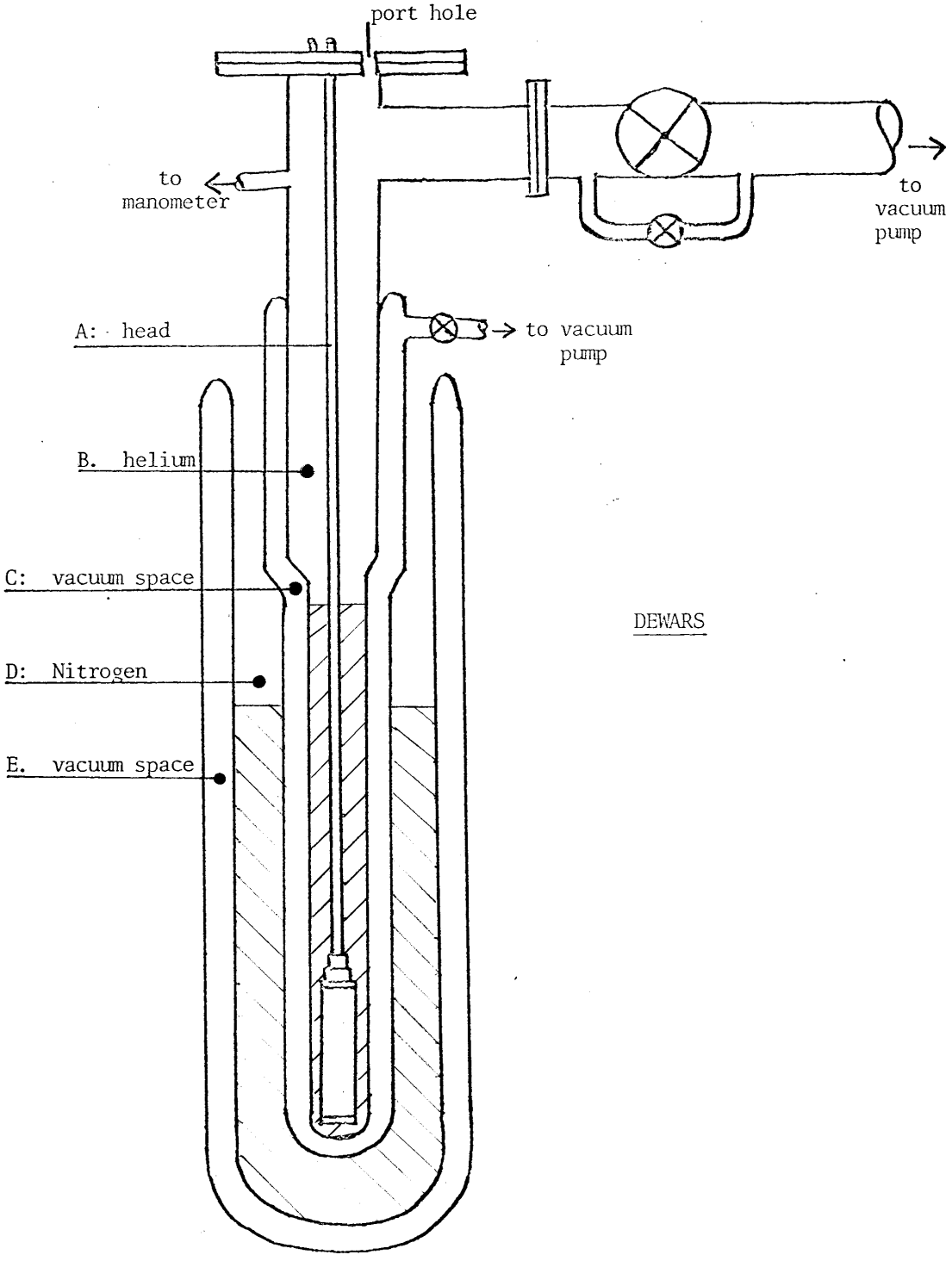

Figure 12. Cross-section of the experimental Dewar

Additional Questions

1. Using the formula $(1/2)m<v^2>=kT$, calculate the root-mean-square speed of helium atoms at 1 Kelvin.

2. For a classical fluid, the speed of sound (and thus of phonons) is $1/\sqrt{3}$ times the root-mean-square speed of the atoms. From the results of problem (1), calculate the speed of sound in 4He at 1 Kelvin.

3. The speed of second sound is $1/\sqrt{3}$ times the speed of phonons. From the results of problem 2, calculate the speed of second sound at 1 Kelvin. Compare your result with Table 6.

REFERENCES

J. Wilks, *The Properties of Liquid and Solid Helium*. Clarendon Press, Oxford (1967).
K. R. Atkins, *Liquid Helium*. Cambridge University Press, Cambridge (1969).

APPENDIX. SOME USEFUL TABLES

T (K)	C (J kg^{-1}K^{-1})	S (J kg^{-1}K^{-1})	c_2 (ms^{-1})	$r = \rho_n/\rho_s$	$\rho_n/(\rho_n + \rho_s)$
1.00	100	17.0	19.40	0.008	0.0080
1.10	190	30.0	18.78	0.015	0.0015
1.20	318	51.5	18.78	0.029	0.0283
1.30	515	84.3	19.03	0.050	0.0472
1.40	786	131.9	19.58	0.081	0.0748
1.50	1142	197.8	20.07	0.128	0.1131
1.60	1598	285.5	20.37	0.197	0.1643
1.70	2174	399.0	20.36	0.300	0.2310
1.80	2896	542.4	19.89	0.463	0.3166
1.90	3804	722.8	18.78	0.740	0.4253
2.00	4990	946.5	16.69	1.289	0.5632
2.10	6972	1231.6	12.39	2.975	0.7484
2.15	8723	1416.1	7.99	7.741	0.8865

Table 6. Various parameters for liquid helium as a function of temperature. C: Heat capacity of normal component. S: Entropy of normal component. c_2: Speed of second sound. r: Normal to superfluid density ratio. ρ_n/ρ: normal to total density ratio.

P (mm Hg)	T (K)		P (mm Hg)	T (K)
4	1.523		40	2.195
6	1.612		50	2.291
8	1.682		60	2.375
10	1.740		70	2.449
11	1.765		80	2.516
12	1.789		90	2.578
13	1.812		100	2.635
14	1.833		150	2.870
15	1.854		200	3.060

16	1.873		250	3.220
17	1.891		300	3.360
18	1.909		350	3.490
19	1.926		400	3.600
20	1.943		450	3.700
21	1.959		500	3.800
22	1.974		550	3.890
23	1.989		600	3.970
24	2.003		650	4.050
25	2.017		700	4.130
26	2.031		750	4.200
27	2.044			
28	2.057			
29	2.071			
30	2.083			
31	2.095			
32	2.107			
33	2.119			
34	2.130			
35	2.141			
36	2.152			
37	2.163			
38	**2.174**			
39	2.185			
40	2.195			

Table 7. Vapor pressure of helium vs. temperature. (T_λ=2.173 K).

SURFACE PLASMON RESONANCE

INTRODUCTION

An ionized gas is called a *plasma*. For example, the gas in a fluorescent lamp is ionized when the lamp is energized, resulting in a plasma. The Geissler tube used in the intermediate lab produces a visible plasma. Most plasmas consist of a free electron gas, capable of flowing through a more or less stationary positive ionic background. One can show that the electrons can exhibit longitudinal[49] density oscillations, called *plasmons*, with a characteristic frequency given by $\omega_p^2 = 4\pi ne^2 / m$, where *n* is the electron number density.[50]

More recently,[51] theorists have shown that it is useful to consider the free electrons in metals and semiconductors as plasmas. Just as with gases, the plasmons exhibit wavelike longitudinal oscillations with a characteristic frequency and wavevector given by the following *dispersion relation* in the so-called random phase approximation:[52]

$$\begin{aligned} \omega^2 &= \omega_0^2 + (3/5)v_F^2 k^2 \\ \omega &\cong \omega_0 + (3/10)(v_F^2 / \omega_0)k^2 \end{aligned} \tag{89}$$

Where, as before, $\omega_0^2 \equiv (4\pi ne^2 / m)$ and $v_F^2 = (\hbar^2 / m^2)k_F^2 = (\hbar^2 / m^2)(3\pi^2 n)^{2/3}$. v_F is known as the *Fermi velocity*, k_F is known as the *Fermi wave-vector*, and *n* is the free electron density.

The plasmon is an outstanding example of a physical phenomenon that can be quantized, and therefore regarded as a *quantum excitation*, or *quasiparticle*.[53] That is to say, the plasmon can be regarded as a particle with energy and momentum given by the following equations, respectively:

$$\begin{aligned} E &= \hbar\omega \\ \mathbf{p} &= \hbar\mathbf{k} \end{aligned} \tag{90}$$

Other examples of such quantum excitations include *phonons* (sound waves), *rotons* (vortices in liquid helium), *Cooper pairs* (electron pairs in superconductors), *excitons*, *helicons*, and so forth.

---

[49] *Longitudinal* density waves are waves whose density varies *along* the propagation direction. Sound waves in a liquid or gas, like plasma waves, are longitudinal density waves.

[50] In this manual we are using so-called esu units. Please refer to the appendix for discussion and conversion factors.

[51] David Pines and David Bohm, *Phys. Rev.* **85**, 338-353 (1952).

[52] P. M. Platzman and P. A. Wolff, *Waves and Interactions in Solid State Plasmas*. Academic Press, New York (1973).

[53] David Pines, *Elementary Excitations in Solids*. Benjamin, New York (1963).

The importance of considering a condensed system as comprised of quantum excitations cannot be overstated. For one thing, material properties can often be ascertained by considering the material as a gas of interacting quantum excitations. At very low temperatures, the densities are low enough that they can be studied, *e.g.* by scattering with more familiar particles such as electrons or light. (In the case of solid-state plasmons, the plasmon energy is of order 10 eV, which is huge compared to kT = 0.025 eV at room temperature.)

It also turns out that a metal can sustain longitudinal *surface* electron density oscillations, known as *surface* plasmons, at the interface between two materials, say metal (*m*) and air (*a*). In this case the dispersion relation is given by:[54]

$$\omega = ck\sqrt{\frac{\varepsilon_m\mu_m + \varepsilon_a\mu_a}{\varepsilon_m\varepsilon_a\mu_m\mu_a}} \tag{91}$$

Here, ε and μ are the (complex) electric permittivities and magnetic permeabilities of the two media, respectively.[55] In our case the magnetic permeabilities are unity, and the dispersion relation for the surface plasmon is given by:

$$\begin{aligned} \omega &= ck\sqrt{(\varepsilon_m + \varepsilon_a)/\varepsilon_m\varepsilon_a} \\ k &= (\omega/c)\sqrt{\varepsilon_m\varepsilon_a/(\varepsilon_m + \varepsilon_a)} \end{aligned} \tag{92}$$

In this experiment we would like to excite surface plasmons by coupling them to a light beam. To couple photons to surface plasmons, both momentum (wave vector) and energy (frequency) need to be matched. However, the dispersion relation of light in a vacuum is $\omega = ck$, which does not match the dispersion of a surface plasmon given in equation (92), for typical values of ε_m. However, if we consider a metal film deposited on a transparent substrate, and have the light incident upon the film by way of the substrate, we can vary the wave vector k_x of the light incident upon the metal at will, by varying the angle of incidence. (Please refer to Figure 13 below). The x-component of the wave vector of the light in the transparent medium (glass in this case) is $k_{gx} = (\omega/c)n_g \sin\theta_g$. Then, the matching condition will be

$$n_g \sin\theta_g = \sqrt{\varepsilon_m\varepsilon_a/(\varepsilon_m + \varepsilon_a)} \tag{93}$$

Here, n_g is the index of refraction of the glass (1.50), ε_m is the complex permittivity of the metal (gold) foil, and ε_a is the permittivity of air (1.00). These quantities at 635 nm (1.95 eV) are tabulated in Table 8.[56]

---

[54] Alexi A. Maradudin, J. Roy Sambles, William L. Barnes, *Modern Plasmonics*. Elsevier, Amsterdam (2014), and Stefan Maier, *Plasmonics: Fundamentals and Applications*. Springer Science (2007).

[55] Please refer to the appendix for definitions.

[56] P. B. Johnson and R. W. Christy, *Phys. Rev.* **B6**, 4370-4379 (1972).

Table 8. The optical properties of various materials at 635 nm.

MATERIAL	n	$\varepsilon = n^2$
Glass (g)	(+1.50 + 0.00i)	(+2.25 + 0.00i)
Gold (m)	(+0.21 + 3.27i)	(−10.7 + 1.37i)
Air (a)	(+1.00 + 0.00i)	(+1.00 + 0.00i)

Inserting these values into equation (93), the electromagnetic wave is matched to the surface plasmon at about $\theta_g = 44$ degrees. When θ_a is tuned to satisfy this condition, the incident light wave will be strongly absorbed, and the normally internally reflected beam will be strongly attenuated. This is known as the Kretschmann configuration.[57]

From a detailed analysis of the coupling of light with surface plasmons,[58] one can show that only the p-waves (also known as TM waves) can excite surface plasmons in our geometry. Thus, s-polarized waves do not excite surface plasmons, but p-polarized do.[59] This follows from the fact that surface plasmons, like bulk plasmons, are *longitudinal* density oscillations. To be excited, the incident electric field must be along the direction of propagation of the plasmon.

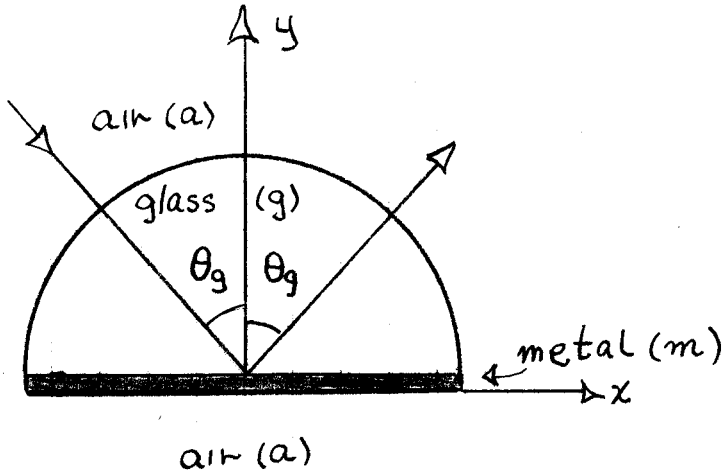

Figure 13. The schematic layout of the Kretschmann configuration. Incident light is totally internally reflected at the glass-metal interface, although the consequent evanescent wave permeates the 50 nm metal film. The surface plasmon excitation occurs at the lower metal (m) − air (a) interface. (In the actual experiment, the glass is configured as a prism rather than a semicylinder).

[57] E. Kretschmann, *Z. Physik* **241**, 313-324 ((1971).
[58] See, *e.g.* pages 24-27 of Stefan Maier, *Plasmonics: Fundamentals and Applications*. Springer Science (2007).
[59] The *plane of incidence*, sometimes known as the *plane of scattering*, is the plane defined by **k** (the incident wave vector) and **n** (the *normal* to reflecting surface). (In our illustrations, the scattering plane is the plane of the paper). See the appendix for more details.

The study of surface plasmons has very practical applications. The manipulation of light on the subwavelength scale is a necessity to further improve photonic circuits, *in situ* bio-sensors, and photolithography.

EXPERIMENTAL PROCEDURES

Overview. The light source with which we will be exciting surface plasmons is a 635 nm laser diode. The light will travel through a polarizer, λ/2 wave plate, and then the right-angle prism. The light shines through the prism and reflects off a layer of gold into the photodetector. The photodetector is a reverse-biased photodiode, which delivers a current proportional to the light intensity. This current is measured by a Keithley digital electrometer, and converted to an output voltage. This output voltage is then delivered to an analog-to-digital converter connected to the computer. The LabVIEW program records the voltage from the electrometer; and it also controls the two DC servo motors to rotate the stages.

Prism. The metal-insulator interface for the Kretschmann configuration will be gold-to-air. A right-angle prism will be used to create total internal reflection conditions. The 50 nm gold layer is deposited on a glass slide using a chromium adhesive layer and attached to the prism via index matching fluid.

Laser Source. The 635 nm laser diode can be focused with the knurled sleeve at the front end of the laser.

Rotating the stages. The orientation of the prism and photodetector with respect to the incident beam are controlled by two rotation stages. The layout of the stages is shown in Figure 14a. The stages can be controlled from the K-Cubes. The top stage controls the prism and the bottom stage controls the photodetector.

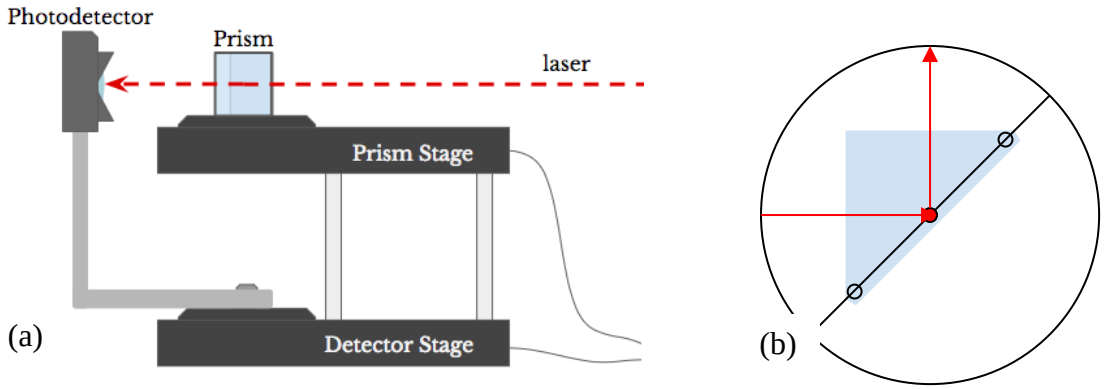

Figure 14. The mechanical rotary stages that support the sample and the detector.

The nominal positions of the stages (see Figure 14b) are such that the laser beam is normal to the entrance surface, and the detector is at 90 degrees from the laser beam. This nominal position has the beam incident upon the gold foil at 45 degrees. At these

positions, the sample dial reads exactly 15 degrees and the detector dial reads exactly 30 degrees.[60]

It is important for the detector to stay aligned with the reflected beam as we change the incident angle. Thus, the photodetector stage needs to move at twice the amount of the prism stage.

Setting the beam polarization. The diode laser emits mostly but not entirely linearly polarized light. To clean up the polarization, the laser beam first passes through a carefully aligned beam splitting cube. This device, as installed, transmits horizontally polarized light, and horizontally reflects, at 90 degrees, vertically polarized light. To get as much intensity as possible, rotate the laser about its axis to minimize the reflected component, using a screen. The result will be a high intensity, high purity horizontally polarized beam. To achieve a vertically polarized beam, follow the beam splitting cube with a half-wave plate, which rotates the plane of polarization by any amount up to 90 degrees.

Alignment of the prism.

1. Use the K-Cube to rotate the prism and detector stage to 15° and 30° respectively.
2. Place the prism (in the prism holder) on the prism rotation stage such that the center of the hypotenuse is at the center of rotation.
3. Rotate the prism holder (glass slide) so that the back reflected laser light is roughly centered on the half wave plate stage.
4. If necessary, position the detector so that the 90 degree reflected beam is centered on the detector sensitive area. This is accomplished by first loosening the brass thumb screw that secures the detector to the stage.

Surface plasmon polariton generation and detection. The LabVIEW program is designed to rotate the stages from the initial position by a given step size; and then record the voltage reading from the Keithley electrometer.

1. Open the program to open the front panel as shown in Fig. 4. Enter a file path for the final csv (comma-separated variable) file.
2. Set start position of the prism to about 12 degrees
3. Set the final position for the prism to about 16 degrees.
4. Set the start position of the detector to be twice the start position of the prism.
5. Assign an appropriate step size (the rotation stages have a maximum resolution of 0.05°) and set the step delay to about 2000 ms.
6. Click the Run button at the top to begin the scan. Note that both rotation stages first go to 0 degrees to properly zero the encoders.
7. After scan is complete check the csv file.
8. Repeat the experiment for s-polarization (polarization perpendicular to the plane of incidence).

[60] This choice of sample and detector dials assures that the dials never go below 0 degrees.

9. Download and plot the respective CSV files. You should plot the data as a function of $k_{||}/k_0$, where $k_0 = \omega/c$. Predict the location of the minimum in reflectivity. Is it near the observed minimum?

APPENDIX. PROPAGATION OF LIGHT IN MATERIALS

The following will be a very condensed account of the propagation and reflection of light in insulators and conductors. For further details, consult any intermediate or advanced text on electrodynamics, *e.g.* Jackson.[61]

Units: In this manual we use so-called electrostatic units (esu), which are commonly employed in solid-state and laser textbooks. Electrostatic units define charge in such a way that the force between two charges is given by $F = q_1 q_2 / r^2$. This system eliminates the cluttering appearance of $4\pi\varepsilon_0$ in countless formulas. Also in this system, the magnetic force per unit length between two wires is given by $dF/dl = 2I_1 I_2 / c^2 d$, likewise eliminating the cluttering appearance of μ_0. The down side is that the unit of charge is the so-called *electrostatic unit* rather than the practical unit of Coulomb; and the unit of charge is the *abamp*, rather than the practical unit of ampere.[62]

We begin with the fundamental harmonic relations between the fields in linear, isotropic media (all systems of units):[63]

$$\mathbf{D}(\omega) = \varepsilon(\omega)\mathbf{E}(\omega) \text{ and } \mathbf{B}(\omega) = \mu(\omega)\mathbf{H}(\omega) \tag{94}$$

Since there may well be a phase shift between the respective quantities, both ε and μ may be complex, and are written $\varepsilon = \varepsilon' + i\varepsilon''$ and $\mu = \mu' + i\mu''$. We further define the complex index of refraction in materials:

$$n(\omega) = n'(\omega) + in''(\omega) = [\varepsilon(\omega)\mu(\omega)]^{1/2} \tag{95}$$

One can show that a transverse electromagnetic wave propagating along the z-axis in a material of index *n* will have the form $\mathbf{E} = \mathbf{E}_0 \exp i(kz - \omega t)$, where $k = n(\omega/c)$ and *n* is complex. As a consequence, a *field* amplitude in a dissipative medium will diminish exponentially with distance, proportional to $\exp[-n''(\omega/c)z]$. The corresponding power will diminish exponentially with distance, proportional to $\exp[-2n''(\omega/c)z]$.

Qualitative Physics: Insulators. We will only consider non-magnetic materials, for which $\mu = 1$. For most materials that are transparent at optical frequencies, $\varepsilon'' = 0$ (no absorption nor phase shift), and $\varepsilon'(\omega)$ is relatively constant, apart from a slight dispersion resulting from absorption in the UV. This follows from the fact that incident quanta are

---

[61] John David Jackson, *Classical Electrodynamics*. John Wiley & Sons (1998).

[62] For the student terminally frustrated by electromagnetic units, I recommend that you consult both the second and third editions of Jackson. The second edition is written with esu units, and the third edition in SI units.

[63] The quantities ε and μ are known as the permittivity and magnetic permeability, respectively.

not energetic enough to excite interband transitions at optical frequencies. Beyond optical frequencies (in the ultraviolet and beyond), ε exhibits complex resonant behavior, incorporating both real and imaginary parts.

Qualitative Physics: Conductors. A useful qualitative model for conductors is the so-called Drude model. In this model, a conductor can be regarded as a uniform, positively charged insulator as described above, plus a sea of conduction electrons that can move with a relaxation time $\tau = 1/\gamma_0$. The permittivity can then be written

$$\begin{aligned}\varepsilon(\omega) &= \varepsilon_b(\omega) + i\frac{4\pi Ne^2}{m\omega(\gamma_0 - i\omega)} \\ &= \varepsilon_b(\omega) + i\frac{\omega_p^2}{\omega(\gamma_0 - i\omega)} \\ &\cong \varepsilon_b(\omega) - \frac{\omega_p^2}{\omega^2} \text{ for } \omega \gg \gamma_0\end{aligned} \tag{96}$$

For good conductors, $\omega \gg \gamma_0$ at optical frequencies, so the final line in Equation (96) applies.

Reflection by conductors. It is well known that polished electrical conductors, such as semiconductors and metals, are shiny. That is, electromagnetic radiation is partially reflected and partially absorbed. For light passing from medium 1 to medium 2 at normal incidence, the reflected and transmitted (absorbed) intensities are given by[64]

$$R = \left|\frac{n_1 - n_2}{n_1 + n_2}\right|^2 \text{ and } T = 4\frac{\mathrm{Re}(n_1)\,\mathrm{Re}(n_2) + \mathrm{Im}(n_1)\,\mathrm{Im}(n_2)}{\left|n_1 + n_2\right|^2} \tag{97}$$

It is straightforward to show that $R + T = 1$. Moreover, in practical cases, material #1 is transparent, in which case $\mathrm{Im}(n_1) = 0$.

The electric field within a medium of index n is proportional to $\exp[-n''(\omega/c)z]$. The time-averaged intensity at depth z is given by the time-averaged square of the magnitude of the electric field, where $\lambda_0 \equiv c/f_0 = 2\pi c/\omega_0$ is the free-space wavelength:

$$\begin{aligned}I &\propto \exp[-2n''(\omega/c)z] \\ &= \exp(-4\pi n'' z/\lambda_0)\end{aligned} \tag{98}$$

[64] John David Jackson, *Classical Electrodynamics*. John Wiley & Sons (1998). See, *e.g.* problem 7.6.

Thus, the intensity diminishes to 1/*e* in a distance $d(\omega) = \lambda_0 / 4\pi n''(\omega)$, which for gold at 635 nm is about (635 nm/4π/3.3) = 15 nm, which is about one-third the 50 nm gold foil thickness.[65]

It should be noted that the above analysis is for normal incidence. The analysis for oblique incidence is much more complicated and is polarization dependent. The interested reader may refer to Stratton.[66]

Reflection and refraction conventions: *s* and *p*. The *plane of incidence*, sometimes known as the *plane of scattering*, is the plane defined by **k** (the incident wave vector) and **n** (the normal to reflecting surface). (It turns out that the incident wave vector, reflected wave vector, refracted wave vector, and normal to the reflecting surface all lie in the scattering plane). The letter *s* stands for the German *senkrecht*, meaning *perpendicular*, signifying that the electric field vector is *perpendicular* to the scattering plane. The letter *p* stands for both the German and the English word *parallel*. For *p*-scattering, the electric field vector lies *in* the scattering plane.

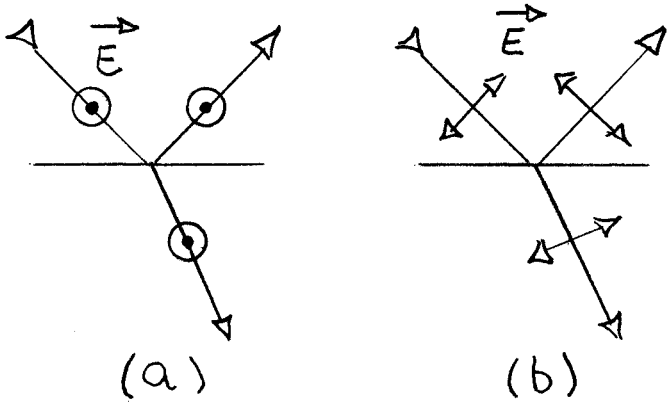

Figure 15. The polarization convention: (a) illustrates *s* polarization (**E** perpendicular to the scattering plane), and (b) illustrates *p* polarization (**E** parallel to the scattering plane). The scattering plane is the plane of the illustration, defined by **k** and **n**.

[65] The distance $d(\omega)$ is known as the *skin depth*.
[66] J. A. Stratton, *Electromagnetic Theory*. McGraw-Hill, New York (1941).

WIND TUNNEL AND AERODYNAMICS

INTRODUCTION

The systematic study of fluid dynamics (also called *fluid mechanics*, *hydrodynamics* and *aerodynamics*, depending upon the emphasis) goes back to the work of Stokes, Navier, Bernoulli, and Poiseuille in the early to mid 1800's.

The flow of a fluid is mathematically characterized by a (vector) velocity field $\mathbf{v}(x,y,z,t)$ and by a (scalar) pressure field $P(x, y, z, t)$. The velocity $\mathbf{v}$ is the velocity of a tiny speck of material at location $\mathbf{X}(t)$. More formally, $\mathbf{v}$ is defined as

$$\mathbf{v}(x, y, z, t) = \lim_{\Delta t \to 0} \frac{\mathbf{X}(t + \Delta t) - \mathbf{X}(t)}{\Delta t} . \tag{99}$$

The complete equation of fluid flow is given by the Navier-Stokes equation:

$$\rho \left\{ \frac{\partial \mathbf{v}}{\partial t} + (\nabla \times \mathbf{v}) \times \mathbf{v} + \frac{1}{2} \nabla v^2 \right\} = -\nabla P - \rho \nabla \phi + \eta \nabla^2 \mathbf{v} + (\eta / 3 + \eta') \nabla (\nabla \bullet \mathbf{v}) \tag{100}$$

In these equations, ρ is the density of the fluid, η is the shear viscosity, ϕ is the gravitational potential, and η' is the bulk viscosity. The shear viscosity, which is of concern to us, reflects the tendency for a fluid to frictionally resist gradients in the flow velocity for parallel streams. The bulk viscosity reflects the tendency of a fluid to resist expansion or compression. Bulk viscosity plays a significant role in the dissipation of sound waves, and in energy dissipation associated with supersonic (shock) waves.

We don't expect you to solve these equations over the next three weeks, mainly because no one has ever yet solved them! As a matter of fact, a $1M prize[67] has been offered to anyone who can exactly solve a certain subset of these equations. A close inspection will reveal that the equations are nonlinear, which means that we can no longer fall back on the principle of superposition, as we could with electrodynamics. We will thus have to content ourselves with very special cases, which can be solved exactly or at least measured phenomenologically in the laboratory. For example, in this laboratory we will make the common assumption that the fluid is incompressible, which enables us to set the last term in equation (100) equal to zero. This is an excellent approximation if the fluid velocities are well below the speed of sound in the fluid, and if we are not interested in the generation, propagation, or attenuation of sound. In what follows, we shall study the effect of either including or neglecting the shear viscosity η.

[67] Keith J. Devlin, *The Millenium Problems: The Seven Greatest Unsolved Mathematical Puzzles of our Time*. Basic Books, 2002.

INVISCID FLOW

Navier stokes with no viscosity. Unfortunately, only two substances are known to have zero viscosity: ^{4}He below 2.7K and ^{3}He below 0.001K. These substances are known as superfluids, and they possess amazing properties. Nevertheless, it turns out that for many purposes we can neglect the fluid viscosity in ordinary liquids and gases as a first approximation. For example, as you learned in freshman physics, for a conservative (non-dissipative) system, conservation of energy for steady fluid flow[68] leads to *Bernoulli's equation*:

$$\frac{1}{2}\rho v^2 + \rho g y + P = \text{constant} \tag{101}$$

The first term, $(1/2)\rho v^2$, is the kinetic energy density; the second term, $\rho g y$, is the potential energy density; and the third term, P (pressure) accounts for internal forces tending to push the fluid one way or another. For horizontal motion, y is constant, and in such cases one can immediately conclude that, along a stream line, high fluid speeds are accompanied by low pressures, and *vice versa*. Bernoulli's equation reflects the fact that in a conservative system a force, and thus pressure difference, is required to accelerate particles from low velocity to high velocity, and vice versa.

Bernoulli's equation explains why a fireplace draws better on windy evenings; how a perfume atomizer works; how a carburetor works; how a garden hose fertilizer dispenser works; how a Venturi tube works; and how you can balance a ping-pong ball on an air stream.

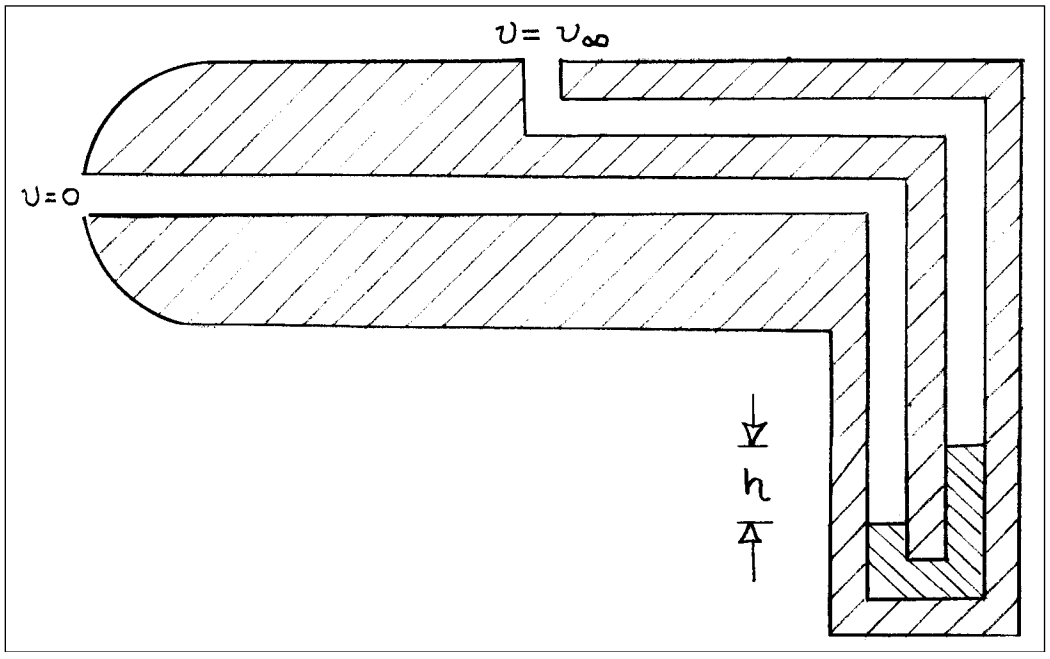

[68] By "steady" we mean that at any point in space, **v** and p do not change with time. In such cases, we can draw "streamlines," which are curves in space everywhere parallel to **v**.

Figure 16. Schematic diagram of a Pitot tube with manometer.

An important application of Bernoulli's principle is the Pitot tube (see Figure 16). The Pitot tube is commonly used to measure airspeed in ventilation ducts, *etc*. It is also used to measure aircraft airspeed (you can usually see the ports on the wing from a passenger seat).[69] The pressure difference between the tip of the tube ($v = 0$) and the side of the tube ($v = v_\infty$) is equal to $\rho_a v_\infty^2 / 2$. Thus, $(1/2)\rho_a v_\infty^2 = \rho_w g h$ if the manometer fluid is water and the height difference is *h*.

Although it is not at all obvious, Bernoulli's principle also explains how an airplane wing has *lift*: A tilted airplane wing, even with a simple elliptical cross-section, will experience lift in an air stream, because the pattern of air flow will result in higher average air speeds above the wing than below the wing, and thus result in lower average pressures above the wing than below it. This effect will depend upon the angle of the wing relative to the flow direction (angle of attack), and can be calculated analytically for many wing shapes. The lift force *F* (perpendicular to the average fluid flow) on an airfoil of length *w* and chord *c* depends upon the angle of attack α, and is usually parameterized by the following expression (see Figure 17):[70]

$$F = K \bullet C_L(\alpha) \bullet (\frac{1}{2}\rho v^2) \bullet (c \bullet w) \qquad (102)$$

For the limiting case of wings with a thin cross-section, and neglecting viscosity, $C_L = 2\pi \sin\alpha$. For thick wings, and incorporating viscosity, the coefficient must either be calculated or measured. *K* is a dimensionless correction factor if the wing is stubby (short relative to the chord); *i.e.* if $c/w > 0.2$. To a good approximation,[71] $K = (1 - 0.86c/w)$.

If the cross section of the airfoil is *up-down symmetric* (as with the elliptical cross section shown in Figure 17), there will be zero lift when the symmetry plane is parallel to the air flow. In this simple case the angle of attack α is just the tilt angle of the symmetry plane of the airfoil relative to the air flow.

Air foils of modern aircraft are usually not perfectly up-down symmetric, in order to reduce drag (the viscous force on the wing in the direction of the air flow). The angle of attack is defined as the tilt angle between the camber plane (Figure 21) and the flow direction. As a consequence, the lift may or may not vanish at zero angle of attack.

---

[69] On June 1, 2009, Air France flight 447 crashed into the Atlantic Ocean when its Pitot tubes iced over. For a fascinating account, and further references, consult the Wikipedia article.

[70] For a given wind speed, if the angle of attack exceeds a certain limit, the lift abruptly vanishes. This is a common cause of airplane crashes.

[71] Ira Abbott and Albert E. Doenhoff, *Theory of Wing Sections.*

It is useful to note that equation (102) is the product of a characteristic pressure, $(\rho v^2 / 2)$; the projected area of the wing ($c \bullet w$); and two dimensionless numbers of order unity. Dimensionally it has the units of force, as it should.

Appendices IV and V give references to simulation software that provides lift and drag coefficients for more complicated wing profiles.

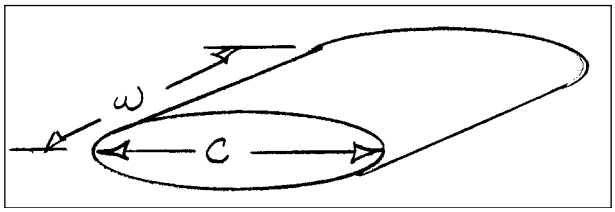

Figure 17. Cross section of an elliptical wing.

VISCOUS FLOW

Alas, all practical fluids have *viscosity*, which is a form of internal friction that resists shearing motion in fluids, resulting in the conversion of kinetic energy into heat. Viscosity accounts for the terminal velocity of falling objects; for the drag force on an airplane wing, boat, or motor vehicle; for the pressure difference required to force a fluid through a tube or pipe of constant cross-section; and so forth.

Drag on a sphere. A smooth sphere will experience a drag force **F** directed parallel to the fluid velocity. The drag force on a sphere immersed in a fluid with asymptotic speed **v** is given by

$$\Re \equiv \frac{\rho v D}{\eta}$$

$$\mathbf{F} = -6\pi\eta R\mathbf{v} \text{ for } \Re(v) < 1000 \text{ (Stokes' law)} \qquad (103)$$

$$|F| = C_D(\Re) \bullet \frac{1}{2}\rho v^2 \bullet \pi R^2 \text{ for } \Re(v) > 1000$$

The quantity $\Re \equiv \rho v D / \eta$, a dimensionless quantity, is known as the *Reynolds number*, where $D=2R$ is the characteristic length scale of the object (in our case, the diameter of the sphere), and $v = |\mathbf{v}|$ is the mean fluid speed. It is roughly a measure of the ratio of inertial forces to viscous forces in the fluid.[72] It is by far the most important constant in fluid dynamics, for the following reason: If two experiments are geometrically similar (that is, all dimensions are reduced or increased by the same scale factor), and if the asymptotic speed v, the viscosity η, and the density ρ are also scaled to keep $\Re$ constant, then the flow pattern will be *exactly* the same. As a consequence, one may build scale models of, for example, an aircraft, and if all parameters are appropriately scaled, the flows will exactly match. It should also be pointed out that for air speeds approaching or exceeding the speed of sound v_s, one must also match the Mach number, $M \equiv v / v_s$.

[72] Stokes law applies, for example, to falling oil drops in the Millikan experiment, molecules in a centrifuge, airborne dust and aerosols, *etc*.

In the second expression in (103), C_D is known as the *drag coefficient*, a dimensionless number of order unity. The measured drag coefficient for a sphere is shown in Figure 19 in the appendices. For an arbitrary object, such as an airplane wing, the drag force will be defined accordingly, by substituting the cross-sectional area of the object for the cross-sectional area of the sphere, πR^2. For modern sedan-style motor vehicles, the drag coefficient, which dominates gasoline mileage at high speeds, is of order 0.3

There is a tremendous amount of physics embedded in equation (103), as described in the chapters in Feynman.[73] However, the complicated physics pretty much boils down to a drag force which is proportional to the speed at low speeds, and proportional to the square of the speed at high speeds.

Viscous Flow in a tube. If we define the Reynolds number $\Re$ for flow in a tube using the diameter of the tube as the characteristic length, and the average velocity $\bar{v}$ as the characteristic velocity (see eq. (105) below), then the pressure drop is related to the mean fluid velocity by

$$\begin{aligned} \Re &\equiv \frac{\rho \bar{v} D}{\eta} \\ P_1 - P_2 &= \frac{8\eta L \bar{v}}{R^2} \quad \Re < 1000 \\ P_1 - P_2 &= f(\Re)\frac{L}{D}\frac{1}{2}\rho \bar{v}^2 \quad \Re > 1000 \end{aligned} \tag{104}$$

The first expression is known as Poiseuille's law, and applies in the limit of high viscosity, low speeds, or small diameters. In this limit, the speed of the fluid depends upon the distance of the streamline from the axis of the tube, and approaches zero at the tube boundaries.[74] The second expression applies in the limit of low viscosity, high speeds, or large diameter tubes. The dimensionless factor $f(\Re)$ is known as the friction coefficient, and is graphed in the Appendix.[75] In this limit the speed of the fluid is approximately independent of the distance of the streamline from the axis, until one reaches very close to the inner surface of the tube, where the velocity drops rapidly to zero.[76] The respective velocities are given as follows, for a tube of radius *R*:

$$\begin{aligned} v(r) &= v(0)(1 - r^2 / R^2) \quad \Re < 1000 \\ v(r) &= v(0) \quad \Re > 1000 \end{aligned} \tag{105}$$

---

[73] Richard P. Feynman, Robert Leighton, and Matthew Sands, *The Feynman Lectures on Physics*, Vol. II. Addison Wesley, 1964.

[74] For example, the flow of blood in capillaries.

[75] James E. A. John and William L. Haberman, *Introduction to Fluid Mechanics***.** (Prentice Hall, 1988)

[76] This thin region is called the *boundary layer*.

EXPERIMENT 1: PITOT TUBE

Using the propeller-based velocity meter, measure the wind velocity in the wind tunnel as a function of the voltage applied to the wind tunnel fans, up to a maximum of 16 volts. At the same time, record the pressure difference in the Pitot tube. Plot the velocity as recorded by the meter versus the velocity as determined by the Pitot tube. How well do they agree?

EXPERIMENT 2: VENTURI TUBE

A Venturi tube is a smooth tube that necks down in a central region. A manometer is set up to measure the relative pressures of the air in the input, central, and output sections of the tube. The Venturi tube is a common instrument for measuring fluid flow.

In order to obtain significant pressure differences, the air velocity will need to be high enough so that it turns out that we will be working in the high Reynolds number regime ($\Re$ >1000) in all sections of the tube. Denote D_1, D_2, and D_3 to be the diameters of the input, central, and output sections (with $D_1 = D_3 = 16$ mm and $D_2 = 5.2$ mm).

Let's define P_1, P_2, and P_3 to be the pressures in sections 1, 2, and 3 as measured by the manometers. Note that the relative pressures will be equal to $-\rho_w gh$, where h is the height of the liquid relative to some fixed base line. The pressure in the Venturi tube as a function of position along the axis is shown schematically in Figure 18. Notice that at the entrance and exit boundaries of the constriction, the pressure first drops abruptly by ΔP_B,

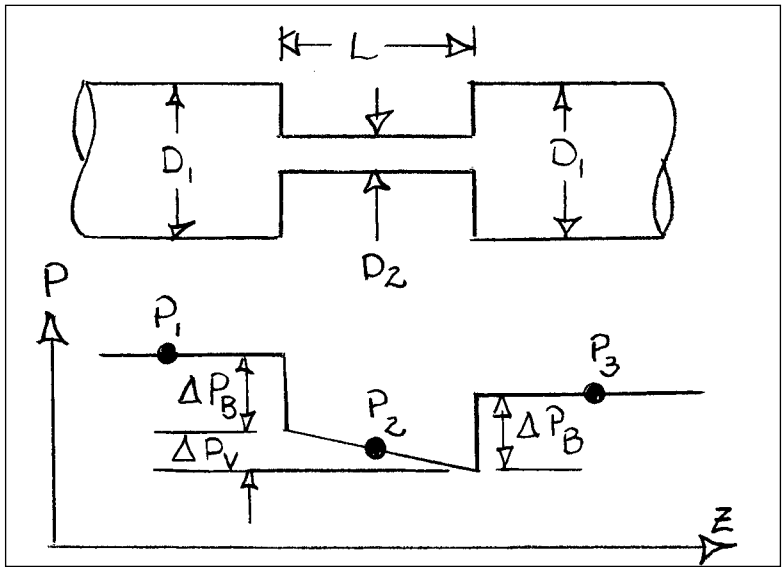

Figure 18. Pressure vs. distance in a Venturi tube.

and then rises abruptly by ΔP_B, due to the Bernoulli effect. Meanwhile, the pressure falls approximately linearly in the constriction itself, by an amount ΔP_V, due to the pressure drop arising from the viscosity of the fluid. From the figure, we can relate these quantities to the actual pressures measured:

$$\Delta P_V = P_1 - P_3$$
$$\Delta P_B = \frac{1}{2}(P_1 + P_3) - P_2 \tag{106}$$

We expect these quantities to be

$$\Delta P_V = f(\Re)\frac{L}{D_2}\frac{1}{2}\rho\bar{v}_2^2 \quad \text{(Due to viscosity)}$$
$$\Delta P_B = \frac{1}{2}\rho\bar{v}_2^2 - \frac{1}{2}\rho\bar{v}_1^2 \quad \text{(Bernoulli effect)} \tag{107}$$

Where L is the length of the constriction, D_2 is the diameter of the constriction, and $\bar{v}_2$ is the average speed of the fluid in the constriction.

Since we may neglect the compressibility of the air, the volume flow rate Q is given by

$$Q = A\bar{v} = \frac{\pi}{4}D_1^2\bar{v}_1 = \frac{\pi}{4}D_2^2\bar{v}_2$$
$$\Rightarrow \frac{\bar{v}_1^2}{\bar{v}_2^2} = \frac{D_2^4}{D_1^4} = 0.011 << 1 \tag{108}$$

Therefore, we can neglect $\bar{v}_1^2$ in comparison with $\bar{v}_2^2$ in the Bernoulli equation, and equations (107) reduce to

$$\Delta P_V = f(\Re)\frac{L}{D_2}\frac{1}{2}\rho\bar{v}_2^2 \quad \text{(Due to viscosity)}$$
$$\Delta P_B = \frac{1}{2}\rho\bar{v}_2^2 \quad \text{(Bernoulli effect)} \tag{109}$$

Notice that both the Bernoulli and viscosity pressure changes are proportional to $\bar{v}_2^2$, so we may write

$$\Delta P_V = f(\Re)\frac{L}{D_2}\Delta P_B \tag{110}$$

Substituting (106) into (110), we can solve for the friction factor:

$$f(\Re) = \frac{D_2}{L}\frac{(P_1 - P_3)}{((P_1 + P_3)/2 - P_2} \tag{111}$$

With these remarkable results, we can calculate the mean air velocities in the pipes from the known pressure differences, and we can evaluate the friction factor from the ratios of the pressures.

Experiment. Using the air supply, blow air into the Venturi tube and measure the relative heights of the manometer liquid (in this case water) in sections 1, 2, and 3. Determine the mean values of the air speed in the wide and narrow sections of the tube, and determine the friction factor.[77] From your velocity calculations, determine the Reynolds number in the central region of the tube.

You may notice that for a given setup, the manometer pressure is bistable. This is because at this flow rate, the flow can alternately fluctuate between a laminar state (low *f*) and turbulent state (higher *f*). Such flows are said to be in the *critical zone*. At significantly lower flow rates the flow is consistently laminar, and at higher flow rates the flow is consistently turbulent.

EXPERIMENT 3: PING-PONG BALL ON A FOUNTAIN

1. If you drop a ping-pong ball, it will accelerate until it reaches a limiting velocity called the *terminal velocity*. This is the speed for which the viscous drag is equal and opposite to the weight force. Referring to equations (103), determine which equation is appropriate and calculate the terminal velocity of a ping pong ball in air. (Hint: the mass is 2.7 grams and the diameter is 4.00 cm.) What is the approximate Reynolds number at the terminal velocity?

2. Balance a ping-pong ball on the output air stream of the air supply.
   a) With the Pitot tube, measure and record the on-axis air speed from the nozzle to past the stability point of the ball.
   b) From the fact that the ball is perched at a stable position above the orifice, estimate the velocity of the air at the ball.
   c) With the Pitot tube, measure and record the air speed as a function of the radial distance from the flow axis, at the stability height. Explain the lateral stability of the ping pong ball.

EXPERIMENT 4: PING-PONG BALL IN THE WIND TUNNEL

1. Calibrate the fan power supply by measuring the wind speed as a function of power supply voltage.

2. Suspend a ping-pong ball in the wind tunnel and measure the angle of the string relative to the vertical direction as a function of wind speed.

   a) Calculate the Reynolds number of the ball at each wind speed.
   b) Derive a formula for the angle of the string as a function of the Pitot tube reading.
   c) Predict the angle of the string as a function of wind speed, and compare with your measurements.

[77] You may notice that your result for the friction factor is significantly higher than the published value. This may be because of turbulence introduced by the manometer connection to the Venturi tube. How would you improve the setup?

EXPERIMENT 5: LIFT ON AN AIRFOIL

There are three model airfoils provided with the experiment. Please measure the lift coefficients of each of these airfoils, and compare the lift with equation (102). You will notice that there is "lift" on the electronic balance in the absence of a wing section. Can you explain this phenomenon? How might you take it into account?

APPENDIX I: USEFUL CONSTANTS

Density of water	$\rho_w = 1.00 \times 10^3$ kg/m^3
Density of air	$\rho_a = 1.20$ kg/m^3
Viscosity of air	$\eta = 1.78 \times 10^{-5}$ SI units
Specific viscosity of air	$\eta/\rho_a = 1.486 \times 10^{-5}$ m^2/s

APPENDIX II: DRAG COEFFICIENT FOR A SPHERE

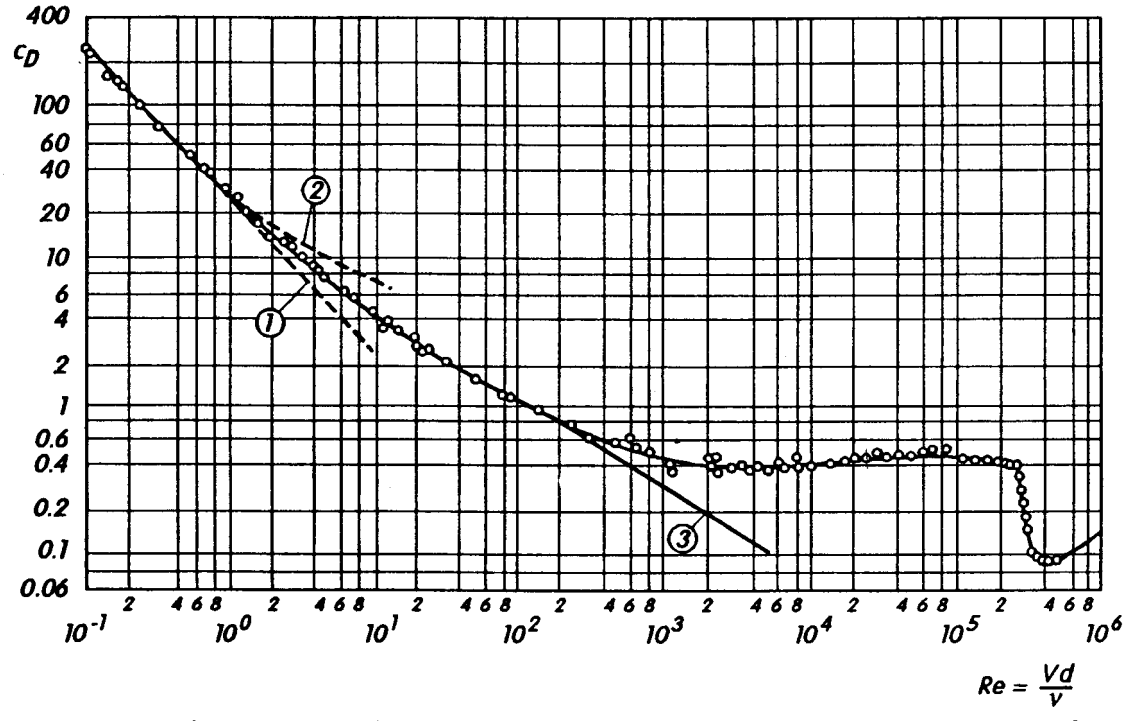

Figure 19. Drag coefficient on a sphere versus Reynolds number.

APPENDIX III. FRICTION COEFFICIENT FOR A SMOOTH PIPE

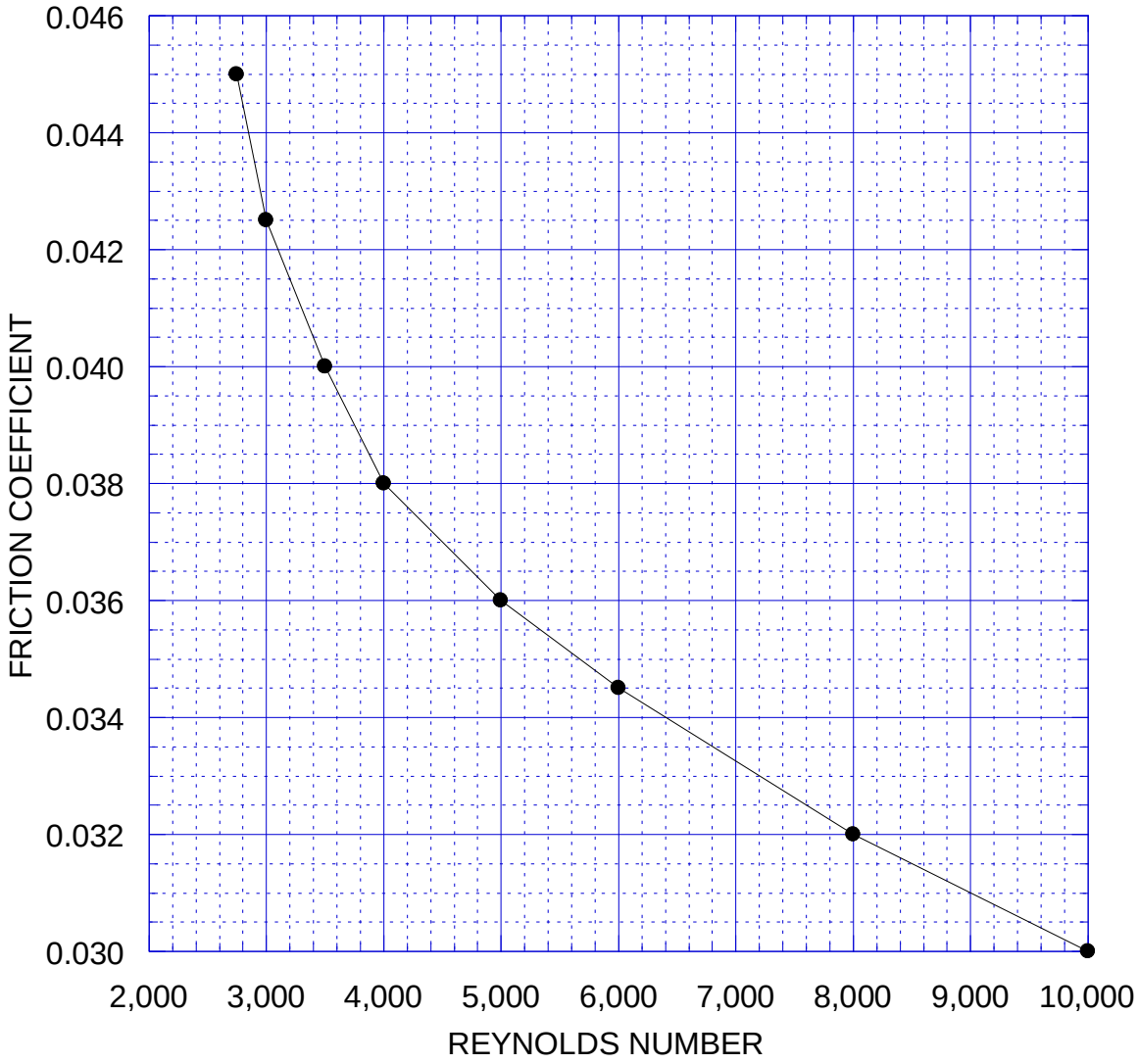

Figure 20. The friction coefficient $f(\Re)$ in a cylindrical pipe as a function of the Reynolds number.

APPENDIX IV. USEFUL VISUALIZATIONS ON THE INTERNET

Reducing Drag: Useful visualization comparing the orientation of an airfoil to its resulting drag. It even compares the airfoil drag to the drag produced by a rod of equal diameter of the maximum thickness of the airfoil. Introduces Bernoulli's principle. Very useful diagrams.
http://techtv.mit.edu/collections/ifluids/videos/32600-fluid-dynamics-of-drag-part-4

Flow Visualization: At 5 min, there is a neat demonstration of flow around an airfoil, clearly showing the relationship between the airfoil angle and the relative velocities of the air above and below the foil.
http://techtv.mit.edu/collections/ifluids/videos/32598-flow-visualization

Drag at low Reynold's number: Interesting explanation of the situational relationship of drag, depending of speed, object size, and fluid viscosity. Shows that inertial forces are negligible at low R (Up to 16 min).
http://techtv.mit.edu/collections/ifluids/videos/32602-fluid-dynamics-of-drag-part-3

Fluid acceleration: Useful to visualize the Venturi tube. See at a little before 4 min. Pitot tube after 8 min.
http://techtv.mit.edu/collections/ifluids/videos/32607-pressure-fields-fluid-acceleration

* indicates the most relevant and useful videos

APPENDIX V. SIMULATION SOFTWARE

Simulating your airfoil using XFLR5

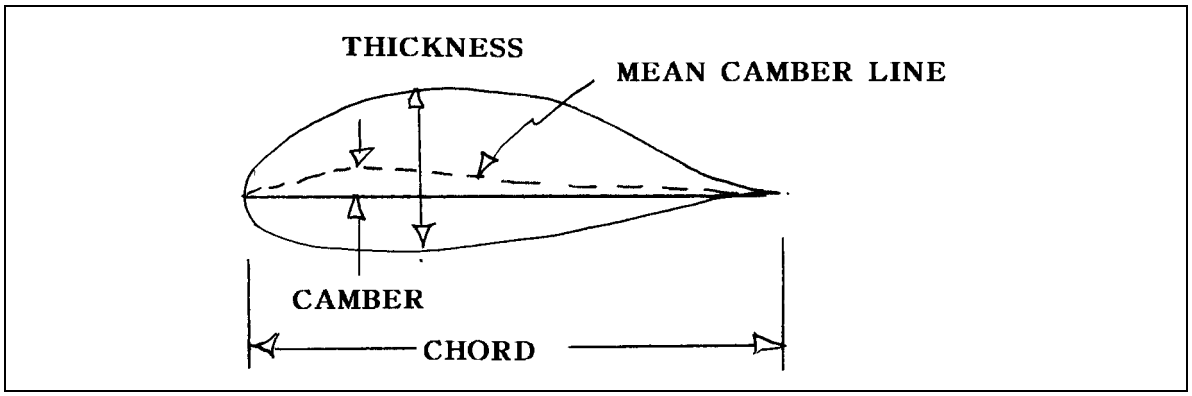

Figure 21. Airfoil nomenclature.

Characterizing Airfoils
In order to simulate your airfoil, you must specify its dimensions. Airfoils are specified by three principal dimensions: chord, camber, and maximum thickness:[78]

- *Chord* - the length of the airfoil from the leading edge to the trailing edge.
- *Mean Camber Line* - Each point on the mean camber line is the halfway point between the upper and lower edges of the airfoil. For a symmetric airfoil, this line will fall directly on the chord.
- *Camber* - the maximum distance between the chord line and mean camber line.
- *Maximum thickness*.

The camber and maximum thickness are usually given as a percentage of the chord length. For instance, if you have an airfoil of chord length 10 cm, a maximum thickness

[78] https://www.grc.nasa.gov/www/k-12/airplane/geom.html

of 2 cm at 3 cm from the leading edge, and a camber of 1 cm at 4 cm from the leading edge, you will define the camber and maximum thickness as follows:

- Camber = 10% at 40% chord
- Maximum thickness = 20% at 30% chord

Loading airfoils on XFLR5

- File > XFoil Direct Analysis
- View > OpPoint View (i.e. Airfoil view)
- There are several databases that describe airfoil specifications and provide .dat files that you can load to XFLR5. Search through http://airfoiltools.com/ and download the source as a .dat file of the airfoil.
- To load airfoil
    - Airfoils from the Naca database, which are already included in the XFLR software:
      Design > Naca Foil > [enter 4 or 5 digit code of desired foil design]
    - Any other airfoil or Naca airfoils with other amounts of digits must be downloaded, and can be loaded from
      File > Open > [select file]
- To ensure a smooth distribution of the airfoil
  Design > Refine Globally > Sets number of panels to somewhere between 100 to 150
- Airfoil parameters can be adjusted from
  Design > scale camber and thickness
- The airfoil used in these experiments has a thickness of 20.3% at 25% chord. You can use the S7055 flat bottom airfoil [http://airfoiltools.com/airfoil/details?airfoil=s7055-il] and adjust its geometry to fit these parameters

Analysis

- Analysis > Define Analysis
- select 'Type 1' [for airfoils], set Reynolds number to 10000
- In 'Direct Foil Analysis' window that pops up, click analyze
    - You can adjust the properties of the graph in this window to make the plots more visible
    - Select 'Show Pressure' for vector visualization of the pressure on your airfoil
    - Select 'BL' for a boundary layer visualization
- To create a simulation, in the 'Direct Foil Analysis' window:
    - Check the 'Sequence' box
    - Set range [in degrees] for start and stop in simulation. First set the positive range (i.e. 0 −10 degree) and analyze, then set the negative range (i.e. −10 - 0 degree) and analyze
    - Delta sets the step size
    - Upon running the simulation, the range of angles in indicated by a pull-down menu with each degree simulated. [If any angles specified in the boundary conditions are missing, this means that the analysis at that degree converged]

- Select a data point to view its results, or right click the plot and select "show all points" to view all
- Select "polar view" to see a polar plots
- C_l is the lift coefficient, C_d is the drag coefficient. The program provides plots of C_l with respect to angle and C_d by default. C_p is a pressure dependent variable.
- The variables plotted can be changed by double clicking a graph and selecting the desired variables.
- Can observe the '*critical Reynold's number*', at which the behavior of the airfoil will be turbulent

If you have time, use XFLR5 to simulate your airfoil and compare to your experimental results and a simulated airfoil of your choice.

Airfoil A dimensions:
Chord = 9.8 cm
Camber = 9.3% at 30% chord (0.9 cm at 3 cm)
Maximum thickness = 18.4% at 30% chord (1.8 cm at 3 cm)

Airfoil B dimensions:
Chord = 9.3 cm
Camber = 0% at 0% chord (symmetric)
Maximum thickness = 19.4% at 32.3% chord (1.8 cm at 3 cm chord)

Airfoil C dimensions:
Chord = 9.8 cm
Camber = 7.7% at 15.3% chord (0.75 cm at 1.5 cm)
Maximum thickness = 15.3% at 15.3% chord (1.5 cm at 1.5 cm chord)

X-RAY FLUORESCENCE

LABORATORY OBJECTIVES

The objective of this laboratory is to understand the phenomenon of x-ray fluorescence, and to understand methods of generating and detecting x-rays.

INTRODUCTION

Fluorescence is the general property of atoms and molecules to emit light subsequent to excitation by light, by electrons, or by other projectiles. Fluorescence is commonly observed at visible wavelengths; it is the workhorse of fluorescent light bulbs. It is also a common property of atoms at x-ray wavelengths.

H. G. J. Moseley was able to subject 21 elements to an x-ray beam, creating single K-shell vacancies, and study the fluorescence resulting from the transition of an L-shell electron into the K vacancy. He discovered an amazing regularity, which settled once and for all the atomic number assignments of the elements.[79] Sadly, Moseley was killed in the collective madness known as World War I, vividly described in a book by Paul Fussel.[80]

X-ray fluorescence is a common and powerful analytical technique for measuring impurity concentrations in materials.

PHYSICS

As you learned from your introductory quantum mechanics courses, negatively charged electrons organize themselves in shells around the positively charged nucleus. Each shell is characterized by a binding energy, which is the threshold photoelectric energy required to remove an electron from a given shell. The correspondence between the x-ray notation for the inner shells, and the atomic spectroscopic notation, is given below. We include the binding energies for metallic copper as a specific example.

K	$1s_{1/2}$	8978.9 eV
L_I	$2s_{1/2}$	1096.7 eV
L_{II}	$2p_{1/2}$	952.3 eV
L_{III}	$2p_{3/2}$	932.7 eV
M_I	$3s_{1/2}$	122.5 eV
M_{II}	$3p_{1/2}$	77.3 eV
M_{III}	$3p_{3/2}$	75.1 eV
M_{IV}	$3d_{3/2}$	1.6 eV
M_V	$3d_{5/2}$	1.6 eV

Table 9. The binding energies of electrons for metallic copper.

If an atom is bombarded by an energetic charged particle or by x-rays, an electron in one of the shells may be removed, leaving behind a vacancy, that has a lifetime of roughly 10^{-16} seconds. (Fast electrons may also create x-rays by colliding with the nucleus,

[79] H. G. J. Moseley, *Phil. Mag*. **26,** 1024 (1913) and **27**, 703, (1914).
[80] Paul Fussel, *The Great War and Modern Memory*.

resulting in continuum x-radiation, known as *bremsstrahlung* or braking radiation.) That vacancy, or hole, will be filled by an electron in a shallower energy shell. As this shallower energy electron falls into the hole, it emits a photon with energy equal to the difference in the respective energy levels. These photons are called fluorescent x-rays. The nomenclature for most x-ray transitions is shown in Table 10 below. For a more complete tabulation, see Figure 22 in the appendix.

	VACANCY→	K ($1s_{1/2}$)	L_1 ($2s_{1/2}$)	L_2 ($2p_{1/2}$)	L_3 ($2p_{3/2}$)
DONOR ↓					
L_1 ($2s_{1/2}$)					
L_2 ($2p_{1/2}$)		**Kα₂**			
L_3 ($2p_{3/2}$)		**Kα₁**			
M_1 ($3s_{1/2}$)				Lη	L*l*
M_2 ($3p_{1/2}$)		Kβ$_3$	Lβ$_4$		
M_3 ($3p_{3/2}$)		**Kβ₁**	Lβ$_3$		
M_4 ($3d_{3/2}$)				**Lβ₁**	**Lα₂**
M_5 ($3d_{5/2}$)					**Lα₁**
N_1 ($4s_{1/2}$)				Lγ$_5$	Lβ$_6$
N_2 ($4p_{1/2}$)		Kγ$_2$	Lγ$_2$		
N_3 ($4p_{3/2}$)		Kγ$_1$	Lγ$_3$		
N_4 ($4d_{3/2}$)				**Lγ₁**	Lβ$_{15}$
N_5 ($4d_{5/2}$)					**Lβ₂**
N_6 ($4f_{5/2}$)					
N_7 ($4f_{7/2}$)				Lγ$_8$	Lβ$_7$

Table 10. Nomenclature for allowed X-ray fluorescence transitions. Entries in boldface are the strongest transitions and are tabulated in the LBNL handbook.

You may recall that electric dipole transitions always satisfy the selection rules $\Delta j = 0, \pm 1$ and $\Delta l = \pm 1$. Therefore, the only transitions resulting in dipole radiation are $s \leftrightarrow p$, $p \leftrightarrow d$, and $d \leftrightarrow f$. And, of course, energy must be conserved. This explains why many of the entries in Table 10 are blank.

The strongest x-ray emission lines resulting from the bombardment of a material with energetic x-rays or electrons are the $K\alpha_1$ and $K\alpha_2$ lines, which are so close together that they can only be resolved with a crystal analyzer. If we suppose that the K and L energies are approximated with an atomic hydrogen model with energies $E_n = -R_y Z_{eff}^2 / n^2$, we get

$$E_K = -R_y (Z - \sigma_K)^2 \quad E_L = -\frac{1}{4} R_y (Z - \sigma_K)^2$$
$$E_L - E_K \approx \frac{3}{4} A (Z - \sigma_K)^2 \tag{112}$$

Where we have introduced the empirical parameters A and σ to account for the screening. The result gives a surprisingly good fit to the data.

EXPERIMENTAL METHOD

In our experiment, continuum bremsstrahlung x-rays are generated by bombarding a silver anode with electrons in vacuum. The resulting x-rays then emerge through a beryllium window into air, and proceed to excite target atoms of our choice.

Note that the anode voltage can be adjusted between 10 kV and 40 kV, and the anode current can be adjusted between 5 and 200 microamperes. You should try to run at the lowest possible current (5 μA), to keep the counter from overloading. Under no circumstances should you run the tube power at levels (V*I) greater than 4,000 milliwatts. Also note that the maximum x-ray energy, by conservation of energy, is equal to the anode voltage. As a consequence, you will only be able to study vacancies with energies less than the anode voltage.

The detector is a single crystal of highly purified silicon, which has a high voltage impressed across it. An incident x-ray deposits all of its energy in the crystal, resulting in a pulse whose integrated charge is proportional to the x-ray energy. This charge pulse, which is very weak, is amplified in a stand-alone amplifier, with adjustable gain. The nominal gain should be around 2.9, but feel free to adjust it to your needs. The amplifier output pulse is then registered by a multichannel analyzer, which records the distribution of pulse amplitudes.

The multichannel analyzer has several important features. The foremost feature is the calibration function, which allows the user to define the relationship between the channel number and the photon energy. here is the basic idea:

1. If you give the calibration routine exactly *one* peak, it will assume a linear fit, with channel 0 defined as $E = 0$.
2. If you give the calibration routine exactly *two* peaks, it will also assume a linear fit, but channel 0 will no longer necessarily correspond to $E = 0$.
3. If you give the calibration routine exactly *three* peaks, it will assume a quadratic fit between channel number and energy.
4. If you give the calibration routine more than three peaks, it will determine the best quadratic fit by minimizing the mean square error.

Regions of Interest. Once you have positively identified a candidate calibration peak, you may define it by a Region of Interest (ROI). With the mouse, place the cursor on the background just below the peak. On the ROI menu tab, click `Mark`. Then, using the right arrow (→), manually move the cursor to the background just above the peak. Then, on the ROI menu tab, click `Unmark`. You should then be left with a peak that is colored red. If , with the mouse, you place the cursor anywhere within the ROI, the energy of the centroid of the peak will be numerically displayed, as well as the energy associated with the location of the cursor.

To calibrate on this peak, click on the `Calculate` menu tab and then on the `Calibration` button. The dialog box will ask you what is the energy you wish to assign to the centroid of the peak. Enter that number in electron volts.

It is best to calibrate with peaks that fall on a low or flat background. A sloping background will shift the peak from where it would be if the background were flat. The software does its best to determine the peak position by subtracting a sloping background (determined by the first and last points of the ROI), but this procedure introduces some error in the peak position.

You will notice from the reference tables that some x-ray energies are very close together and therefore unresolvable (e.g. $K\alpha_1$ and $K\alpha_2$). In such cases you should take the weighted average of the peak energies as the energy that you observe. Here are the weighting factors.[81]

1. $K\alpha_1 : K\alpha_2 = 2.0 : 1.0$
2. $L\alpha_1 : L\alpha_2 = 9.1 : 1.0$
3. $L\beta_1 : L\beta_2 = 2.61 : 1.0$

Example: for copper, $K\alpha_1$ = 8047.78 eV and $K\alpha_2$ = 8027.83 eV. So the mean energy is (2.0 x 8047.78 + 1.0 x 8027.83)/(2.0 + 1.0) = 8041.13 eV.

Dead Time. The x-ray generator is not capable of running at a current below 5 microamps. As a consequence, the x-ray count rate for pure materials may saturate the detector if the sample is placed too close to the detector. Saturation manifests itself as a very high "dead time." At dead times greater than about 5%, pulse pileup will cause the peak positions to significantly shift, depending upon the count rate.

To reduce the dead time, simply use one or two of the aluminum rings to offset the sample from the base of the fixture, and run at the lowest possible current. This has the beneficial effect of reducing the count rate.

PROCEDURE

NOTE: PLEASE LEAVE THE SAMPLES IN THE PLASTIC ENVELOPES, WHICH ARE TRANSPARENT TO X-RAYS.

1. Calibrate the multichannel analyzer using the ROI method, with at least three samples; *e.g.* silver (L lines), zirconium, and tin.
2. Record the spectra of at least five of the known samples, and compare the energies observed with the tabulated values.
3. The atomic weight of cobalt is greater than the atomic weight of nickel. From x-ray fluorescence spectra that you take, determine which has the higher atomic number. (Moseley first settled this question in 1914).[82]
4. Determine the chemical composition of a penny, a nickel, a dime, a quarter, a 50 cent piece, a silver dollar, and of the given pottery shard. Would you drink fruit juice from a cup made of similar pottery?

[81] X-Ray Data Booklet

[82] H. G. J. Moseley, *Phil. Mag.* **26,** 1024 (1913) and **27**, 703, (1914).

5. Determine the chemical composition of the three unknown samples.
6. Determine the chemical composition of 316 stainless steel.
7. Determine the chemical composition of one or more samples of your choosing.

FURTHER QUESTIONS

1. Plot the K-shell energies taken from the tables for all of the elements for $Z > 1$ as a function of Z, and fit to the function $E(Z)=A(Z-\sigma)^2$. Is it a reasonable fit? Determine the constant A and the effective screening charge σ. Interpret your results.

REFERENCES

1. The Lawrence Berkeley National Laboratory x-ray data booklet, http://xdb.lbl.gov
2. *Handbook of Chemistry and Physics*. CRC Publishing Company.
3. J. A. Bearden, *Rev. Mod. Phys.* 39, 78 (1967).

APPENDIX

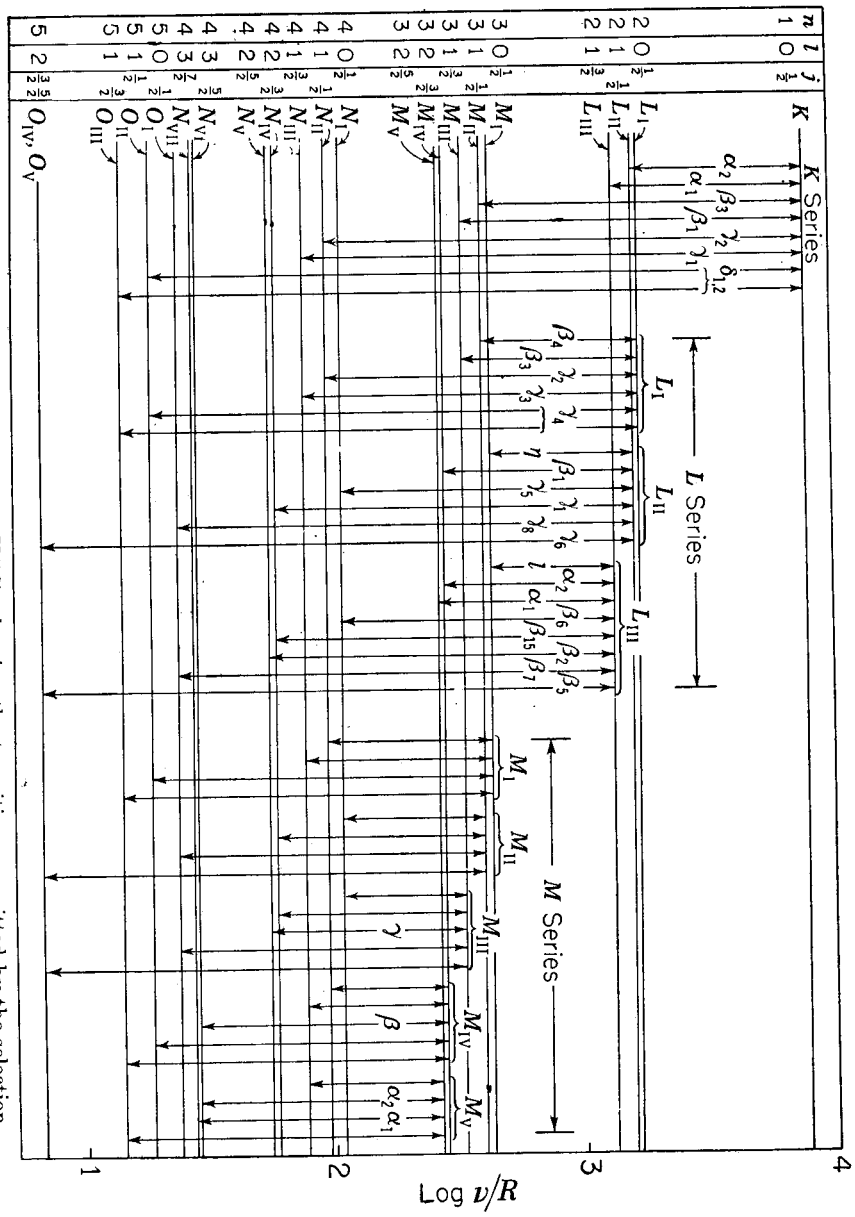

FIG. 137. X-ray energy-level diagram for U(92), showing the transitions permitted by the selection rules $\Delta l = \pm 1$; $\Delta j = \pm 1, 0$.

Figure 22. Atomic shell structure and X-ray emission lines for uranium. (Taken from Richtmeyer, Kennard, and Lauritsen, *Introduction to Modern Physics*, 5th Edition.

THE ZEEMAN EFFECT

I. INTRODUCTION

In this experiment we will study the effect of a magnetic field upon the wavelength and polarization of photons emitted by excited states of atomic mercury. This effect, discovered by Pieter Zeeman in 1896, won him the Nobel Prize in 1902. Twenty-five years later, this discovery provided the first convincing evidence for the half-integer nature of the spin of the electron.

The atomic number of mercury is Z=80. The electrons of mercury arrange themselves in the following shells, known as the atomic *configuration*:[83]

$$[\mathrm{Xe}]4f^{14}5d^{10}6s^2$$

For example, the notation $6s^2$ means two s ($l = 0$) electrons with principal quantum number $n = 6$. This so-called *shell model* treats the atomic electrons as independent of one another. As we shall see below, the electrons are not entirely independent, and we will have to take some pairwise correlations into account in this experiment.

When gaseous mercury is subjected to an electrical discharge, such as in a fluorescent light bulb, street lamp, or laboratory discharge tube, the collisions between the mercury atoms and the electrons are energetic enough to excite one of the 6s electrons to a higher energy state, while the remaining 79 electrons (including the other 6s electron) remain undisturbed. Depending upon which empty shell the excited 6s electron occupies, the excited electron will eventually return to successive lower energy states by emitting packets of light, called photons, whose energy reflects the energy difference between the two levels. That is,

$$\begin{aligned} E &= hf = \hbar\omega \\ \lambda &= c/f = hc/E \end{aligned} \tag{113}$$

In this experiment we will examine the following excitation and de-excitation steps of the 6s electrons:

$$(6s)\bullet(6s) \rightarrow (6s)\bullet(7s) \Rightarrow (6s)\bullet(6p) \rightarrow (6s)\bullet(6s) \tag{114}$$

That is, by some complex process, one of the 6*s* electrons is excited to the 7*s* state, while its companion 6*s* electron remains in its equilibrium configuration. Then, after some period of time, on the order of 10^{-9} seconds, the 7*s* electron decays into a 6*p* state, the transition that we are investigating. Eventually, this 6*s*6*p* state will decay into the ground state 6*s*6*s*, a transition that does not concern us in this experiment.

Unfortunately, the simple shell notation above does not account for the fact that there are many states with distinct energies associated with both the initial and final configurations

[83] The *Handbook of Chemistry and Physics* is an excellent reference for atomic energy levels.

indicated above. This is because the actual energy of the pair of electrons depends upon the combined spin of the pair, the combined orbital angular momentum of the pair, and the combined (spin plus orbital) angular momentum of the pair of electrons. Moreover, this manifold of distinct energy states is further split if the atom is subjected to a magnetic field *B*.

A remarkable consequence of quantum mechanics is that angular momentum is not simply additive as it is in classical mechanics; instead, there is a spectrum of possibilities. There are six energetically distinct levels, known as *terms*, associated with the 6s7s and 6s6p configurations:

Configuration 6s7s: terms $^1S_0$ or $^3S_1$
Configuration 6s6p: terms $^1P_1$ or $^3P_0$ or $^3P_1$ or $^3P_2$

The term notation has the following meaning. The symbol $^{2S+1}[X]_J$ for <u>two</u> electrons means the following:

- The superscript S numerically designates the *total spin* quantum number of the two electrons. For two electrons, S=0 (antiparallel spins) or S=1 (parallel spins).
- [X] = S (L = 0), P (L = 1), D (L = 2), F (L = 3), ... alphabetically designates the *total orbital* angular momentum quantum number L of the two electrons.[84]
- J numerically designates the *total* (spin *plus* orbital) angular momentum quantum number of the two electrons.[85]

In principle, there are eight possibilities for transitions from the two 6s7s terms to the four 6s6p terms. Each transition is characterized by its own characteristic wavelength, or color. We concern o
urselves in this experiment with the transition $^3S_1 \rightarrow {}^3P_2$, which results in the bright green line at λ = 546.07 nm. The other seven transitions are well-separated from this one. This transition has the following properties:

$2S+1=3 \rightarrow 2S+1=3$:The total spin quantum number (S = 1) of the pair is unchanged.
$S \rightarrow P$:The orbital angular momentum quantum number of the pair increases by one unit.
$J=1 \rightarrow J=2$:The total angular momentum quantum number of the pair increases by one unit.

[84] *Important warning*: the symbol S has two distinct meanings in atomic physics. The superscript 2*S*+1 refers to the total *spin* quantum number *S* of the two electrons. However, the S in the sequence [S], [P], [D], [F], *etc*., signifies that the total *orbital* angular momentum quantum number is zero. In this context, *S* stands for "Sharp," *i.e. L* =0; *P* stands for "Principal," *i.e. L*=1; "*D*" stands for "Diffuse," *i.e. L*=2; and "*F*" stands for "Fundamental," *i.e. L*=3; which were crude descriptions given by Rydberg in 1890 of the appearance of the spectral lines in alkali metals. See, *e.g.* Richtmeyer, Laurtison, and Kennard, *Introduction to Modern Physics*, McGraw-Hill Publishing Company.

[85] Beware that *S*+*L* does not always equal *J* , although it fortuitously happens to in this case. This mysterious but important and fundamental fact is explained at length in every introductory quantum mechanics textbook under the heading "*Addition of Angular Momenta*."

Magnetic field dependence: If $B = 0$, the transition ${}^3S_1 \rightarrow {}^3P_2$ would manifest itself as the emission of light of a single wavelength of 546.07 nm. However, because the total angular momentum quantum number of the two electrons in the *initial* state is $J = 1$, there are three sublevels, $m_J = -1, 0, 1$, corresponding to different *z*-components of angular momentum.[86] These states will have slightly different energies in a magnetic field. Similarly, because the total angular momentum quantum number of the two electrons in the *final* state is $J = 2$, there are five sublevels in the final state, $m_J = -2, -1, 0, +1, +2$, each with slightly different field-dependent energies. Thus, in principle, there are $3 \times 5 = 15$ possible distinct transition energies for the ${}^3S_1 \rightarrow {}^3P_2$ transition in a magnetic field.

Fortunately for us, quantum mechanics only allows transitions for which $\Delta m_J = -1, 0$, or $+1$. Hence there can only be 9 allowed transitions (see Figure 23**).** Furthermore, if our line of sight to the source is perpendicular to the magnetic field direction (as it is in this experiment), the polarization of the light has the following interesting property: Light emitted from the three possible $\Delta m_J = 0$ transitions will be polarized *parallel* to the magnetic field direction; these are called π (or p) (for *parallel*) transitions.[87] Conversely, light emitted from the three possible $\Delta m_J = -1$ or three possible $\Delta m_J = +1$ transitions will be polarized *perpendicular* to the magnetic field direction; these are called σ (or s) (for *senkrecht*, or perpendicular) transitions.[88]

The shift in the energy levels of an atomic state is proportional to the z-component angular momentum quantum number, m_J. The shift (in cgs units[89]) is given by $\delta E = g \mu_0 B m_J$, where g is the dimensionless Lande g-factor, $\mu_0 = e\hbar / 2m_e c$ is the Bohr magneton, and B is the magnetic field in Gauss. The dimensionless number g is calculable using quantum mechanics; it is given by

$$g = 1 + \frac{J(J+1) + S(S+1) - L(L+1)}{2J(J+1)} \tag{115}$$

For the ${}^3S_1$ initial level (+), $g = 2$; for the ${}^3P_2$ final level (−), $g = 3/2$ (please verify!). By referencing the bottom of **Figure 23**, we see that the nine possible energy shifts are evenly and symmetrically spaced about the zero-field transition.

---

[86] For convenience, we take the z-axis to be the direction of an externally applied magnetic field, which in our case is horizontal.

[87] Not to be confused with the *p* that means one unit of orbital angular momentum!

[88] In this experiment we will view the source along a line that is perpendicular to the field direction. It turns out that if we view the light along a direction parallel to the field direction, the light would be circularly polarized. This experiment is beyond the scope of the present lab.

[89] In cgs units, $e = 4.803 \cdot 10^{-10}$ esu, $\hbar = 1.05459 \cdot 10^{-27}$ erg-sec, $h = 2\pi\hbar$, $m_e = 9.108 \cdot 10^{-28}$ grams, $c = 2.998 \cdot 10^{10}$ cm/s, and $\mu_0 = 9.2741 \cdot 10^{-21}$ erg/Gauss.

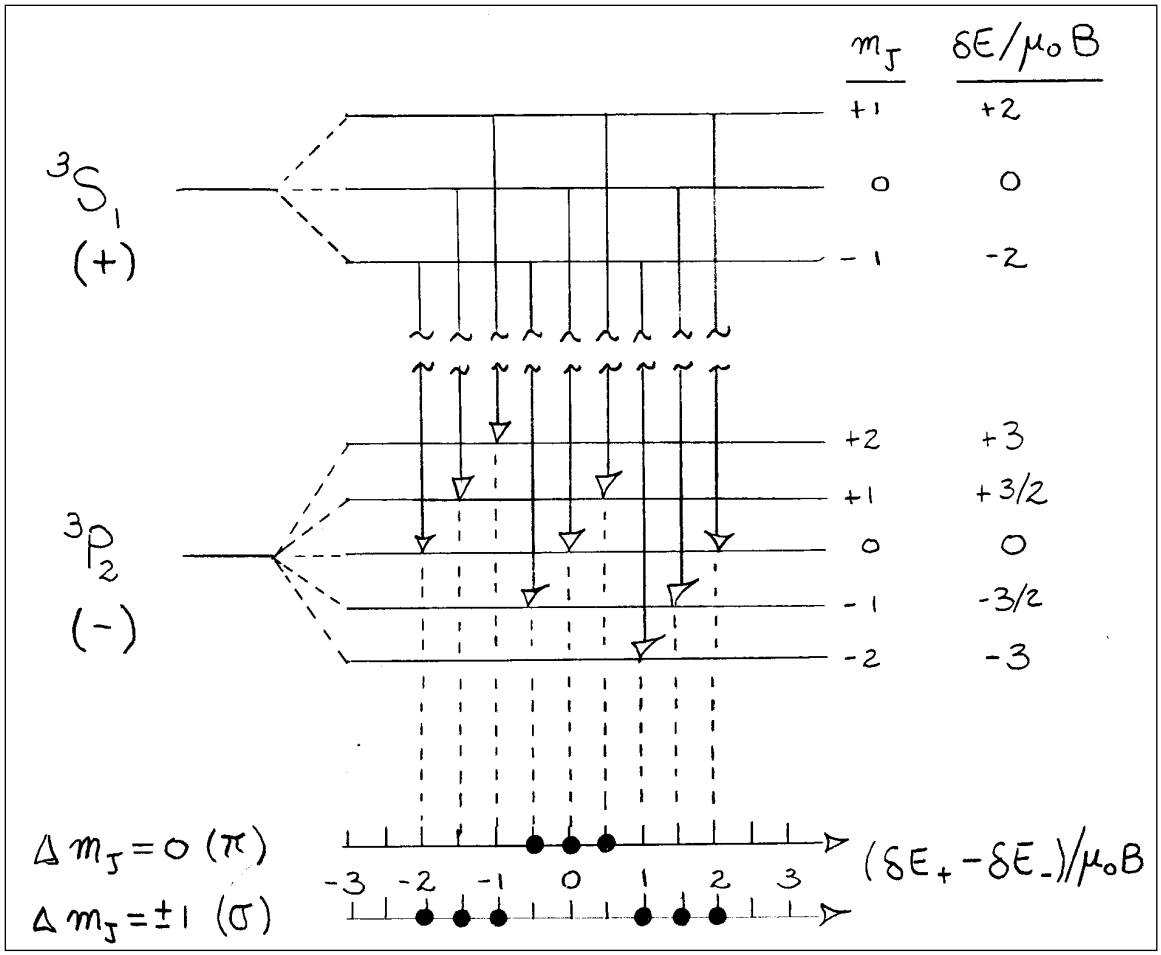

Figure 23. The energy levels for the $^3S_1 \rightarrow {}^3P_2$ transition in mercury.[90]

Note that in Figure 23, we have classified the transitions into two categories:

$$\begin{aligned} \Delta m_J &= 0 \quad (\pi \text{ polarization}) \\ \Delta m_J &= \pm 1 \ (\sigma \text{ polarization}) \end{aligned} \tag{116}$$

In our experiment, the light is always viewed perpendicular to the direction of the magnetic field. The three π lines are linearly polarized, along the direction of the magnetic field (horizontal). By contrast, the six σ lines are polarized perpendicular to the direction of the magnetic field (vertical). With a linear polarizer one may select either set.

Finally, the line intensities are not all equal. The relative line intensities for the lines are shown in Figure 24. Since our interferometer is not capable of resolving the individual

[90] Adapted from Figure 7.8 of Melissinos, *Experiments in Modern Physics***,** Academic Press (1966).

lines within a triplet, the triplet appears as a single line with a position that is the weighted average of the individual three lines.[91]

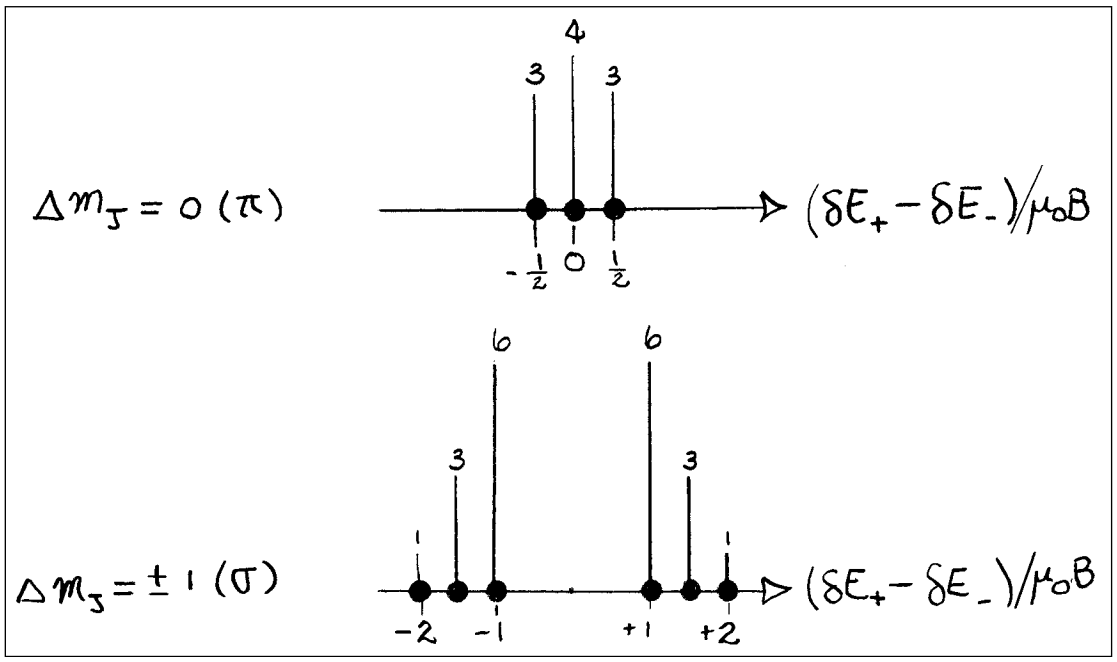

Figure 24. Relative intensities of the Zeeman lines.

II. THE MAGNET

CAUTION: THE MAGNET PRODUCES A FAIRLY HIGH MAGNETIC FIELD AND ATTRACTS FERROMAGNETIC OBJECTS. BE SURE NOT TO BRING SUCH OBJECTS INTO THE VICINITY OF THE MAGNET WHILE THE MAGNET POWER IS ON. A FLYING SCREWDRIVER COULD EASILY SHATTER THE DISCHARGE TUBE.

The magnetic field for this experiment is produced by a conventional iron-core electromagnet, arranged in a horseshoe configuration. The power supply (KEPCO, Inc.) for the magnet can furnish a maximum of 80 volts and a maximum of 2.0 Amperes. There are two controls on the chassis: voltage limit and current limit. In this experiment the magnet excitation should be controlled with the current limit knob, by setting the voltage limit knob to its maximum. Please note that the magnetic field at a given current is not unique; it depends upon the history of the excitation. This is called hysteresis. You should measure the field with the Hall probe each time you change the current.

[91] See, *e.g.* E. U. Condon and G. H. Shortley, *The Theory of Atomic Spectra* (Cambridge University Press, 1963). This important point is not discussed in Melissinos.

IMPORTANT NOTICE: ALWAYS RUN THE CURRENT CONTROL DOWN TO ZERO BEFORE SWITCHING THE POWER SUPPLY ON OR OFF. OTHERWISE, THE SUDDEN CHANGE IN CURRENT GIVES RISE TO A HIGH VOLTAGE SPIKE AT THE POWER SUPPLY OUTPUT TRANSISTORS.

The magnetic field is measured by means of a Gaussmeter using a Hall Probe. The probe measures the field perpendicular to the tip.

PLEASE NOTE: THE PROBE TIP IS VERY DELICATE AND EXPENSIVE. BENDING THE TIP RELATIVE TO THE PROBE HANDLE MAY DESTROY THE TIP.

III. THE LIGHT SOURCE

The light source in this experiment is a simple hollow-cathode mercury discharge tube, known as a Geissler tube, after its inventor in the 1860's. It is powered with alternating current, originating from a step-down autotransformer connected to a step-up high voltage transformer. This experiment runs well with the autotransformer set at 40-50 volts. Running the tube at a higher voltage risks overheating the tube. The lamp is immediately followed by a 4.0 mm diameter aperture to assure that only light from the center of the magnet is viewed by the optics.

Ideally, for the purposes of this experiment, we would like a lamp with a single, even-numbered isotope. However, the mercury in the lamp comprises the naturally occurring isotopes, with atomic mass number A = 198, 199, 200, 201, 202, and 204. The isotopes with an odd value of A have an odd number of neutrons, for which there is a definite spin to the nucleus. Since the nucleus is charged, these nuclei possesses a nonzero magnetic moment. This nuclear moment interacts with the electron's magnetic moment to produce energy shifts leading to the so-called *hyperfine* structure, which is present even in the absence of an externally applied magnetic field. Since some of these lines are closely spaced, they will manifest themselves as a broadening of the spectral lines rather than as sharply resolved individual lines. A few of the lines are actually resolved by our spectrometer.

To make matters even slightly worse, even if our mercury lamp contained only the even numbered values of A (198, 200, 202, and 204), there would still be a slight shift due to the fact that the nucleus is not a point charge, but rather an extended charge whose size grows with atomic number. This is the so-called *isotope effect*.

IV. THE CONDENSER

The principal lens in the optical system is a simple bi-convex lens with a focal length of 150 mm. The lens is placed approximately 300 mm from the source, resulting in a real image of the source at about 300 mm downstream, with about unity magnification. The purpose of this lens is to collect as much light as possible from the source and convey it to the subsequent optical elements.

V. THE POLARIZER

As mentioned in the introduction, the radiation from atomic transitions in a magnetic field can be polarized, the nature of which is determined by the transitions themselves, and by the direction of emission relative to the magnetic field direction. In this experiment we will be investigating cases in which the radiation is linearly polarized. The analysis of linear polarization is made by rotating the polarizer about the beam axis.

VI. THE INTERFERENCE FILTER

The visible spectrum of atomic mercury excited by a discharge tube is exceedingly complex. In order to study a given spectral line, it is important to remove the light from all other lines in the spectrum. Fortunately, there exist commercially available interference filters that are opaque to all wavelengths except those within a narrow band in the vicinity of the desired spectral line. The spectral response of our filter is shown in Figure 25.

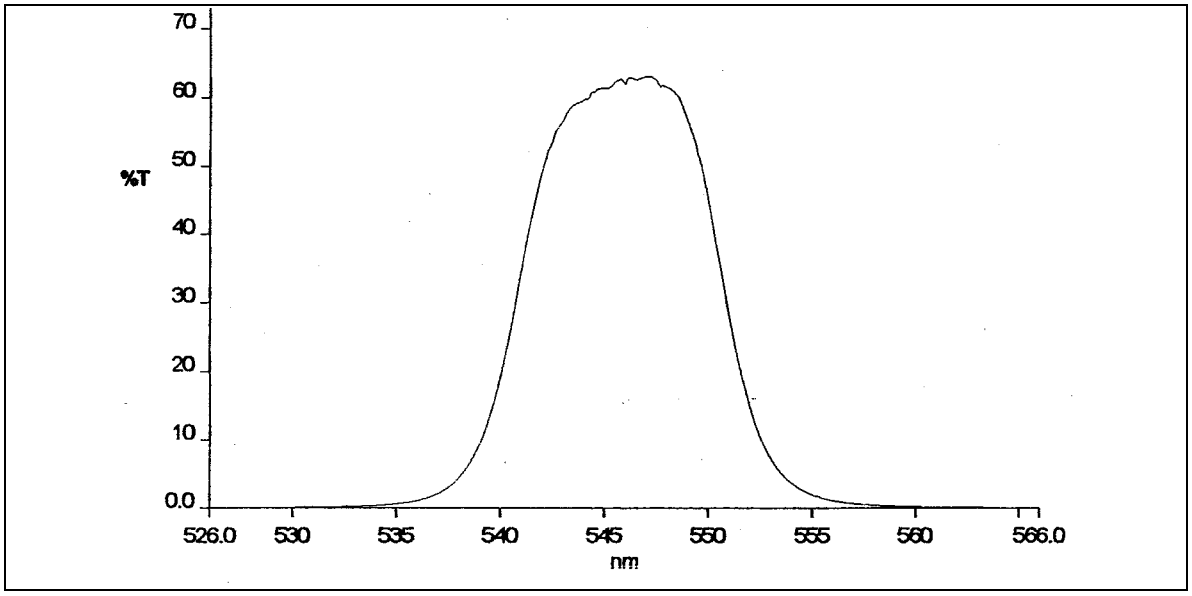

Figure 25. The spectral response of the 546 nm interference filter.

VII. THE FABRY-PEROT INTERFEROMETER

The Fabry-Perot interferometer is an extremely high resolution interferometer, discussed in detail in the appendix (refer to Figure **27**). The geometry is extremely simple: it consists of two optical flats, separated in our case by t = 0.6499 cm., using a rigid, precision-ground hollow spacer. The flats are coated with an aluminum or silver coating with a reflectivity of about 90%.

We will be studying the splitting of the green mercury line at $\bar{\lambda}$ = 546.07 nm. In the absence of a magnetic field, and, neglecting hyperfine shifts and nuclear-size (isotope) shifts, the output of the interferometer, as imaged by a telescope focused at infinite distance, will be a series of concentric sharp rings (p = 1,2,3,…) of angular size given by

$$\theta_p^2 = \frac{\lambda_0}{t}(p - e(\lambda_0)); \quad p = 1, 2, 3, \ldots \tag{117}$$

Where $e(\lambda_0)$ is an unimportant constant (discussed in the appendix).

For purposes of analysis of the spectrum in a magnetic field, assume that the magnetic field results in two closely spaced lines, λ_a and λ_b. Constructive interference of each respective wave will occur at discrete polar angles, $\theta_a^{(p)}$ and $\theta_b^{(p)}$. For a fixed p, the lines will be displaced by the amount

$$\boxed{(\theta_p^{(a)})^2 - (\theta_p^{(b)})^2 = 2\bar{\lambda}\left(\frac{1}{\lambda_a} - \frac{1}{\lambda_b}\right) = 2\frac{E_a - E_b}{\bar{E}}} \tag{118}$$

A perfectly constructed étalon will yield rays of sharply defined angles with a sharpness given by Equation (130) in the appendix.

VIII. THE CAMERA

The final optical element is an f = 135 mm focal length lens attached to an astronomical CCD camera. (The camera is preceded by an adjustable aperture, to ensure that only light emerging from the center of the source falls on the camera. The aperture should be set to slightly larger than the lamp aperture, or about 5 mm). When the focus is adjusted to give the sharpest rings, the lens will be focused at infinity, so that incoming parallel rays making an angle θ with respect to the optic axis are focused at a distance $f\theta$ from the center of the image. The CCD camera has an array of 510×765 pixels, each 9 μm × 9 μm square.

The camera software is extremely easy to use. For preliminary measurements, where you don't need to save the image files, perform the following steps:

1. Connect AC power to the camera.
2. Load CCDOps.
3. Under the CAMERA tab, select FOCUS.

When you are ready to take images to save, under the CAMERA tab, select GRAB, and take the image.

To analyze the data,

1. Load the desired image.
2. Under DISPLAY, select SHOW CROSSHAIRS.
3. Move the origin to the origin of the image.
4. Under DISPLAY, select SHOW HORIZONTAL PROFILE.

You can now easily see the peaks, and measure their intensities and positions.

The full optical system is depicted in Figure 26, which illustrates two extreme sample rays emerging from the source. Note that the centers of each optical element should be

about 11.5 cm above the table. Otherwise, you may be viewing a part of the lamp outside the magnetic field (the lamp has a small aperture at its center point).

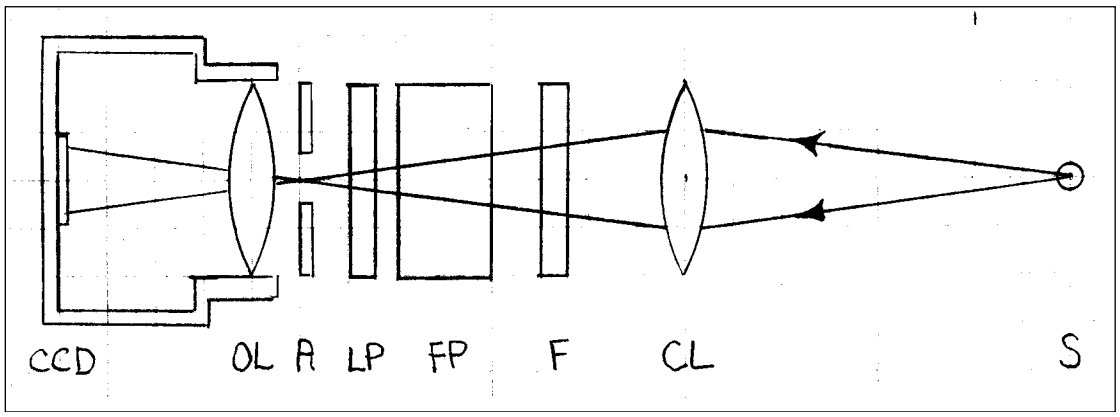

Figure 26. Schematic of optical layout. S=Source, CL=Condenser Lens, F=Interference Filter, FP=Fabry-Perot Interferometer, LP=Linear Polarizer, A=Aperture, OL=Camera Objective Lens, CCD=Charge Coupled Device.

IX. THE EXPERIMENT

The following steps are intended to be suggestive. Feel free to explore the various parameters available to you. The book by Melissinos is a good overall reference. Note: It is a good idea to calculate your line splittings before measuring. Often, lines from different orders can overlap.

1. With the magnetic field set to zero, observe and record the Zeeman rings. Measure the angular radius of the rings, using the known pixel size and camera lens focal length. Make a plot of θ^2 versus the ring index (1, 2, 3, ...). From this straight line determine the slope $d\theta_p^2 / dp$. Compare this with the theoretical value, λ/t. [t=6.499 mm]
2. With the magnetic field on, perform the Zeeman experiment.
   2.1. For the polarizer set to observe π polarization, measure the energy shift as a function of the magnetic field. From your results determine the value of the Bohr magneton μ_0.
   2.2. Exercise: show that the centroid of each σ triplet is $<(\delta E_+ - \delta E_-)>= \pm 1.25\mu_0 B$.
   2.3. For the polarizer set to observe the σ polarization, record the Zeeman pattern as a function of magnetic field. From your results determine the value of the Bohr magneton μ_0.

APPENDIX: THE FABRY-PEROT INTERFEROMETER

INTRODUCTION

Two plates of flat, transparent material, aligned mutually parallel, may give rise to important interference effects. In particular, if the inner surfaces of the two plates have a high reflectivity, the cavity can sustain multiple reflections of light if the wavelength and the angle satisfy certain conditions, which we shall derive shortly. If the spacing of the plates is adjustable, the device is called a Fabry-Perot *interferometer*, and if the spacing of the plates is fixed, the device is called a Fabry-Perot *étalon*. Our étalon consists of two flat, transparent discs, with the inner surfaces coated with a highly reflecting material, separated by a precision spacer. Another version of the étalon is a solid transparent rod of index of refraction *n*, reflectively coated at each end.

THEORY

If a plane wave of wavelength λ is incident upon the étalon at incident angle θ, the light will enter the cavity and bounce back and forth, with some light eventually transmitted and the remainder back-reflected.

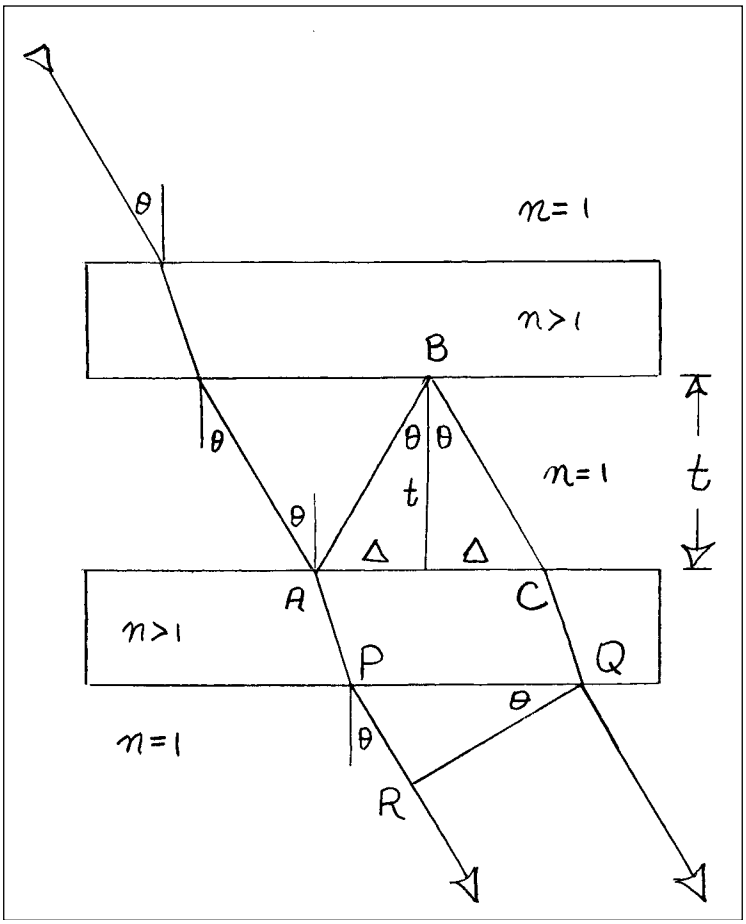

Figure 27. Ray diagram of the Fabry-Perot Interferometer

In order for the primary ray to interfere constructively with the reflected ray, the extra phase advance caused by the extra distance traveled, and by the phase shift φ at each surface, must be a multiple of the wavelength. Referencing Figure 27, the extra distance is

just AB + BC – PR. Simple trigonometry tells us that AB = BC = $t/\cos(\theta)$, and PR = PQsin(θ). But PQ = AC = $2\Delta = 2t\tan(\theta)$, so PR = $2t\tan(\theta)\sin(\theta)$. Thus the extra distance is $2t/\cos(\theta) - 2t\tan(\theta)\sin(\theta) = 2t\cos(\theta)$ (please verify!). Hence we have the requirement for constructive interference

$$\boxed{\frac{2t\cos(\theta)}{\lambda} + 2\frac{\phi}{2\pi} = m}. \tag{119}$$

At this angle and for this wavelength, the incident wave will be transmitted with 100% efficiency. If, for a given wavelength, the angle does not exactly satisfy equation (119), but is close, then the transmission coefficient will be less than 1, and will be given by[92]

$$T = \frac{1}{1 + \frac{4R}{(1-R)^2}\sin^2(\frac{\delta}{2})} \qquad \frac{\delta}{2} = \frac{2\pi t}{\lambda}\cos\theta + \phi \tag{120}$$

To get a feel for equation (119), take λ =546.07 nm (the green line of mercury); t = 0.500 cm. (not quite our value), and $\phi/\pi = 0$.[93] Then

$$\cos(\theta_m) = \frac{m}{18312.536} \tag{121}$$

The smallest angle satisfying this equation will be when the right hand side is less than or equal to 1; *i.e.* for m = 18312, 18311, 18310, ... = $m_{\max}, m_{\max}-1, m_{\max}-2, \ldots$. To each of these decreasing values of m corresponds a small but increasing angle θ_m where the light is transmitted with unity probability. For the angles θ_m close to 0, we can set $\cos(\theta_m) \simeq 1$, yielding from (119) the following useful approximation:

$$\frac{1}{\lambda} \simeq \frac{1}{2t}(m - \phi/\pi) \tag{122}$$

We now carry out the analysis of equation (119) to higher order. We will consider only angles small compared to unity; in this cases we can use the small angle approximation $\cos\theta \simeq 1 - \theta^2/2$ and express Eq. (119) as

$$\frac{2t}{\lambda}(1 - \frac{\theta_m^2}{2}) + \frac{\phi}{\pi} = m \tag{123}$$

---

[92] See, e.g. Born and Wolf, *Principles of Optics***,** or Pedrotti and Pedrotti, *Introduction to Optics***.**

[93] Since $0<\varphi<\pi$, this qualitative argument is not changed by setting $\varphi=0$.

Solving this equation for θ_m, we get

$$\theta_m^2 = 2 + \frac{\lambda}{t}\left[\frac{\phi}{\pi} - m\right] = \frac{\lambda}{t}\left[\frac{2t}{\lambda} + \frac{\phi}{\pi} - m\right] \tag{124}$$

Recalling that the allowable values of *m* are a set of very large, but descending, integers $m = m_{\max}, m_{\max}-1, m_{\max}-2,...$, we associate with them the respective ascending sequence of integers $p = 1, 2, 3,...$, corresponding to increasing angles of incidence θ_p. One will then observe unity transmission at angles given by

$$\boxed{\theta_p^2 = \frac{\lambda_0}{t}(p - e(\lambda_0)); \quad p = 1, 2, 3, \ldots} \tag{125}$$

where $0 \le e(\lambda_0) \le 1$ is the fractional part of $(2t/\lambda_0 + \phi/\pi)$. Thus $e(\lambda_0)$ is a wavelength-dependent residual phase number arising from the fact that *t* is not an integer multiple of λ_0. For our purposes $e(\lambda_0)$ does not play a significant role.

With monochromatic incident radiation, we can measure the angles of maximum intensity, and plot θ_p^2 versus *p*. From (125) we should get a straight line, with slope λ / t. Figure 28 shows an example of such a plot for *t* = 0.5 cm. and λ = 546.06 nm.

In practice, we cannot predict beforehand the precise values of θ_p because we do not know the phase shift ϕ, nor do we know the value of $2t/\lambda$ to six significant figures. However, the usefulness of the Fabry-Perot étalon lies in our ability to determine wavelength *differences* to very high precision. In what follows we will show how this is accomplished.

Suppose two closely spaced wavelengths of light, λ_a and λ_b, are incident upon the étalon. Let us compare the angular separation of the rings *that occur for the same order m*. From equation (124) we have

$$\begin{aligned}(\theta_m^{(a)})^2 &= 2 + \frac{\lambda_a}{t}\left(\frac{\phi}{\pi} - m\right) \\ (\theta_m^{(b)})^2 &= 2 + \frac{\lambda_b}{t}\left(\frac{\phi}{\pi} - m\right)\end{aligned} \tag{126}$$

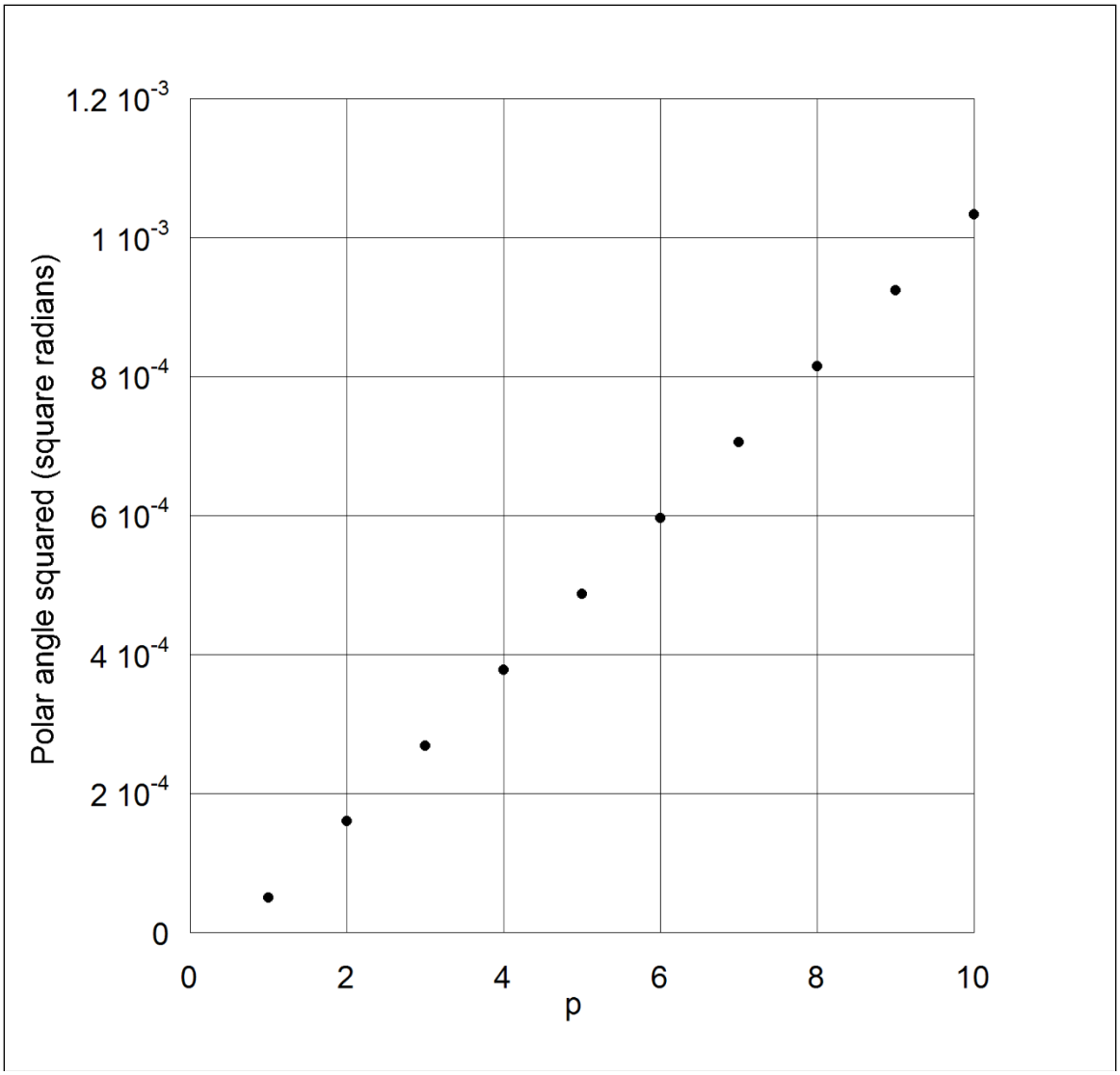

Figure 28. A plot of θ_p^2 versus *p*, for λ = 546.074 nm, *t* = 0.500 cm, and $\phi = 0$.

Subtracting the two equations,

$$(\theta_m^{(a)})^2 - (\theta_m^{(b)})^2 = \frac{\phi/\pi - m}{t}(\lambda_a - \lambda_b) \tag{127}$$

Using the approximation given in equation (122), we may write

$$\frac{m - \phi/\pi}{2t} \approx 1/\lambda_a \approx 1/\lambda_b \approx 1/\bar{\lambda}\,. \tag{128}$$

We therefore obtain the very simple and elegant result[94]

[94] Inexplicably, this simple expression is neither derived in Born and Wolf, nor in Melissinos.

$$\boxed{(\theta_m^{(a)})^2 - (\theta_m^{(b)})^2 = 2\frac{\lambda_b - \lambda_a}{\bar{\lambda}} \simeq 2\bar{\lambda}\left(\frac{1}{\lambda_a} - \frac{1}{\lambda_b}\right) \simeq 2\frac{E_a - E_b}{\bar{E}}} \qquad (129)$$

In our case, the application of a magnetic field to our sample will split a line $\bar{\lambda}$ into two or more lines λ_a and λ_b; the difference in the square of their angles will be given by (129). This result is central to many kinds of high resolution spectroscopy, including Zeeman spectroscopy.

In practice, a Fabry-Perot étalon is usually *deliberately* illuminated by an extended, uncollimated source. Contrary to one's intuition, and contrary to the situation with grating spectrometers, this is not only *easy*, it is also a *good* thing.[95] Then, if the étalon is illuminated with monochromatic light and then viewed with an astronomical telescope or a camera focused at infinity, one will observe sharp rings at successively larger polar angles.

RESOLUTION OF A FABRY-PEROT INTERFEROMETER

The resolving power of any spectrometer is usually specified in terms of the full-width at half maximum (FWHM) of the spectral lines. If you analyze Equation (120) in detail, you will find that, for an otherwise perfect Fabry-Perot étalon, the FWHM is given by a very simple expression,

$$\frac{\Delta\lambda}{\lambda} = \frac{\lambda}{2t}\frac{1-R}{\pi\sqrt{R}} \qquad (130)$$

where the variables have been defined earlier. For our étalon, t = 0.6499 cm and $R \approx$ 0.9.[96] For our experiment, λ = 546 nm. This leads to $\Delta\lambda / \lambda$ = 1.4x10^{-6}!

[95] A Fabry-Perot étalon is, in effect, a filter; a plane wave incident with a certain direction results in a plane wave transmitted with *exactly* the same direction, but with transmittance *T*. Therefore, there *must* be an angular spread of the source comparable to the angular range of the rings that one wishes to observe. However, the transverse *size* of the beam does not matter, unless the étalon has inhomogeneities.

[96] You might think that the resolution should go to zero as *R* goes to 1. Theoretically this is the case; however, for values of *R* greater than about 0.9, surface imperfections dominate and larger values of *R* do not help.

APPENDIX. INTERACTION OF RADIATION WITH MATTER

1. NOMENCLATURE

Because of the historical evolution of the subject, the nomenclature of electromagnetic radiation is a bit ambiguous. We may always use the modern terms *quanta*, or *photons*, to describe the quantized particles of electromagnetic radiation. High energy quanta (E >100 eV) are called x-rays if they originate from atomic transitions, and gamma rays if they originate from nuclear transitions. However, they are fundamentally identical, apart from their origin.

2. GENERAL THEORY

Photons of energy $E_\gamma = \hbar\omega$ interact with matter in one of three ways: quasi-elastic scattering, Compton scattering, and the photoelectric effect. We will discuss these three processes in turn.

Quasi-elastic scattering: Quasi-elastic scattering may consist of one of the following three processes:

$$\begin{aligned} &\hbar\omega + \text{crystal} \rightarrow \hbar\omega + \text{crystal (Diffraction)} \\ &\hbar\omega + \text{crystal} \rightarrow \hbar\omega' + \text{phonon} + \text{crystal (Brillouin Scattering)} \\ &\hbar\omega + \text{atom} \rightarrow \hbar\omega' + \text{atom (Quasi-elastic scattering)} \end{aligned} \tag{131}$$

The photon may scatter from a crystal with no energy loss; in this case the process is called x-ray diffraction. On the other hand, a photon may scatter from a solid or a liquid and create (or possibly absorb) a lattice vibration (phonon); in this case the photon emerges with a slightly lesser (or greater) energy. Phonon energies are of order 10^{-2} electron volts, so the energy loss is extremely difficult to detect. In this case, such scattering may be accompanied by a large angular deflection. Finally, a photon may scatter elastically from a single atom in a liquid or a gas, transferring both energy and momentum to the atom.

Compton Scattering: Compton scattering is defined by the following process:

$$\hbar\omega + \text{atom} \rightarrow \hbar\omega' + \text{e}^- + \text{atom*} \tag{132}$$

In this process, the photon may be thought to scatter from a single electron in an atom, ejecting the electron from the atom. As a consequence, the atom is left in an excited state (atom*), which then relaxes to its ground state (after stealing a nearby electron to make up for the one it lost), in a very short time, of order 10^{-15} seconds. Meanwhile, the photon emerges with considerably less energy, having conveyed energy both to the scattered electron and to the atom.

Two experiments observing the Compton effect were pivotal in the early development of quantum mechanics. The second, most famous experiment demonstrated that gamma rays had the same kinematic properties as ordinary, massive particles, except that they were

massless. Compton observed that the reaction given in equation (132) could be thought of as the collision of a massless particle (the photon) with a massive particle (the electron). From simple kinematic arguments, he confirmed the following formula:

$$\frac{1}{E'}-\frac{1}{E}=\frac{1}{m_e c^2}(1-\cos(\theta)) \tag{133}$$

Where E is the energy of the incident photon, E' is the energy of the scattered photon, m_e is the mass of the electron, and θ is the polar angle of the scattered electron.

The first experiment, published in 1929, had an equally profound effect upon the development of quantum mechanics. To understand this experiment, it must first be understood that J. J. Thomson had predicted that the scattering of unpolarized electromagnetic waves by an electron should obey the relation

$$\frac{d\sigma}{d\Omega}=\frac{1}{2}r_0^2(1+\cos^2\theta) \tag{134}$$

Where r_0 is the so-called classical radius of the electron, $r_0=e^2/mc^2 = 2.818\text{x}10^{-13}$ cm.

However, the Thomson result was derived before the special theory of relativity had been put forward by Albert Einstein, and it was subsequently clear that a relativistic formulation was required when the photon energy was comparable to the rest energy of the electron. Dirac's famous relativistic formulation of the electron, which required the existence of anti-electrons (positrons), led to the generalization of the Thomson formula, the famous Klein-Nishina cross section for unpolarized incident radiation:[97]

$$\frac{d\sigma}{d\Omega}=\frac{1}{2}\left(\frac{E'}{E}\right)^2 r_0^2\left[\frac{E}{E'}+\frac{E'}{E}-\sin^2\theta\right] \tag{135}$$

A comparison of equations (134) and (135) show that, while the Thomson formula predicts equal forward-backward scattering probabilities, the Klein-Nishina formula predicts a substantial forward-backward asymmetry, which is straightforward to observe in the laboratory.

Photoelectric Absorption: The previous two processes describe scattering: the incident photon survives, albeit with changed energy. The photoelectric effect is quite different: the incident photon is entirely absorbed, resulting in an ejected photoelectron, whilst leaving the target atom in a highly excited state. This process results in the deposit of the entire incident energy into a small volume surrounding the target atom. The reaction can be describe symbolically as

$$\hbar\omega+\text{atom}\rightarrow e^-+\text{atom}^* \tag{136}$$

[97] J. J. Sakurai, *Advanced Quantum Mechanics*. Addison-Wesley, Co.

For the x-ray fluorescence laboratory, this is the key reaction. The incident photon, from the x-ray source, ionizes the atom, forming an exited state, atom*. This excited atom, in turn, may relax in any number of ways. For example, if the incident photon collides with one of the most tightly bound electrons, the so-called K shell electrons, the resulting vacancy may be re-filled by an L-shell electron dropping into the K-shell. The L-electron, in the process, radiates a photon of energy equal to the energy gained; namely, 8,038 eV in the case of copper.

The above process is of extreme technological importance. K-shell vacancies in any material can be made by bombarding atoms with x-rays, electrons, and even protons. The result is the characteristic fluorescent line, which unambiguously identifies the element.

3. DETECTION OF ELECTROMAGNETIC RADIATION

There are many practical methods of utilizing the physics described above to detect high energy x-rays. We will describe five such methods, as manifested in the upper division x-ray experiments.

Ion Chambers: As an x-ray passes through matter, the processes of Compton scattering and x-ray absorption lead to the ionization of the material, both through the direct process and through the subsequent atomic relaxation processes. Although the detailed relaxation processes are complex, the net effect is an average ionization energy, expressed in electron volts per ion pair. For example, in air, the average ionization energy is about 33 eV per ion pair. Thus, a Cu Kα x-ray of energy 8038 eV, if completely absorbed in an ion chamber, deposits about 244 electrons and creates 244 singly ionized atoms or molecules.

If the volume of air is subjected to a modest electric field, of order 100 Volts per centimeter, the electrons will be attracted to the positive electrode and the positive ions will be attracted to the negative electrode. If the field is much weaker, the electrons and ions, which strongly attract one another, will recombine.

Intrinsic Silicon Detectors. Pure silicon, sometimes referred to as *intrinsic* silicon, is conceptually identical to an ion chamber. Because of its purity, in principle it behaves like an insulator at zero degrees Kelvin; but because of the low ionization energy, there will be some conductivity above absolute zero. However, the conductivity will be still far less than that of typical semiconductors that are doped with electron donors or acceptors. Because of the high resistivity, it is possible to collect all of the charge from a single x-ray as a pulse, whose charge is accurately proportional to the energy deposited by the x-ray. This is the detector used in the x-ray fluorescence experiment.

Proportional Counters: Proportional counters are designed to be sensitive to photoelectric absorption in a gas. A proportional counter is invariably a fine wire surrounded by a conducting cylinder. The wire is held at a positive potential of several hundred volts with respect to the outer cylinder. Electrons migrating to the wire gain enough kinetic energy to further ionize the gas. Thus, if an x-ray or gamma ray is photoelectrically absorbed, the resulting ionization is amplified by the cascade process, leading to a pulse of charge on

the wire that is large enough to be detected by electronics. Although this is a common technique, at the moment we have no examples of proportional counters in the lab.

Geiger Counters: A Geiger counter is a proportional counter operated at a sufficiently high voltage to cause an avalanche pulse whose amplitude is independent of the original amount of charge deposited. That is, when the avalanche reaches a certain amplitude, the discharge is quenched by a trace gas in the tube. Geiger counters are typically used in hand-held radiation monitors because they are relatively rugged and repeatable. However, they give no information about the incident radiation other than its presence.

Scintillation Counters: The interaction of high energy quanta, through Compton scattering and through photoelectric absorption, leave the target atom in a highly excited state. The details of the relaxation of the atom are extremely complicated, but they often result in the emission of one or more quanta in the visible part of the spectrum. Thus, if our target material is a transparent crystal, viewed by a light-sensitive detector such as a photomultiplier, we can in principle detect residual effects of the incident photon, with time resolution of order 10^{-6} seconds. A favored material is the crystal NaI, pioneered by the Nobel Laureate Robert Hofstader. The key result is that if all of the energy of the incident quantum is absorbed by the crystal, a pulse of light is produced with total intensity proportional to the incident energy.

4. MULTI CHANNEL ANALYZERS

The pulse of visible light resulting from the scintillation is converted to an electrical pulse by the photomultiplier. The multi channel analyzer, in turn, produces a histogram of the distribution of pulses, and thus an energy distribution of the incident quanta.

A monochromatic beam of quanta will result in a pulse-height distribution of finite width. This is because only a finite number of photons are created by the incident high energy photon; and only some fraction of them create photoelectrons at the first stage of the photomultiplier. For example, the pulse height distribution of photons from a ^{137}Cs source is about 7% wide. We know that the statistical uncertainty arising from N photons is about $N^{1/2}$, so the relative uncertainty is about $N^{-1/2}$. Thus, the 661.7 MeV ^{137}Cs gamma ray results in about 200±14 photoelectrons at the input stage of the photomultiplier.